VARIATION AND THE EVOLUTIONARY DRIVERS OF DIVERSITY IN THE GENUS *PARANTHROPUS*

by

Nomawethu Hlazo

B.Sc., B.Sc. (Hons)

Thesis Presented for the Degree of

Masters of Science

in the Department of Archaeology

Faculty of Science

UNIVERSITY OF CAPE TOWN

06 February 2018

Cape Town, South Africa

Supervised by:

Professor Rebecca Rogers Ackermann

Co-supervised by:

Dr. Terrence Ritzman

Declaration

I, Nomawethu Hlazo, hereby declare that the work on which this thesis is based is my original work (except where acknowledgements indicate otherwise) and that neither the whole work nor any part of it has been, is being, or is to be submitted for another degree in this or any other university. I authorise the University to reproduce for the purpose of research either the whole or any portion of the contents in any manner whatsoever.

Signature: Signed by candidate Date: 06 February 2018

ABSTRACT

Craniodental robusticity in *Paranthropus* has led many researchers to posit that all the species in this genus share a common adaptation to a diet of hard foods. Recent research on craniodental morphology, microwear, biomechanics, and isotopes, by contrast, has suggested that substantial variation exists within the genus *Paranthropus*, both in terms of ecological niches occupied by the three recognized species within the genus and the amount of consumed hard and compliant foods. Rather than pointing to a common adaptive suite, these studies suggest that the species were adaptively distinct from each other. However, current approaches to understanding craniodental morphology do not present a clear picture of how these species-specific adaptations differ. It is also not clear whether all aspects of morphology that have been attributed to adaptation are indeed adaptive, rather than the products of non-adaptive processes. This study examines variation across the three known *Paranthropus* taxa (*P. aethiopicus*, *P. boisei* and *P. robustus*; N=39) using an approach that tests for adaptive morphology against a null hypothesis of random change (i.e. drift). Extant species (*Homo sapiens* (N=150), *Gorilla gorilla* (N=150), *Pan troglodytes* (N=143) act as analogues for *Paranthropus* variance/covariance (V/CV). Results reveal a high magnitude of variation within and between species across mandibular and cranial regions, especially when including the *P. robustus* individuals DNH 7 & 8 from Drimolen. Drift cannot be rejected for the bulk of comparisons. Neutrality tests detect adaptive divergence between *P. robustus* and the other two species, but not between *P. aethiopicus* and *P. boisei*. Reconstructed selection vectors indicate that both positive and negative directional selection have driven diversification in mandibular and tooth dimensions and in the cranium, resulting in variable morphological responses including considerable evidence for correlated selection.

TABLE OF CONTENTS

LIST OF TABLES

CHAPTER 3

CHAPTER 4

CHAPTER 5

LIST OF FIGURES

CHAPTER 2

CHAPTER 4

CHAPTER 5

LIST OF APPENDICES

ACKNOWLEDGEMENTS

To my parents, mama, I want to thank you for always pushing me to do my best and work hard. Thank you for telling me that I have it in me to achieve whatever I want in this life if I just focused and pushed forward. You are the epitome of what it means to work hard and strive for what one wants in this life. I am forever indented to you for your encouragement, support and love.

Thank you to my friends, family and God. There are no words to say how much I appreciate and am grateful for your time, your patience, your love and support. It's been quite a long road, a longer one yet to come but you have and will always be my rocks.

TO THE LAB (Tessa, Robyn, Kerryn, and Lauren) THANK YOU. Thank you for letting me vent and cry. Thank you for helping me EVERY step of the way and talking me through this process. Lauren thank you again for your data.

I am forever grateful to the National Research Foundation, Palaeontological Scientific Trust and the Centre of Excellence (Co-Pal) for awarding me the bursaries needed to complete this project and obtain this degree. Thank you to Dr. Christine Steininger (and the Gondolin team) for their support.

I also extend a warm thanks to the Drimolen team Dr. Stephanie Baker (including Ashleigh and Tash for their support), Professor David Strait and Dr. Colin Menter (University of Johannesburg). Assisted by Dr. Kieran McNulty and Dr. Caley Orr who made application for scanning the specimens.

Thank you for the data collected by Jesse Martin, Angeline Leece and Dr. Andy Herries (La Trobe University) by funded by the Australian Research Council Discovery Grant through The Australian Archaeomagnetism Laboratory and a Society of Antiquaries of London grant to Jesse Martin that allowed them to conduct this research towards the Drimolen specimens.

To the Ditsong Museum and Stephany Potze for allowing me access to the collections, thank you for your hospitality, it was much appreciated.

Furthermore, I would like to thank the Smithsonian's Division of Mammals (Dr. Kristofer Helgen) and Human Origins Program (Dr. Matt Tocheri) for the scans of USNM specimens used in this research. These scans were acquired through the generous support of the Smithsonian 2.0 Fund and the Smithsonian's Care and Preservation Fund.

I would extremely love to personally meet (hopefully soon) and thank Dr. Lynn Copes for her scans. I thank you for your continuous support throughout this project and answering my late night e-mails. Thank you.

Thank you to the smartest and most inspirational people that I know to my supervisor Professor Rebecca Rogers Ackermann and my co-supervisor Dr. Terrence Ritzman. Thank you for constantly helping me throughout this project including the devotion you have to me and this project. I am so grateful for your patience, support, kindness, spirit and time.

CHAPTER 1

INTRODUCTION

Previous studies of the morphology of the genus *Paranthropus* have tended to focus on inter-specific variation (e.g. Kimbel and White, 1988; Wood and Lieberman, 2001; Rak, 1988), with an eye towards understanding phylogenetic relationships as well as shared adaptations. These studies have separated the genus *Paranthropus* into three species (Wood, 2010; Strait et al., 1997). These species are thought to share an adaptation for feeding on tough and/or hard foods, which is reflected in their possession of extremely large jaws and teeth (hence the term "robust") (Brain, 1967; Rak, 1983). Therefore, the tacit assumption with regard to the craniodental morphology of the genus *Paranthropus* has traditionally been that features shared by its members were driven by natural selection. Less attention has been paid to exploring intra-individual variation and to understanding the potential role of non-adaptive processes in the diversification of this genus. This thesis attempts to fill some of these gaps.

The overall objective of this study is to understand intra- and inter-specific variation in the genus *Paranthropus* by comparing within-group craniofacial variation with between-group craniofacial variation. This is achieved by applying models of variation based on extant ape species as models to estimate variation (see Ackermann and Cheverud, 2000, 2002; Harvati, 2003 and various others). This thesis will also attempt to determine the roles of adaptive and non-adaptive processes in shaping the morphology and evolution of the genus *Paranthropus* using a methodological approach adopted from previous studies (Ackermann, 1998; Ackermann and Cheverud, 2002, 2004; Schroeder, 2007, 2014, 2015). The remaining chapters of this thesis, which are summarized below, provide the background information relevant to achieving these overall objectives.

CHAPTER 2 (Background) will provide information about the genus *Paranthropus* that is critical for framing the research objectives of this research (Ackerman and Cheverud, 2002; 2004; Schroeder, 2007; 2015; Wood and Schroer, 2017). Particular attention will be paid to the morphological features that define the genus and each of the three species and how morphological, temporal, and geographic information has been used to make inferences about the evolutionary relationships among these species (Constantino and Wood, 2007).

Since previous attempts to understand the craniodental morphology of *Paranthropus* have largely hinged on ideas about dietary adaptations and feeding mechanics, this chapter also summarizes research that has offered evidence about the diet of these species (Lucas et al., 2013; Ungar and Sponheimer, 2011). This chapter outlines previous work that has examined the role of non-adaptive processes in driving craniodental diversity and evolution in primates. Lastly, **Chapter 2** introduces the specific research objectives and questions that are addressed in this thesis.

CHAPTER 3 (**Materials)** will introduce the samples used in this study; *Paranthropus* as well as a comparative sample of *Australopithecus africanus* specimens. This includes a description of the fossil specimens assigned to the genus. These descriptions include information on the fossil localities and specific details about fossil specimens that were used in this study. This chapter also provides detail about the comparative sample of extant apes, which includes samples of *Gorilla gorilla*, *Pan troglodytes* and *Homo sapiens*.

CHAPTER 4 (**Methods**) will provide specific details about the methods that were used to address the research objectives and questions. The descriptions of the methods include both those that were used to collect the data and the statistical methods that were used to analyze the data. Data collection methods included collecting landmark data and calculating inter-landmark distances. Statistical methods included the use of Mahalanobis' distance statistic and geometric morphometrics. A hypothesis testing framework tested for adaptive morphology against the null hypothesis of random change, where drift was rejected selection required to produce change was reconstructed.

CHAPTER 5 (**Results**) presents the results of the thesis. Taken together, these results indicate that within-group craniofacial and between-group craniofacial variation in both East and South African specimens is significant. The results also highlight the relatively large degree of intra-specific variation in *P. robustus.* Lastly, the findings show that the null hypothesis of genetic drift cannot be rejected for the majority of the regions that were analyzed. However, selection was indicated for some regions, including some (but not all) regions related to the masticatory apparatus.

Finally, **CHAPTER 6** provides a brief Discussion/Conclusion, addressing the main findings and future research. The main findings of the results indicated that variation within and between groups of the genus *Paranthropus* was significant. Evolutionary relationships among and across the species have proven to be much more complex in the context of their variation and moreover "adaptations". This evidence changes the approach and understanding of which "morphological features" in *Paranthropus' "*uniquely" designed characteristics are distinguished by adaptive and non- adaptive forces.

CHAPTER 2

BACKGROUND

Introduction

The genus *Paranthropus* was first discovered in Kromdraai B, South Africa by Robert Broom in 1938, attributed to the holotype TM 1517, along with species *Paranthropus crassidens* from neighboring sites such as Swartkrans (Broom, 1938a, 1938b, 1950:, Wood 1988), later renamed *Paranthropus Paranthropus robustus* and finally *Paranthropus robustus* (Broom, 1938b; Cofran and Thackeray, 2010; Constantino and Wood, 2004; Wood, 1988; Wood and Schroer, 2017). Since their discovery both Kromdraai and the neighboring site of Swartkrans have contributed immensely to the *P. robustus* hypodigm (Cazenave et al., 2017; Cofran and Thackeray. 2010). In addition, not only have thousands of fossils been retrieved from the site but there is still contention on whether these sites gave rise to one single species (*P. robustus*) or two separate species (*P. robustus* and *P. crassidens*); however, researchers have reached a general consensus for the name *P. robustus* for both sites and sites in South Africa (Cofran and Thackeray, 2009).

Subsequently, "*Zinj*" was uncovered in East Africa, and ultimately placed in the taxon *Paranthropus boisei* (Constantino and Wood, 2004; Leakey, 1959; Walker and Leakey, 1988). The third species of *Paranthropus*, *Paranthropus aethiopicus*, was named with the discovery of the "Black skull", discovered by Arambourg and Yves in 1967 (Wood, 2010). Since the discoveries of each species, the cranial and dental morphology of *Paranthropus* has been described, discussed and debated. Several researchers (e.g. Kimbel, 2006; McCollum, 1999; Wood, 2010; Rak, 1983) have described the morphology of the face in *Paranthropus*; these descriptions include characterizations of the cranial and dental features of the genus, with a focus on the adaptations that make this masticatory complex unique. Relatively less work has focused on intra-specific variation of the face and mandible.

The phylogenetic relationships among these three species and between them and other hominins have been debated since the earliest discoveries. Some researchers consider the species

members of a monophyletic group, with all *Paranthropus* species being more closely related to each other than to other species, while others consider *Paranthropus* paraphyletic, with other non-paranthropine taxa more closely related to various species within the genus (Kimbel, 2006). In particular, researchers have argued that *P. aethiopicus* retains more primitive characteristics similar to and shared with *Australopithecus afarensis* (Kimbel and White, 1988; Suwa, 1988; Wood, 2010). It has also been argued that *P. robustus* shares characteristics with *A. africanus* (Vrba, 1988, Wood, 1988; Wood and Schroer, 2017).

Much of the phylogenetic debate (and research more generally) has revolved around the shared adaptations of these "robust" australopiths (Brain, 1967; Conroy and Pontzer, 2012; Rak, 1988) linked to a diet of hard and/or tough foods, including their large posterior dentition, "hyper-thick" enamel, thick robust jaws and flared zygomatic arches (Kimbel, 2006; Lee-Thorp, 2011; Wood, 2010). Indeed, the genus *Paranthropus* is generally characterized by a shared dietary adaptation resulting in the robust "hyper megadont" morphology (Kimbel, 2006; Wood and Schroer, 2017). Recent research on craniodental morphology, macrowear and microwear, isotopes, and biomechanics, however, has suggested that substantial variation exists within *Paranthropus*, both in terms of the ecological niches occupied by the species and the amount of hard and complacent foods that were consumed (Lucas et al., 2013; Martinez et al, 2016; Sponheimer et al., 2013; Ungar et al., 2008).

Although fossil remains are abundant, they mostly consist of teeth (best preserved) and cranial and mandibular elements (Kimbel, 2006). The small sample of post cranial remains (e.g. *P.robustus* at sites such as Kromdraai and Swartkrans; Susman, 1988) has made it challenging for researchers to establish sexual dimorphism (and body size generally) within the genus (Cazenave et al., 2017; Wood and Boyle, 2016; Wood and Schroer, 2017). However, Conroy and Pontzer (2012) have suggested that the high variation in craniodental elements may indicate high levels of sexual dimorphism in *P. boisei*. Patterns of sexual dimorphism have provided some indications of social structure and other behaviors in *Paranthropus* (Lockwood et al. 2007; Lockwood, 1999)

This chapter will provide background to all of the topics mentioned above, including a description of *Paranthropus* morphology (generally and for each species), their geographical and temporal context, and proposed phylogenetic relationships. Diet and dimorphism in this genus will also be considered. This chapter will also briefly outline the adaptive hypothesis that has

been proposed to explain paranthropine craniodental morphology and will provide context for testing hypotheses of drift versus selection, in order to understand drivers of paranthropine diversity. Finally, I will present the hypotheses to be tested in this research.

Paranthropus

The genus *Paranthropus* is made up of three morphologically similar species: *P. aethiopicus* and *P. boisei* from East Africa, and *P. robustus* from South Africa –**Figure 2.1**- (McCollum, 1999: Wood and Schroer, 2017). The first specimens of *Paranthropus* – *P. robustus* – were recovered at Kromdraai B in South Africa in 1938, just over a decade after the discovery of *Australopithecus africanus* (Broom, 1938b, 1950; Kimbel, 2006). Since then more than 200 *Paranthropus* fossil specimens have been found in South African sites such as Gondolin, Drimolen, Swartkrans and Coopers cave (Kimbel, 2006; Wood, 2010). Specimens include crania, post crania and teeth fragments (Kimbel, 2006; Wood, 2010). Over the decades other *Paranthropus* specimens have also been discovered throughout East Africa – in Kenya, Ethiopia, Malawi and Tanzania – from the taxon *P. boisei* (previously known as "*Zinjanthropus boisei*") (Constantino and Wood, 2004; Wood, 2010; Wood and Schroer, 2017) and subsequently *P. aethiopicus* (Kimbel, 2006; Walker and Leakey, 1988). Although the dates of the three species differ (Conroy and Pontzer, 2012; Kimbel, 2006; Wood, 2010), as a group the genus *Paranthropus* dates to between 2.7-1.0 Ma (Constantino and Wood, 2004; Wood and Boyle, 2016; Wood and Schroer, 2017).

As a collective this genus is highly distinctive from other hominin species by its suite of morphological characteristics. All three species exhibit similar craniodental features such as a robust thick mandible, small anterior dentition (lateral incisors are larger than central incisors) and large postcanine dentition with thick enamel whereby the premolars and molars are "molarized" (Clement and Hillson, 2013; Grine et al., 2012; Rak, 1983). The small nature of the canine and incisors create a narrow anterior tooth row. In addition, the crania display severe postorbital constriction with flaring and anteriorly positioned zygomatic arches, creating a flat

broad dish-shaped face (Broom, 1938b; Leakey and Walker, 1988; Rak, 1983). The robust nature of the mandible and cranium of *Paranthropus* has led many researchers to posit that all the species in this genus shared a diet of hard foods in open grasslands (Rabenold and Pearson, 2011). New research using macrowear, microwear, stable isotopes and biomechanics show that this genus ate a combination of C^3/C^4 foods and that tough fibrous and abrasive foods were fallback foods which broadens their ecological niche (Cerling et al., 2011; Williams, 2015). Martinez (2016) conducted a study which revealed that perhaps these abrasive foods were strictly a fallback food and they required robust teeth and jaws as a "precaution" (Rabenold Pearson, 2011; Ungar and Sponheimer, 2011).

Despite an abundance of craniodental remains, the fossil record of *Paranthropus* is represented by few postcranial remains. *P. robustus* has definitively been associated with postcranial remains (Susman, 1988; Wood, 2010) while the two East African species have not been found in clear association with post cranial evidence (Constantino and Wood, 2007; Kimbel, 2006), though there are a few specimens from Laetoli and Olduvai Gorge that may be attributable to *P. aethiopicus* and *P. boisei*, respectively (see below). However, even with limited post cranial remains, researchers have concluded with the help of cranial evidence (i.e. anteriorly positioned foramen magnum) that this hominin was bipedal (Broom, 1938b; Kimbel, 2006; Tobias, 1988; Wood, 2010; Williams, 2015). Given the nature of the remains, this study will focus on the craniofacial and mandibular remains of *Paranthropus*.

All these shared derived features distinguish *Paranthropus* from other genera, however there are clear inter-specific differences across the genus (Kimbel and White, 1988; Wood and Lieberman, 2001). These differences will be outlined in the following sections.

P. aethiopicus

The "Black Skull" was discovered in 1985 by Alan Walker, and placed in a new species, *P. aethiopicus* (Walker et al., 1986; Walker and Leakey, 1988). This species has the smallest sample size within the genus and includes a well-preserved cranium from West Turkana (KNM-

WT 17000), and mandible (e.g. KNM-WT 16005) and isolated teeth from the Shungura Formation (Kimbel, 2006; Leakey and Walker, 1988). Additionally, in recent years researchers have assigned a proximal tibia and juvenile cranium (L. 338y-6) to the hypodigm (Wood, 2010; Wood and Boyle, 2016; Wood and Schroer, 2017). This species dates to roughly 2.7-2.3 Ma (Kimbel, 2006; Wood, 2010). The current sample was recovered from sites in Tanzania (i.e., Laetoli), Kenya (i.e., West Turkana) and Ethiopia (Omo River basin-Shungura Formations) (Walker et al., 1986; White, 1988; Wood and Boyle, 2016).

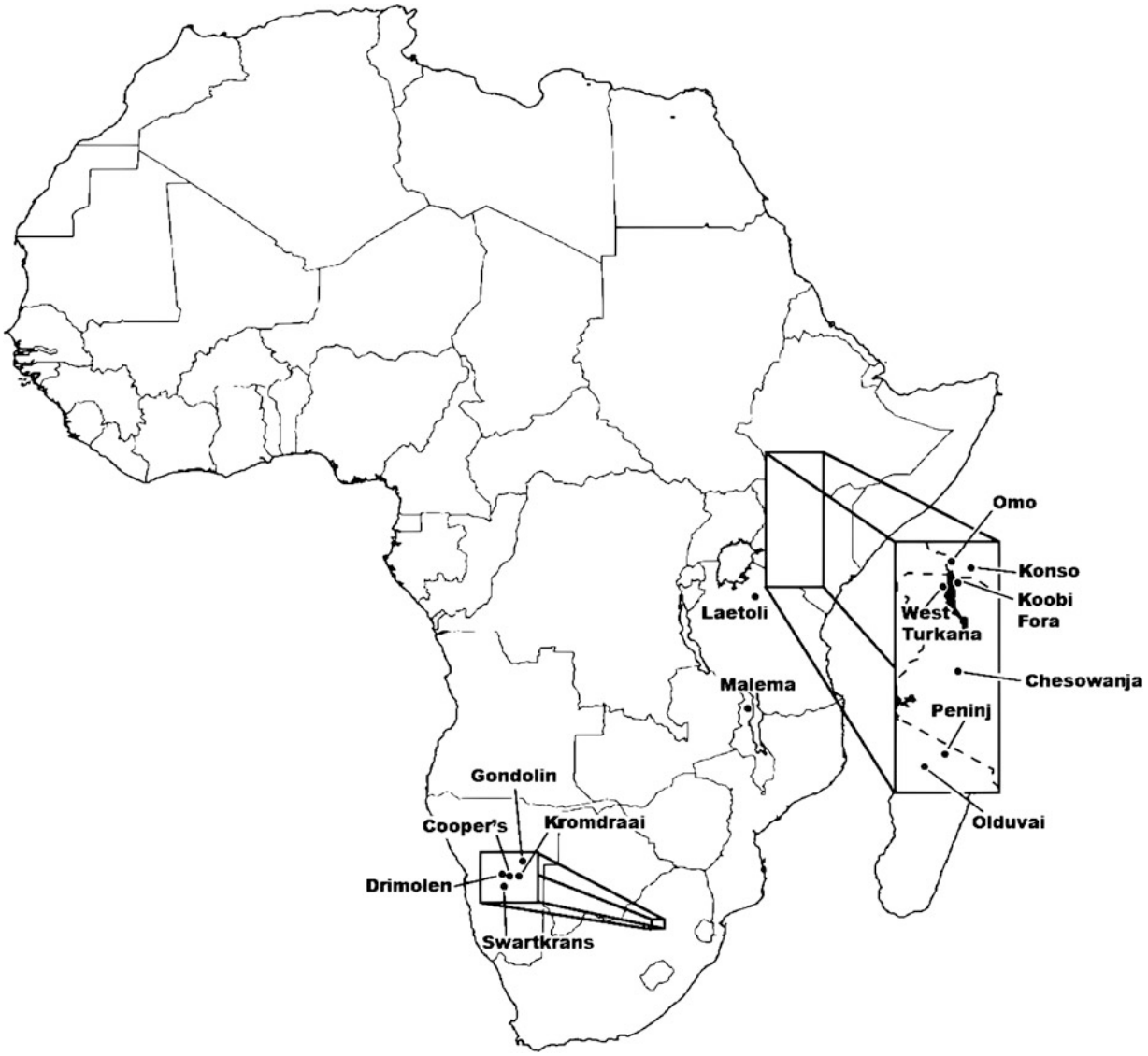

Figure 2.1. Map of East and South African discovery sites of the genus *Paranthropus* (Wood and Schroer, 2017).

Variation within this taxon is poorly understood because it is represented by such a small sample. However, the available material indicates that this species possesses a mosaic of features including those that are shared with other *Australopithecu*s species (which are considered more primitive), derived features that are shared with other species in the genus and features that are solely distinct to this species alone (Kimbel, 2006, Wood, 2010). Those features that are shared with species in the *Australopithecus* genus include a short midface, prognathic subnasal region and increased "zygomaticomaxillary" area (Walker et al., 1986). Features that are more derived and shared with the other *Paranthropus* species consist of a low braincase relative to the face, anteriorly placed large zygomatic bones, robust zygomatic arches including a high height of origin of the masseter muscle and broad nasals above the frontonasal suture (Walker et al., 1986; Rak, 1983). Like the other species within the genus *Paranthropus, P. aethiopicus* exhibits premolar and molar expansion together with molarization in the postcanine dentition (Kimbel, 2006; Walker et al., 1986; Wood and Schroer, 2017).

Among the features that are distinct to *P. aethiopicus* solely are a less "flexed" cranial base, the largest sagittal crest witnessed in any hominid species and a heart shaped foramen magnum (Clarke, 1988; Tobias, 1988; Wood and Schroer, 2017). The anterior teeth (primarily the incisors) are larger than both *P. boisei* and *P. robustus* with canines that are blunter than the latter species as well as a posterior dentition that is relatively smaller (Wood, 2010; Wood and Schroer, 2017). This species exhibits a less pronounced glabella (yet still pronounced in general) and supraorbital region with a lower forehead relative to *P. robustus* and *P. boisei* (Walker et al., 1986).

.*P. boisei*

Once known as "*Zinjanthropus boisei*" this taxon was first discovered in 1959 by Mary Leakey (Hay, 1990; Leakey, 1959; Wood and Harrison, 2011). It dates to approximately 2.4-1.4 Ma (Kimbel, 2006). This species has been discovered at sites throughout East Africa: Tanzania (i.e., Olduvai Gorge and Peninj), Kenya (i.e., Koobi Fora, West Turkana and Chesowanja), Ethiopia (i.e., Konso and Omo River basin) and more recently Malawi (i.e., Malema-Chiwondo) (Constantino and Wood, 2007; Kimbel, 2006; Shipman and Harris, 1988). This species is thought to have lived in proximity to water sourced woodlands and/or wetlands (Macho, 2014).

P. boisei has the most abundant number of specimens attributed to it of all the paranthropine taxa, including isolated teeth, mandibles and crania which are also rather well preserved (Constantino and Wood, 2007; Kimbel, 2006). However, no post crania have been assigned to this species yet (Vrba, 1988; Wood and Boyle, 2016).

Many researchers have termed this species as "hyper-robust" because of its exaggerated suite of features that are shared with and more derived than *P. aethiopicus* and *P. robustus* (Rak, 1988; Smith et al., 2015). These features include a bulkier face with a protruding and pronounced supraorbital torus and extreme post orbital constriction (Wood, 2010; Rak, 1983). Derived features also include an infraorbital "visor" with a nonexistent anterior pillar (Kimbel et al., 1988; Rak, 1983). This species displays a flat and wide face which is in both respects larger and broader than the southern African taxon (Kimbel, 2006; Wood and Boyle, 2016). *P. boisei* anterior dentition is smaller in comparison to the other paranthropine species in addition to a P4 talonid expansion and "hyper-thick" enamel (Dean, 1988; Suwa, 1988). To accommodate the large postcanine dentition, both the mandibular corpus and ramus are thick, and robust (Cerling et al., 2011; Wood and Harrison, 2011).

P. robustus

P. robustus dates to approximately 2.0-1.0 Ma (Constantino and Wood, 2004; Wood and Boyle, 2016; Wood and Schroer, 2017). Historically, it is the first taxon discovered in the genus and the only species of *Paranthropus* discovered in South Africa (Kimbel, 2006). The first

specimen, discovered by Broom (1938a,b; 1950) in Kromdraai, was followed by many more discoveries of this fossil hominin species throughout South Africa at sites such as Sterkfontein, Gondolin, Drimolen, Coopers Cave and Swartkrans (Ackermann, 1998; Brain, 1967; Keyser, 2000; Keyser et al., 2000; Menter et al., 1999).

The *P. robustus* hypodigm consists of a wide collection of fossil specimens consisting of crania, post crania, mandibles and isolated teeth (Brain, 1967; 1988; Susman, 1988). However, samples are often not well preserved, distorted and disintegrated as they were retrieved from quarry's and breccia with the use of explosives (Broom, 1950).

P. robustus features are neither as "hyper-robust" as *P. boisei* or as primitive as *P. aethiopicus,* but have been described as less derived more "general" features that are shared with both East African species (Rak, 1983; Walker and Leakey, 1988). Features possessed by *P. robustus* that are shared characteristics with both East African species – i.e. features that are less derived relative to *P. boisei* - include small anterior dentition with large posterior dentition where the M1 has an oval form (Walker et al., 1986). The premolars are "molarized" with thick dental enamel in conjunction with thick robust mandibular corpi and tall rami (Kimbel, 2006). Moreover, the cranium exhibits large robust zygomatic arches, relatively high masseter origin, a low cranial base relative to the calvarium, including infraorbital foramina that are situated high in the maxillary region (Kimbel, 2006; Walker et al., 1986).

Phylogenetic Relationships

Since the discovery of *Paranthropus* in 1938 (Broom, 1938a, b; Wood and Schroer, 2017), the taxonomy and phylogenetic relationships of these fossils has been a topic of debate (Kimbel et al., 1988). Early on, Robinson (1954), in an attempt to classify *P. robustus* (Wood, 1988), experienced back lash from researchers about the taxonomic diversity of this species - i.e., whether to treat the species as *Australopithecus* or *Paranthropus* (or both) and whether these two genera should be treated as separate and distinct or merely one in the same (Constantino and Wood, 2007;; Wood and Schroer, 2017).

Over the years researchers have generally come to a consensus that all the species within *Paranthropus* are separate distinct species (Constantino and Wood, 2007; Grine, 1988; McCollum, 1999). However, some authors (Conroy and Pontzer, 2012) continue to group *P. aethiopicus* and *P. boisei* (and sometimes refer to them as *Australopithecus* rather than *Paranthropus*) as one species - i.e. *Paranthropus boisei sensu lato* (Wood and Schroer, 2017).

The distinctiveness of *P. boisei* and *P. robustus* has been fairly well determined (Wood, 1988; Wood and Strait, 2004); what is at issue is the distinctiveness of the earlier East African species. However, Kimbel (2006), among other researchers (Kimbel et al., 1988; Walker and Leakey, 1988), have consistently (and convincingly) argued that *P. aethiopicus* is its own separate species, with craniodental evidence for this such as smaller anterior dentition with larger incisors and more facial prognathism (Dean, 1988; Kimbel and White, 1988; Wood and Boyle, 2016). Chronologically, *P. aethiopicus* is also older, and does not share the derived features *P. boisei* and *P. robustus* have in common (Strait et al., 1997).

Although the distinctiveness of the three taxa is largely accepted, considerably more disagreement exists between researchers around the relationships between these three taxa, and between them and other australopiths, including whether species within the genus should be considered monophyletic or paraphyletic. If they are monophyletic (i.e., all these species have a common ancestor and represent all its descendants), this indicates that they are more closely related to each other than any other species (Hlazo, 2015; Grine, 1998; Strait et al., 1997). In other words, species within the genus *Paranthropus* share one common ancestor and *P. aethiopicus, P. boisei* and *P. robustus* are more closely related to each other than any of the other hominin taxa (Kimbel, 2006). This interpretation is based on evidence of shared derived characteristics that define "robust" australopiths through their craniofacial morphology.

Alternatively, if these taxa are paraphyletic (i.e. one common ancestor but all ancestor's descendants are not included in the group), species within the group are closer in ancestry to other species outside the genus than to each other (Skelton and McHenry, 1992). Examples of paraphyletic interpretations include morphological evidence linking *A. afarensis* and *P. aethiopicus,* who share "primitive" features, as well as craniodental evidence (e.g. anterior pillars) linking *A. africanus* and *P. robustus* (Clarke, 1988; Kimbel and White, 1988; Lockwood, 1999; Wood and Schroer, 2017). However, Wood and Harrison (2011) caution that because

species share skeletal features, it may not necessarily indicate a "shared recent evolutionary history", (Wood and Harrison, 2011:347) genetic relationship or otherwise. The genus name *Paranthropus* should hold if these species fall under a monophyletic group, however if they do not then *Australopithecus* is a perfect umbrella term (Constantino and Wood, 2004, 2007; Wood, 2010).

Homoplasy – characteristics that are shared (due to shared function/adaptations) but not present in the most recent common ancestor – has also played a significant role when it comes to interpreting data and determining phylogenetic relationships, as it can bias these interpretations, especially when considering species relationships within the genus *Paranthropus* based on their "robust" morphology (Wood, 1988, 2010). In his review, Wood (1988) outlines how tempting the notion of paraphyly is to many researchers considering the contribution homoplasy has on skeletal features (Skelton and McHenry, 1992). Fossil data uses hard skeletal tissue which is highly prone to homoplasy and can skew data (Skelton and McHenry, 1992; Wood and Harrison, 2011).

To get at the root of these issues, in the past three decades researchers such as Wood (1988) and Strait et al. (1997) have carried out cladistics studies analyzing morphological (character) states that compare different (australopith/paranthropine) species. The analyses have shown that the "robust" australopiths form their own monophyletic clade (Strait et al., 1992; Wood, 1988). *A. afarensis* was categorized as a sister taxon to the paranthropine (monophyletic clade) species –and *A. africanus* (Strait et al., 1997; Wood, 1988). Resulting cladograms grouped *Paranthropus* into a monophyletic clade even when character states were removed from the analysis (Grine, 1988). Character states such as masticatory morphology may introduce bias through homoplasy (Skelton et al., 1986: Skelton and McHenry, 1992; Wood, 1988; Wood and Harrison, 2011).

After all the debates throughout the decades, most scientists support the general notion of monophyly among the species (and the name *Paranthropus)* (Grine, 1988; Strait et al., 1997; Ward, 1991; Wood, 1988). There are however, scholars in the community who believe that species within *Paranthropus* form a paraphyletic group (Skelton and McHenry, 1992; Skelton et al., 1986). In their study Skelton and McHenry (1992) investigated traits according to region and

function. Their results showed that *A. aethiopicus* was rather a sister taxon to *P. robustus*, *P. boisei* and the likes of *A. africanus* and *Homo* forming its own separate lineage (Skelton and McHenry, 1992; Skelton et al., 1986). The authors follow up study (Skelton and McHenry, 1998) used a similar methodology as Strait et al. 1997 by omitting character states. The authors maintain their conclusion for *A. aethiopicus* as a sister taxon to other hominin species, i.e. *P. boisei, P. robustus* and *A. africanus*.

Diet

Since the first discoveries, researchers have speculated that the uniquely derived dental and craniofacial characteristics of *Paranthropus* – robust crania with a pronounced sagittal crest, large thick mandible and megadont or "hyper" megadont posterior dentition – indicate that this genus is characterized by a diet of tough, fibrous and abrasive foods that consisted of hard objects (seeds and nuts), and occupies savanna biomes (Clement and Hillson, 2013; Daegling et al., 2011; Macho, 2014). Most of this speculation contextualizes this morphology firmly within an adaptive framework postulating that the unique *Paranthropus* morphology is a direct result of selection acting on it (see Ackermann and Cheverud, 2004). This has led researchers to try and reconstruct diet and paleohabitats occupied by the species within this genus. Countless studies conducted in recent years such as macrowear, microwear, isotopes and biomechanics show that *Paranthropus* diet and ecological niche is quite broad. Researchers have deliberated diet and ecological niches but have not reached a general consensus.

Macrowear studies investigate wear patterns on teeth to evaluate diet, taking into consideration contact between teeth and foods that are consumed that result in "abrasion- loss of volume" (Lucas et al., 2013; Wood, 2013:2). There are two types of wear: occlusal (due to grinding of upper and lower teeth) and approximal (wear between adjacent teeth in the same tooth row) (Clement and Hillson, 2013). Microwear texture analyses look at pits on the surface to determine whether a diet consists of crushing nuts or hard foods, and at scratches ("striations")

to determine whether a diet consists of leaves, grasses and sedges (Kay and Grine, 1988; Ungar and Sponheimer, 2011). However, microwear studies can only infer direct consumption activities of individuals leading up to their last weeks, not their entire lifespan (Grine et al., 2012; Lucas et al., 2013). Isotopic studies (isotopes in organic material consumed, then mineralized in dental enamel and bone) inform researchers about C^4/C^3 photosynthetic pathways which infer diet and possible habitats occupied by hominin species (Sponheimer et al., 2005; Ungar and Sponheimer, 2011). More recently, biomechanical studies investigating movement in the cranium, particularly areas involved in mastication, can reveal patterns in diet (Macho, 2014).

Specialized craniodental features in *Paranthropus* such as large "hyper" thick enameled postcanine dentition, together with earlier macrowear studies, have led researchers to conclude that this genus consumed tough, hard foods and had a specialized diet (Ungar et al., 2008).

However, recent studies using microwear (Lucas et al., 2013) and isotopes (Cerling et al., 2011) proposed that species within the genus may have had a more generalized diet (Sponheimer et al., 2005; 2013). If resources were not available they integrated hard and complacent foods as seasonal or rather "fallback" foods (Lee-Thorp et al., 2010; Martinez et al., 2016)

Recent microwear studies using complexity (roughness) and anisotropy (toughness and degree to which striations are aligned) analyses (Sponheimer et al., 2013; Ungar and Sponheimer, 2011) showed that East African species have a low complexity and low anisotropy (degree to which striations are unaligned or heavy pitting) similar to *Homo* (Martinez et al., 2016). These data revealed that there was no evidence of abrasive hard object feeding (Cerling et al., 2011; Martinez et al., 2016). The same data demonstrated that *P. robustus* had high complexity and low anisotropy (no heavy striations) combining hard foods/fruits and grasses (Daegling et al., 2011; Sponheimer et al., 2005; Ungar and Sponheimer, 2011). Martinez (2016) conducted a study that revealed that abrasive tough foods were "fallback" foods and were sought after seasonal changes or when normal resources were not available (Grine et al., 2012; Williams, 2015). Moreover, foods that were consumed were not so tough and abrasive at all (specialist feeder) but more general and soft (Daegling et al., 2011; Macho, 2014; Martinez et al., 2016; Ungar and Sponheimer, 2011).

Researchers using carbon isotopes have shown that diet in *Homo* (as well as gracile australopiths) leans toward "C^3" shrubs and plants while the "robust" clade consumed more "C^4/CAM" low quality grasses and sedges (Cerling et al., 2011; Lee-Thorp, 2011). The notion behind stable carbon isotopic studies stems from C^4 plants absorbing more ^{13}C isotopes into their cellular walls than C^3 plants do leaving "signatures" (Sponheimer et al., 2013). As such the dietary signature consumed from the plant or the animal that has consumed the plant will show in the organism, unfortunately there is no way to distinguish between these two possibilities (Sponheimer et al., 2013). In their study Sponheimer et al. (2013) use carbon signatures to evaluate consumption of foods showing that *P. boisei* and *P. robustus* had a significantly different diet (Lucas et al., 2013; Sponheimer et al., 2005; Vrba, 1988). The diet of *P. boisei* is thought to have comprised of majority C^4 foods while *P. robustus* combined both C^3 and C^4/CAM foods (Cerling et al., 2011; Smith et al., 2015; Sponheimer et al., 2005, 2013; Williams, 2015). Although these two species share similar morphological features (Walker et al., 1986; Wood, 2010), research shows that there is evidence of variation in the diet and habitats these species occupied (Kay and Grine, 1988).

According to many researchers, grasses and sedges make up approximately 70%- 80% of the diet (Cerling et al., 2011; Martinez et al., 2016; Sponheimer et al., 2013). Macho (2014) uses a baboon (*Papio*) model to describe how ill-efficient *P. boisei* morphology would be to "laterally directed loads of shearing tough foods" compared to the beneficial vertically directed motion (Macho, 2014:2; Smith et al., 2015). Although this species has thick enamel – perhaps an adaptation to foods rich in abrasive silica phytoliths (Daegling et al., 2011; Lucas et al., 2013) – thick enamel does not equate sufficient enamel prism decussation (Dean, 1988). Prism decussation prevents the enamel from cracking by strengthening the structural components (Macho, 2014). This study concludes that 80% of C^4 grasses is a gross overestimation, and approximates 30%, especially considering corms into the diet. With that said, other than brittle hard foods, C^4 foods can also consist of invertebrates, flowers, fruits and corms (Macho 2014; Martinez et al., 2016; Sponheimer et al., 2013).

Specialized morphology may have very well come into play for *P. robustus* (hard shelled invertebrates, termites and very little leaves) and *P. boisei* for chewing repetitive loads (Cerling et al., 2011; Daegling et al., 2013; Smith et al., 2015; Williams, 2015). However, new evidence

supports that not only was *Paranthropus* (especially *P. robustus* exhibiting a C^3 and C^4 diet) a generalized mixed feeder but for *P. boisei*, tough or hard foods may not have played such a big role in the diet (Clement and Hillson, 2013). These studies suggest that the genus occupied diverse ecological niches. Based on these finding *P. robustus* is thought to have occupied a vast ecological niche because of its mixed C^3/C^4 diet, whereas *P. boisei* is suggested to not only have inhabited closed water sourced woodlands and wetlands but also open savannas based on their C^4/CAM diet (Clement and Hillson, 2013; Cerling et al., 2011; Lucas et al., 2013; Shipman and Harris, 1988; Williams, 2015).

Despite all the new evidence that informs us of the diet and paleohabitat of *Paranthropus* species, there is still no hard evidence as to the exact type of foods the species consumed and what ecological niches they occupied. Nevertheless, these studies do indicate that regardless of the shared robust morphology seen among the species, variation in the diet is significantly large across the genus, suggesting that these taxa were adapted in similar ways to different

dietary/ecological contexts. More so, this evidence further suggests that selection (adaptive forces) may not be the result of a tough hard diet.

Sexual Dimorphism

Gorilla gorilla and *Pan troglodytes* exhibit higher degrees of skeletal sexual dimorphism relative to modern humans (Lockwood, 1999; McHenry, 1988; Plavcan, 2001), and are often used as models for considering early hominin dimorphism. Sexual dimorphism in these apes allow researchers to differentiate the sex of individuals readily through differences in body size/shape, canine size and sharpness and cranial size and robusticity (Ahern et al., 2005). Unfortunately, for *Paranthropus* postcranial material is limited, and the genus does not exhibit large/sharp canines, making the process of distinguishing the sexes more difficult (Ahern et al., 2005; Lockwood et al., 2007; Plavcan, 2001; Williams, 2015). Distinguishing sexes allows for researchers to infer social, behavioral and equally important cultural aspects of fossil hominins.

Nevertheless, researchers have discovered individuals (based largely on cranial data) that are both small and large sized with distinctive morphological features (Leakey, 1976; Dean,

1988; Rak, 1988). This has prompted scientists to identify male and female individuals primarily in *P. boisei* and *P. robustus. P. boisei* has the most abundant collection of fossil specimens among the two taxa that have allowed researchers to distinguish between size/sex in fossil specimens (Kimbel, 2006; Wood, 2010). *P. boisei* is thought to have a higher degree of sexual dimorphism relative to *P. robustus,* based primarily on fossil evidence of crania (Jungers, 1988; Plavcan, 2001); this is despite the lack of sexual dimorphism found in canine morphology (Kimbel and White, 1988; Walker and Leakey, 1988; Wood, 2010).

Degree of sexual dimorphism is often used to infer social structure in primates. However, researchers such as Lockwood et al. (2007) note the difficulties of inferring social structure and behavior through sexual dimorphism without prevalent distinguishing morphological characteristics (Lockwood, 1999). Through morphological evidence, DNH 7 is a presumed female and DNH 8 male, authors concluded that there is a distinguishable level of sexual dimorphism that exists within *P. robustus* hominin species (Keyser, 2000; Lockwood et al., 2007), however neither degree nor pattern of sexual dimorphism is similar in any species (Lockwood, 1999). In short, given the morphological evidence and size differences found in each species, *Paranthropus* shows significant variability not only in size but in varying degrees of sexual dimorphism particularly with new evidence from Drimolen attributed to *P. robustus*.

Evolutionary processes shaping paranthropine diversity

The emergence and diversification of the hominin lineage has largely been framed as resulting from adaptation with little consideration of contributions from random divergence, with natural selection acting on the phenotype in tune with changes in climate and environmental conditions. Ackermann and Cheverud (2002, 2004) proposed that perhaps diversity in hominin evolution was not only driven by non-random forces but also neutral – random – evolution acting on morphological features (see also Schroeder, 2015; Schroeder et al., 2014; Weaver et al., 2007), including in the genus *Paranthropus*. In this scenario divergence between taxa is brought about by a combination of forces: genetic drift, mutations, gene flow and natural selection (Kimura, 1968, 1991). These forces work together to create change at a molecular and phenotypic level (Kimura, 1955a, b, 1968, 1991).

Kimura (1968, 1991) outlines how random changes in allele frequency and/or random mutations occurring at different loci elicit evolutionary change. This theory has allowed researchers to use genetic drift as a null hypothesis, natural selection as an alternative hypothesis, when examining evolutionary change in a way that is statistically testable and allows for predictions (Lande, 1977,1979) in different populations at a molecular level (Kimura, 1991) and phenotypic level (Ackermann and Cheverud, 2004; Lofsvold, 1988; Marriog and Cheverud, 2004; Roseman, 2004; Schroeder et al., 2014; Weaver et al., 2007). If the null hypothesis of drift is rejected then adaptive non-random forces may contribute to evolutionary change (Ackermann and Cheverud, 2002). However, if the null hypothesis is not rejected, it gives an indication that perhaps these neutral forces contribute to evolutionary changes (Ackermann and Cheverud, 2004).

This neutral theory of evolution has been used successfully to investigate evolutionary changes in different hominin lineages (Ackermann and Cheverud, 2004; Roseman, 2004, Schroeder et al., 2014; Schroeder and Ackermann 2017; Weaver et al., 2007). This approach has also provided a means to understand and characterize the action and effects of selection, when it is shown to play a role in diversification (e.g. Ackermann and Cheverud 2004; Schroeder and Ackermann 2017).

In the case of *Paranthropus*, hypotheses for diversification both of this genus from other genera, and the species from each other, have largely been couched in adaptive assumptions. The "megadont" *Paranthropus* taxa are defined by: large "molarized", "hyper-thick" and expansive posterior dentition, small anterior dentition (Kimbel, 2006; Lee-Thorp, 2011; Wood, 2010), a large thick mandible in combination with a flat, broad dished shape induced by anteriorly placed flaring zygomatic arches (Broom, 1938b; Leakey and Walker, 1988; McCollum, 1999; Rak, 1983). These features have collectively been considered adaptations for a specialized diet of tough and hard abrasive foods and occupation of a specific ecological niche. In other words, they result from natural selection acting to shape morphology, and drive morphological divergence.

However, there have been some recent indications that the different taxa within *Paranthropus* are eating different things and possibly living in different environments (Martinez et al., 2016; Sponheimer et al., 2005; 2013; see also discussion above). This suggests that they

are under different selective pressures, but nevertheless maintain similar morphology. What is not clear is the role that drift might play in determining these morphologies. This study aims to understand the drivers of morphological differentiation in the genus, both in terms of the role that drift has played as well as the potentially different ways in which selection has acted on the three taxa.

Objectives of this Thesis

Objective 1: To understand and quantify inter-individual variation in *Paranthropus.*

- Question 1a: Are there significant differences in craniodental morphology between East and South African *Paranthropus* specimens for the variables being examined?
- Question 1b: Does intra-specific variation (to the degree that it can be quantified) in East and South African paranthropine species differ?
- Question 1c: Do DNH 7 and DNH 8 differ significantly from other *P. robustus* specimens?

Objective 2: To understand the effects of extant model choice on interpretations of morphological distance.

- Question 2a: Do different extant species provide different estimates of morphological distance among *Paranthropus* individuals*?*
- Question 2b: Are ape extant models more appropriate models of *Paranthropus* variability than human models (possibly because of different magnitudes/patterns of sexual dimorphism)?

Objective 3: To understand the evolutionary processes underlying diversification in *Paranthropus*.

- Question 3a: Did the diversification of *Paranthropus* species from each other occur through random processes (i.e. drift), or did adaptation play a role?

- Question 3b: If natural selection acted to diversify species within the genus, then which region(s) was selection acting on? Is this consistent with our understanding of morphological/functional differences in these taxa?
- Question 3c: Did the morphological response to selective pressures change in concert with these pressures, or is there evidence of correlated response due to selection on other variables?

CHAPTER 3

METHODS

The *Paranthropus* fossil sample consists primarily of isolated teeth, mandibles and crania (including maxilla) (Kimbel, 2006; Wood, 2010). Craniodental remains allow researchers to study diet, paleohabitats and are also used to form hypotheses on phylogenetic relationships within species of *Paranthropus*, as outlined in the previous chapter. This study concentrates on variation in the face and mandible. Facial and mandibular variation is important for understanding taxonomic diversity, but also provides some of the best sample sizes when comparing across taxa. Here measurements in the face and mandible are used to investigate morphological relationships and understand processes driving taxic diversity across *Paranthropus* using different multivariate statistical methods and models.

Fossil Hominin Sample

The fossil material used in this study comprises cranial and mandibular samples from eastern and southern African collections described in **Table 3.1**. Detailed descriptions of individual specimens and their localities are found in **Table 3.2** and **Table 3.3**. Three-dimensional surface scans were obtained from a previous study (Schroeder, 2015). Three-dimensional surface scans derived from an Artec Spider Scanner which uses fixed position video cameras for specimens DNH 7 and DNH 8 were obtained directly from the University of the Witwatersrand.

All analyses were constructed to maximise sample size and/or region analysed, given the constraints of shared preservation. Several analyses and sub-sets of analyses were created and introduced into the study to obtain the most information possible from individual specimens. A small sample (n=3) of well-preserved australopiths from South Africa was also included as a comparative dataset. *A. africanus* served to further investigate the magnitude and pattern of intra and inter specific variation in the "robust" clade, more specifically *P. robustus* (DNH 7) in

South Africa. Overall, a total of 42 (both mandibular and cranial specimens) fossil specimens were incorporated into this study. 41 of the fossil samples consist of adult and young adult specimens, with Sts 52b also included as a juvenile specimen (Schroeder, 2015).

Comparative Extant Sample

In studies using fossil hominins small sample sizes and lack of preservation are often a concern. The methods used here require large samples (>30) to ensure accuracy of mathematical and statistical analyses, especially when it comes to the estimation and accuracy of variance/covariance. The smaller the sample size the less accurate estimates of variance/covariance become (Ackermann, 2002; 2009). Comparative samples drawn from extant apes and humans are therefore used as analogues/models to estimate intra-specific variation within *Paranthropus* species (see Ackermann, 2002). Three different hominoid species were used in this study to serve as "models" in order to make allowances for all possible effects (e.g. different patterns of covariation) various models could have on the results.

Homo sapiens sapiens

Three-dimensional laser scans were obtained of approximately equal numbers of male and female Bantu-language and Khoesan African individuals. These scans were collected from the Raymond Dart Collection (RDC), housed at the University of the Witwatersrand, Johannesburg and the Iziko Museums of South Africa (SAM) for a previous study (Schroeder 2015). Reabsorption, missing and/or broken elements meant that pertinent information could not be obtained –mostly in regards to teeth and mandibular elements – and therefore supplementary scans were obtained from other sources. The remaining scans (crania n=5; mandibles n=35) were sourced from the Smithsonian Collection and Human Origins Program with females (n= 16) and males (n= 23) that were both Caucasian (n= 17) -due to limited sources of scans- and of African American (n=22) descent from the Terry Collection (Copes, 2012; Copes and 2016) and Duke University, Evolutionary Anthropology in Durham, North Carolina

(mandible n= 1) from the Churchill Human Skeletal Collection (unknown descent). In total, the final dataset comprised of 50 crania and 50 mandibles.

Pan troglodytes

Three-dimensional laser scans of 44 crania and 37 mandibles were obtained from the Hamann-Todd Collection at the Cleveland Museum of Natural History in Cleveland, Ohio. Because of preservation and distortion concerns, and in order to capture as much data as possible, other scans were obtained from: Morphosource.org database, Duke University, Evolutionary Anthropology in Durham, North Carolina (crania = 1; mandible n = 1) and the Museum of Comparative Zoology in Harvard University in Cambridge, Massachusetts (cranium n=1). The remaining scans (crania n= 4; mandible n= 5) were obtained from the Smithsonian Institute (Copes, 2012; Copes and Kimbel 2016). In total the final dataset amounted to 50 crania and 43 mandibles, with approximately equal males and females.

Gorilla gorilla

Three-dimensional laser scans of 50 crania and 49 mandibles were obtained from the Hamann-Todd Collection at the Cleveland Museum of Natural History in Cleveland, Ohio. An additional three-dimensional scan (mandible n=1) was also obtained from the Smithsonian Institute (Copes, 2012; Copes and Kimbel, 2016) in order to have equal numbers of both cranial (n=50) and mandibular (n=50) elements and of female and male specimens.

Table 3.1. List of repositories, repository accession abbreviations and sites for all hominin specimens used in this study.

Repository	Abbreviations	Site Description
The University of the Witwatersrand, Johannesburg, South Africa	DNH	Drimolen
Ditsong National Museum of Natural History, Pretoria, South Africa	SK	Swartkrans pre -1968
	SKW	Swartkrans 1968-1979
	Sts	Sterkfontein pre-1968
The National Museums of Kenya, Nairobi	KNM-ER	Kenya National Museums East Rudolf
	KNM-WT	West Turkana
The National Museum of Tanzania, Dar es Salaam National Museum	OH	Olduvai Hominid

Table 3.2. Fossil crania specimens used in this study.

Species	Specimen	Sample
A. africanus	Sts 5	Cranium
A. africanus	Sts 71	Hemicranium (right side only)
Total	2	
P.aethiopicus	KNM-WT 17000	Cranium
Total	1	
P.boisei	KNM-ER 405	Partial maxilla
	KNM-ER 406	Cranium
	KNM-ER 732	Hemicranium (right side only)
	OH 5 face	Face
Total	4	
P.robustus	DNH 7	Partial cranium
	SK 11	Maxilla
	SK 12	Maxilla
	SK 46	Hemicranium (left side only)
	SK 48	Cranium
	SK 65	Partial maxilla
	SK 79	Cranium
	SK 83	Partial cranium
	SK 845	Maxilla, Basicranium
	SK 1512	Partial maxilla
	SKW 8	Partial maxilla
	SKW 12	Partial maxilla
	SKW 29	Maxilla, Basicranium
Total	13	

Table 3.3. Mandibular fossil specimens used in this study.

Species	Specimen	Sample
A. africanus	Sts 52b	Mandible missing left ramus
Total	1	
P. aethiopicus	KNM-WT 16005	Distorted mandible, partial corpi
Total	1	
P. boisei	KNM-ER 403	Right mandibular corpus
	KNM-ER 404	Right mandibular corpus
	KNM-ER 725	Left mandibular corpus
	KNM-ER 729	Mandible (missing ramus)
	KNM-ER 733	Right mandibular corpus
	KNM-ER 3230	Mandibular corpus
Total	6	
P. robustus	DNH 21	Left mandibular corpus
	DNH 7	Mandible missing rami
	DNH 8	Detached mandibular corpi
	SK 10	Distorted mandible, partial left corpus
	SK 12	Mandible missing right ramus
	SK 23	Mandible
	SK 34	Mandible in two halves
	SK 74a	Partial mandible
	SK 81	Mandible in breccia
	SK 844	Left mandibular corpus and ramus
	SK 858, 861, 883	Mandible missing ramus
	SK 876	Crushed mandible missing rami
	SK 1587	Left mandibular fragment
	SKW 5	Mandible
Total	14	

Fossil Hominin Specimens

The fossil hominin specimens in this study include material from South Africa, Tanzania and Kenya, detailed in **Tables 3.1-3.3**. The geographical distributions and sites of the genus *Paranthropus* were illustrated in the previous chapter (**Figure 2.1**). Below is information on the sites and individual specimens used in this study.

Swartkrans

Swartkrans is a cave comprised of dolomite limestone (Brain, 1988; Lacruz, 2008; Pickering et al., 2011; Robinson, 1956; Schwartz and Tattersall, 2003). It is situated approximately 30-40 km away from Johannesburg, South Africa in a "brecciated cavity-fill" (Schroeder, 2015: 49) located North of the Blaauwbank River (Brain, 1967; Constantino and Wood, 2004; Pickering et al., 2011; Schroeder, 2015; Schwartz and Tattersall, 2003). The first hominids to be excavated at this site were discovered by Broom and Robinson in 1948 (Balter et al., 2008; Brain, 1967, 1988; Broom et al., 1950; Broom and Robinson, 1952; Lacruz, 2008; Robinson, 1956). Robinson sustained excavations until 1953 (Brain, 1988). Excavations were resumed by Brain from 1965-1979 (Brain, 1967; Grine, 1988; Grine and Strait, 1994; Schwartz and Tattersall, 2003). Pickering et al. (2011) state because fossil remains are primarily found in the clastic sediments it has been termed "fossil bearing clastic sediments" otherwise known as breccia (Pickering et al., 2011: 23).

The Swartkrans Formation was originally separated into two members (Butzer, 1976). However, later research at the Swartkrans cave revealed that it is comprised of six distinct units organized into five compartments (Brain, 1988; Pickering et al., 2011; Schroeder, 2015; Schwartz and Tattersall, 2003). According to Schwartz and Tattersall (2003) considerably more *Paranthropus* than *early Homo* individuals are found in Members 1 and 2 (Tobias, 1988). Fossil materials collected from the Swartkrans cave were the first to include both hominid species occurring in one deposit and site (Brain, 1967; 1988; Grine, 1988; Pickering et al., 2011; Lacruz, 2008; White, 1988). As such, hominins can only be found between Members 1-3 (Brain, 1988; Grine, 1988; Lacruz, 2008; Schroeder, 2015).

Member 1 is made up of the Hanging Remnant and Lower Bank (Brain, 1988). Recent research undergone by Pickering et al. (2011) uses Uranium-Lead dating to date the flowstone that caps each Member. Given this new data, Pickering et al., (2011) concludes that Member 1 dates to 2.31-1.64 Ma (Herries and Adams, 2013; Sutton et al., 2009). Member 2 dates to 1.5 Ma (Pickering et al., 2012; Wood, 2011). Member 3 dates from approximately 1.0 Mya to 600 Ka (Sutton, 2013). Wood (2011) dates this Member 4 to less than 100 Ka. The youngest of the members, Member 5 dates to approximately 11 ka (Lacruz, 2008; Sutton et al., 2009; Wood, 2011).

Crania

SK 11 is a partial adult maxilla with both lower and upper body alveolar processes including the presence of the palate and hind teeth (lt: P3-M3; rt: P3-M2) Robinson, 1956). It was discovered in 1949 by Broom and Robinson. This specimen was found in Member 1 dated to 2.31–1.64 Ma (Pickering et al., 2011).

SK 12 is an almost complete maxilla with some dentition preserved (Broom and Robinson, 1956). It was discovered by Robinson in 1949 and found below the Hanging Remnant and Lower Bank of Member 1 (Pickering et al., 2011) dating from 2.3-1.64 Ma.

SK 46 is a female adult hemi cranium (majority left side preserved) with incomplete posterior dentition. This hemi cranium also has a partially complete right maxilla (Broom and Robinson, 1952). It was discovered in 1936 by Robert Broom in Member 1 (Schwartz and Tattersall, 2003) dating between 2.31-1.64- Ma (Pickering et al., 2011).

SK 48 is a slightly crushed nearly complete cranium displaying some minor distortion (Broom and Robinson, 1952; Robinson, 1956). According to Wood (2011) this cranium is a young adult male that was discovered by Broom and Robinson in 1949. It was found in Member 1(Schwartz and Tattersall, 2003) dating between 2.31-1.64 Ma (Pickering et al., 2011)

SK 65 is the left side of a partial maxilla (Schroeder, 2015). It is presumably an adult male (Broom and Robinson, 1952). The partial maxilla was discovered by Broom and Robertson in 1949 from Member 1.

SK 79 is a heavily crushed and distorted partial adult cranium (Robinson, 1956). This individual was discovered by Broom and Robinson between 1949 -1953 (Brain, 1988). This specimen was found in Member 1 Hanging Remnant (Schwartz and Tattersall, 2003) dated to between 1.8-1.7 Ma1 Ma (Pickering et al., 2011).

SK 83 is a distorted and crushed partial adult cranium with maximum preservation around the palatal and zygomatic regions (Robinson, 1956). This specimen was discovered by Broom and Robinson in 1949. This individual was found within Member 1 which dates to between 2.31-1.64 Ma (Schwartz and Tattersall, 2003).

SK 845 is a crushed and highly distorted partial cranium with the most preserved regions surrounding the maxilla and palate (Robinson, 1956). This particular individual was discovered by T.J Robinson in his last years of excavation at the Swartkrans site in 1952 (Schroeder, 2015). It originates from Hanging Remnant Member 1.

SK 1512 is a crushed and distorted partial maxilla with a preserved palate (Brain, 1967). Specimen SK 1512 was discovered by Broom and Robinson between 1948 -1952 within Member 1 dating between 2.31-1.64 Ma (Pickering et al., 2011).

SKW 8 is the right side of a partial maxilla (Brain, 1981). It was discovered by Brain in 1971 within the Hanging Remnant of Member 1.

SKW 12 is a partial left fragment of a maxilla discovered by Brain in 1972 (Brain, 1981; Pickering et al., 2011). It was found within Member 1 of the Hanging Remnant (Schwartz and Tattersall, 2003).

SKW 29 is a crushed partial cranium with most of the hard palate, regions of the maxilla and posterior dentition preserved (Brain, 1981). This specimen has a crushed partial basicranium with only some parts of the hard palate and maxilla preserved and incomplete dentition (Brain, 1981). This specimen comes from the Hanging Remnant of Member 1 (Ackermann, 1998).

Mandibles

SK 10 is a crushed and highly distorted section of a partial ramus (Broom, 1949). This specimen discovered by Broom and Robinson in 1949 is presumably an adult individual found within the Hanging Remnant of Member 1 (Schwartz and Tattersall, 2003).

SK 12 is a mandible lacking the ramus (Broom and Robinson, 1950). It was discovered in 1949 by Robinson. It was found within the Hanging Remnant of Member 1 (Schwartz and Tattersall, 2003).

SK 23 is a slightly distorted mandible in the midline region (Broom and Robinson, 1952). This individual is suggested by researchers to be an adult female. It was discovered in 1950 (Brain, 1967) by a quarryman working with Broom and Robinson enclosed in Hanging Remnant Member 1 (Schwartz and Tattersall, 2003).

SK 34 is an adult male mandible split into two halves (Broom and Robinson, 1952). It was discovered by Broom and Robertson in 1949. It was found within the Hanging Remnant of Member 1(Schwartz and Tattersall, 2003).

SK 74a is a distorted mandible with an incomplete (partial) left corpus (Broom and Robinson, 1952). This presumed adult female specimen lacks both left and right rami. It was discovered by Broom and Robinson in 1949 within Member 1 of the Swartkrans Formation (Schwartz and Tattersall, 2003) dating between 2.31-1.64 Ma (Pickering et al., 2011)

SK 81 is a brecciated mandible (Broom and Robinson, 1952). This individual was found in Member 1 of the Swartkrans Formation (Schwartz and Tattersall, 2003).

SK 844 is a distorted partial adult mandible comprising of the left corpus and ramus (Robinson, 1956). It was discovered by Robinson in 1952 with Swartkrans Formation Member 1 (Schwartz and Tattersall, 2003).

SK 858, 861, 883 is an amalgamation of mandibles into one distorted partial adult mandible lacking the left ramus (Robinson, 1956). The head of the right ramus is incomplete. This specimen was discovered by Robinson in 1952 within Swartkrans Member 1 (Schwartz and Tattersall, 2003).

SK 876 is a crushed mandible without the left and right rami (Robinson, 1956). This specimen was discovered by Robinson in 1952. It was found within Swartkrans Member 1 (Schwartz and Tattersall, 2003).

SK 1587 is a left fragment of the mandible (Brain, 1967). This specimen contains P3-M1. It was discovered in the Swartkrans Formation Member 1 (Schwartz and Tattersall, 2003).

SKW 5 is a mandible lacking the right ramus and also lacks both left incisors and canines (Brain, 1981). This specimen was discovered within Swartkrans Formation Member 1 (Pickering et al., 2011; Schwartz and Tattersall, 2003) which dates between 2.31-1.64 Ma (Pickering et al., 2011).

Koobi Fora

Koobi Fora is located East of Lake Turkana in northern Kenya (Ackermann, 1998; Schwartz and Tattersall, 2003). The "area extends from the inland eastern shore of the lake; from Ileret to Allia Bay" (Schwartz and Tattersall, 2003:132). It was formerly called East Turkana or Lake Rudolf (Wood, 2011), however, presently it is named after the area of exposures i.e. Koobi Fora Formation (Schwartz and Tattersall, 2003). Richard Leakey first discovered the site in 1967 (Schwartz and Tattersall, 2003). Excavations began in 1968 by Richard Leakey and Glynn Isaac (Isaac, 1978; Schwartz and Tattersall, 2003). The site proved to be rich in fossil material. Excavations carried on from 1968-1982 resulting in the discovery of more than 100 hominid specimens and excavations still continue today (Schwartz and Tattersall, 2003). Hominin fossils discovered included *Paranthropus* specimens ranging from teeth to a partial skeleton (Schwartz and Tattersall, 2003; Wood 2010).

The Koobi Fora Formation is comprised of 8 distinct members that have been dated (Schwartz and Tattersall, 2003). Member Moiti is 3.9 Ma and Locochart is dated to between 3.6-3.4 Ma (Isaac, 1978). Tulu Bor member is dated at 3.18 Ma (Isaac, 1978). KBS member is dated to between 2.61-1.82 Ma (Isaac, 1978). According to researchers such as Schwartz and Tattersall (2003) more recent studies date the KBS tuff to 1.88 Ma. The Koobi Fora member is dated to 1.57 Ma (Isaac, 1978). The next member, Okote, was previously dated by Isaac (1978) to 1.53 Ma; however recent studies have shown that the Okote member dates to 1.6 Ma (Schwartz

and Tattersall, 2003). The Karari member is dated to 1.32 Ma (Isaac, 1978). Burgi member dates to 1.48 Ma (Isaac, 1978). Chari dates to 1.22 Ma (Isaac, 1978). The Galanoi Boi beds are in the Holocene epoch (last ten thousand years); these beds date from 10 Ka to present day (Rowan et al., 2015).

Crania

KNM-ER 405 is a maxilla with the alveolar processes and right roots from the M1-M3 preserved. The left roots are only partially preserved (Isaac, 1978; Leakey et al., 1971). It was discovered in 1969 by the Leakey's in the "upper member, above post KBS erosion surface" (Isaac, 1978:93). As mentioned above KBS tuff dates to; 1.88 Ma, Schwartz and Tattersall, 2003).

KNM-ER 406 is an edentulous (lacking teeth) adult male cranium (Howells and Coppens, 1976; Isaac, 1978). The mastoid processes and occipital condyles have been eroded (Isaac, 1978). It was discovered in 1969 by Richard Leakey and a member of his team, Harrison Mutua (Isaac, 1978). The cranium was found on top of the KBS tuff which dates between 1.88 Ma (Schwartz and Tattersall, 2003; Wood, 2013-1).

KNM-ER 732 is an adult female hemicranium; the occipital condyle (right) and incisor crown are worn and not well preserved (Isaac, 1978; Howells and Coppens, 1976). The right side of the face is preserved, however areas of the zygomatic region are lacking (Leakey et al., 1972; Walker, 1976). "The dentition is represented by only half of the P4 crown and parts of the roots of P4-M3" (Isaac, 1978:104). This specimen was discovered by Harrison Mutua in 1970 (Isaac, 1978; Wood, 2011). It was found within the KBS member (*in situ*) (Isaac, 1978).

Mandibles

KNM-ER 403 is a right mandibular corpus, segmented through the M3 (Isaac, 1978; Leakey et al., 1971). Roots P3-M3 are preserved including the 1st incisor and canine. It was discovered by M. Muoka in 1968 (Isaac, 1978). It was found within the KBS tuff, 1.88 Ma (Schwartz and Tattersall, 2003).

KNM-ER 404 is a right mandibular corpus broken after the M3(Leakey et al., 1971). The crowns of M2-M3 in addition to the partial roots of P3-M1 are still preserved. It was discovered by K. Kimeu in 1968 (Isaac, 1978).

KNM-ER 725 is a left mandibular corpus (Isaac, 1978). The roots from P4-M3 are preserved and only the partial root of P3 is preserved (Leakey et al., 1972). The corpus lacks the alveolar process except in the molar region. It was discovered by N. Mutiwa in 1970 (Isaac, 1978). It was found within the Okote member dated to 1.6 Ma (Schwartz and Tattersall, 2003).

KNM-ER 729 is a mandible with dentition that is almost complete, with the right ramus preserved (Isaac, 1978; Howells and Coppens, 1976). This specimen was discovered by P. Abell in 1970 (Issac, 1978; Leakey et al., 1972). It was discovered in the Okote member, dated to 1.6 Ma (Schwartz and Tattersall, 2003).

KNM-ER 733 is a right mandibular corpus found in association with cranial fragments (Isaac, 1978; Leakey and Walker, 1973). P3-M2 roots and the alveolar process are still preserved. P4 and M3 are broken. This specimen was discovered by Richard Leakey in 1970 (Isaac, 1978; Walker, 1976). The specimen was found within the Okote member and dates to 1.6 Ma (Schwartz and Tattersall, 2003).

KNM-ER 3230 is an entire mandibular body with complete dentition (Isaac, 1978). The posterior edges of the mandible are missing. It was discovered in 1974 by K. Kitibi when the site was managed by J.W.K. Harris (Isaac, 1978). It was found within the Okote tuff which dates to 1.6 Ma (Schwartz and Tattersall, 2003).

West Turkana

West Turkana is the name given to the area West of Lake Turkana, originally named after the Turkana group otherwise known as the Nilotic tribe. This part of the lake forms part of the Omo (Turkana) basin shared with Ethiopia (Howell and Coppens, 1976). Expeditions (excavations) started in 1964 led by Richard and Meave Leakey (Wood, 2011).

The Omo Turkana basin comprises of seven Formations. The stratigraphy uncovered at West Turkana is from the Nachukui Formation that dates to between 4.3-0.7 Ka (Wood, 2013). The Nachukui formation consists of eight members named

after ephemeral streams (Wood, 2011). The first member of the Nachukui Formation is Lonyumun, dated to between 4.2-3.9 Ma (Delson et al., 2004). Kataboi is the second member that dates to 3.36 Ma (Harris et al., 1988). Following Kataboi is Lomekwi; this member dates from 3.6-3.2 Ma (Harris et al., 1988). Lokalalei subsequently is dated to 2.52 Ma (Harris et al., 1988). The fifth member of the formation is the Kalochoro member that dates to 2.32 Ma (Wood, 2011). Kaitio is the 6th member of the Formation dated to 1.88 Ma (Harris et al., 1988). The seventh member in the Formation is Natoo which dates between 1.6-1.8 Ma (Harris et al., 1988). The last and youngest member of the Formation is called Nariokotome, spanning 1.3-0.7 Ma (Harris et al., 1988).

Cranium

KNM-WT 17000 is an edentulous adult male cranium (Kimbel et al., 1988; Walker and Leakey, 1988). This specimen lacks portions of the neurocranium (frontal and temporal processes), calvarium and to a lesser degree fragments of the basicranium (Walker et al., 1986). Only the left side of the hard palate is intact but it is highly distorted (Walker and Leakey, 1988). It was discovered by Arambourg and Coppens in 1985 (Kimbel, 2006; Wood, 2011). It was discovered in the Nachukui Formation in the Lokalalei tuff dated to 2.5 Ma (Kimbel, 2006; Wood, 2011).

Mandible

KNM-WT 16005 is an adult mandibular body (Leakey and Walker, 1988; Walker et al., 1986; Wood, 2011). The fragmentary mandible is broken from the right M1 and left M3 posteriorly, with some roots and crowns still intact (Leakey and Walker, 1988). It was discovered in 1985 by Alan Walker and Richard Leakey in the upper Lomekwi member (Wood, 2011). Lomekwi 1 dates to between 3.6-3.2 Ma (Harris et al., 1988), although some studies say it was discovered in the KBS member that dates to 1.88 Ma (Schwartz and Tattersall).

Olduvai Gorge

Olduvai Gorge is a ± 40 km long valley situated in the Serengeti Plain in the northern region of Tanzania (Hay, 1976, 1990). The Gorge is separated into branches and the main branch is known as the Main Gorge, originating from Lakes Ndutu and Masek (Hay, 1990). The sediments date to between 2.0 Ma and 1500 years BP (Hay,

1976). The sediment exposures are known as the Olduvai Beds and are divided into seven units. The units (beds) from oldest to youngest are: Beds I (last unit) to IV, Mazek, Ndutu (lower and upper units) and Naisiusiu (Hay, 1976; 1990). Hominin fossils have been recovered from all geological beds.

Cranium

OH 5 face is an almost complete young adult cranium with a complete set of dentition, which was also found with the mandible (Wood, 2011) which is not included in the study. The specimen was discovered in Bed I at site FLK and dates to approximately 1.7 - 1.85 Ma (; Hay, 1990; Leakey, 1959).

Drimolen

Drimolen is a brecciated cave that constitutes of dolomite (limestone) from the Chunniespoort group (Keyser, 2000; Wood, 2011). The cave forms part of the Cradle of Humankind in Gauteng and is situated North of the Sterkfontein caves. Drimolen was discovered by Andre' Keyser in 1992 (Keyser, 2000; Wood, 2011) upon which the site was named after the farmer (van Drimolen) on whose farm the site was discovered (Wood, 2011).

The Monte Christo formation that is exposed at the site (Keyser et al., 2000; Wood, 2011) is currently dated between 2.0-1.5 Ma (Keyser, 2000; Keyser et al., 2000). Since its discovery, Drimolen Main Quarry has contributed significantly to the sample of *P. robustus* (Keyser, 2000), including samples DNH 7 & DNH 8.

Cranium

DNH 7 consists of a partial adult female cranium and mandible. Unfortunately, when the specimen was discovered the skull, which is distorted, was occupied by vegetation (plant roots) and a colony of ants, hence its fragmentary nature (Keyser, 2000). The cranium is missing the left zygomatic arch, the "superolateral" aspect of the left orbit, nasal bones and part of the basicranium (Keyser, 2000:189; Wood, 2011).

Mandible

DNH 7 is a partial female mandible with complete dentition where the corpi are intact and well preserved; it lacks the inferior margins and both rami (Keyser, 2000; Keyser et al., 2000; Wood, 2011).

DNH 8 is a detached adult male mandible with complete dentition and corpi (but missing both rami) (Keyser, 2000).

DNH 21 is a partial adult mandible with the left mandibular corpus (fragment) preserved (Keyser et al., 2000). It was discovered by Keyser and members of his team in 1992. The presumed age for the specimen spans between 2.0-1.5 Ma (Keyser et al., 2000).

Sterkfontein

Sterkfontein is a dolomitic (limestone) cave (Brain, 1967) situated South of the Blaauwbank river approximately 50 km northwest of Johannesburg at the Cradle of Humankind in Gauteng (Partridge et al., 2003; Pickering and Kramers, 2010). Although it has been difficult to date this site (Herries and Shaw, 2011; Pickering and Kramers, 2010), geologists have discovered six members (M1-M6) in what they call the "Sterkfontein Formation" (Clarke, 1988; Partridge and Watt. 1991; Partridge et al., 2003; Schroeder, 2015; Wood, 2011). Member 1 is older than 2.8 Ma (Pickering and Kramers, 2010). Member 2 dates to between 2.8-2.6 Ma (Pickering and Kramers, 2010). Member and 3 and Member 4 are "subsumed" into the same member which dates to approximately 2.65-2.01 Ma (Pickering and Kramers, 2010). Herries and Shaw (2011) date Member 5-which has been separated into different sections- to less than 1.8 Ma. Member 5A dates to between 1.78-1.49 Ma, and Member 5 B-C where both *Homo* and *Paranthropus* fossil samples are found date to 1.40-1.07 Ma (Clarke, 1988; Herries and Shaw, 2011). Sterkfontein is also home to gracile australopiths, i.e. *Australopithecus africanus* (Brain, 1967; Clarke, 1988).

Cranium

Sts 5, otherwise known as “Mrs Ples” (Brain, 1967; Pickering and Kramers, 2010), is a complete female cranium though some researchers consider it a male (Thackeray et al., 2002a). This cranium, as well as the two listed below, is from the species *Australopithecus africanus*, first described by Dart in 1925 (Broom, 1947). This fossil was found in Member 4 of the Sterkfontein Formation (Clarke, 1988) dating to approximately 2.65 – 2.01 Ma (Pickering and Kramers, 2010)

Sts 52 is partial male (Broom et al., 1950; Kimbel and White, 1988) hemicranium. It was discovered in Member 4 of the Sterkfontein Formation (Clarke, 1988; Benazzi et al., 2013) which dates to approximately 2.65-2.01 Ma (Pickering and Kramers, 2010).

Sts 71is a male (Broom et al., 1950; Kimbel and White, 1988) adult cranium. It has fragmentary left P3 and P4 including broken right M1-M3 (Conroy et al., 2000) This specimen was found in Member 4 (Wood, 2011), which dates to approximately 2.65-2.01 Ma (Pickering and Kramers, 2010).

CHAPTER 4

METHODS

This chapter will include a detailed description of data collection/capture. This chapter will also introduce the multivariate statistical models and approaches that were used in this study in order to: (1) assess patterns and magnitude of variation in *Paranthropus*, (2) investigate shape change, (3) test against a null hypothesis of drift, and (4) reconstruct selection vectors to characterise the nature of selection where relevant

Data Collection

The bulk of the data used in this study were collected from three-dimensional surface scans, acquired using a NextEngine™ Laser Desktop Scanner for a previous study (Schroeder, 2015). Surface scans have become very useful throughout many disciplines and particularly in palaeoanthropology because of the delicateness of fossils specimens. This allows for skulls to be scanned at higher resolutions and minute details are visible (Schroeder, 2015). Once skulls are scanned they can be used repeatedly in studies without compromising or using the fossil itself.

Due to the nature of the analyses (and study) and to increase the sample size, additional non-human primate 3D surface scans were obtained from the Morphosource.org database hosted by Duke University, and from Harvard University (Copes, 2012; Copes and Kimbel,2016). Supplementary human CT scans were obtained from the Smithsonian Institute, Washington, U.S.A. (Copes, 2012; Copes and Kimbel, 2016). These CT scans were subsequently converted to PLY files using Avizo Fire 8.1 ™. Thereafter, three-dimensional landmarks were collected from the PLY surface scans. Due to the delicate and fragmentary nature of the Drimolen samples these specimens were scanned using an Artec Space Spider Scanner for higher resolution and intricacy (unpublished study Herries, 2017), and surface renderings of those scans were used for analyses of DNH 7 and DNH 8.

Landmark Protocol

Standardized three-dimensional landmarks were collected from the fossil and extant material. Landmarks are defined as "homologous points that can be reliably and repeatedly located in all specimens under study" (Bookstein et al., 1985; Harvati, 2003:111). Bookstein (1991) further classifies the type of landmarks: (1) intersection of sutures; (2) "fuzzy" landmarks surrounding curvatures; and lastly (3) surrounding bony structures/ processes. Overall, 62 landmarks were collected for the cranium, 24 mandibular and a further 21 palatal landmarks. Detailed descriptions of cranial, mandibular and densified palatal landmarks are listed in **Tables 4.1, 4.2** and **4.3**. See **Figure 4.1**, **Figure 4.2,** and **Figure 4.3** for landmark localities. These landmarks were chosen to obtain sufficient information on shape variation, without redundancy. Landmarks were collected subject to preservation. If the region in question was damaged or distorted then the landmark was not collected.

Table 4.1. Craniodental landmarks used in this study (adapted from Bass 1987; Freidline et al., 2012; Schroeder, 2015; Stansfield and Gunz, 2011; Von Cramon-Taubadel, N. and Smith, 2012).

	Landmark Abbreviation	Landmark	Landmark Description
1	FMT	Frontomalare temporale	The most lateral point on the frontozygomatic suture
2	GLA	Glabella	Most anterior midline point on the frontal bone
3	ZMF	Zygomaticofacial foramen	The most anterior inferior point on the border of the zygomaticofacial suture
4	NA	Nasion	The point at the intersection of the nasofrontal suture and the midsagittal plane
5	OR	Orbitale	The most inferior point on the midpoint of the lower edge of the orbit
6	DAC	Dacryon	The point of intersection of the frontolacrimal and lacrimomaxillary sutures
7	SON	Supraorbital notches	The most lateral point on the supraorbital notch
8	ZS	Zygomaxillare superior	The most superior point on the zygomaticotemporal suture
9	ZI	Zygomaxillare inferior	The most inferior point on the zygomamaxillary suture
10	FMN	Frontomalare maxillary nasal suture	The most superior point of the suture where the maxilla articulates with the frontal and nasal bones
11	OPH	Ophryon	Midline of the forehead immediately above the orbits
12	LA	Lacrimale	The point of intersection of the posterior lacrimal crest with the fronotolacrimal suture
13	SO	Superior Orbitale	The most superior midpoint on the orbital margin
14	MF	Maxilllofrontale	The point of intersection of the anterior lacrimal crest (medial edge of eye orbit), or the crest extended, with the frontomaxillary suture
15	IOF	Infraorbital foramen	The most inferior lateral point on the border of the infraorbital foramen
16	ALR	Alare	The most lateral point on the nasal aperture
17	ANS	Anterior Nasal spine	The most anterior midpoint of the anterior nasal spine of the maxilla
18	PRO	Prosthion	The most anterior point in the midline of the maxillary alveolar process
19	RHI	Rhinion	The anterior tip at the end of the suture of the nasal bones
20	IDS	Infradentale superius (alveolare)	The upper alveolar point; the apex of the septum between the upper central incisors
21	MMC	Max maxillary curve	The point in the depth of the notch between the zygomaxillary suture and the alveolar process
22	MT	Maxillary tuberosity	The most distal point on the maxillary alveolar process
23	M2D	Distal M2	The most distal point on M2/The most mesial point on M3
24	M1D	Distal M1	The most distal point on M1/The most mesial point on M2

25	ALV	Alveolon	The intersection of the interpalatal suture and a line tangent to the posterior margins of the alveolar processes
26	INC	Incisivon	The most posteroinferior point on the border of the incisive foramen
27	GPF	Greater palatine foramen	The most posterolateral point on the border of the greater palatine foramen
28	OL	Orale	The point where a line drawn tangent to the inner margin of the sockets of the two middle incisors of the upper jaw and projected onto the hard palate intersects the midsagittal plane
29	STA	Staphylion	The point in the midline of the back of the hard palate (interpalatal suture) where it crosses
30	IC	Incision	The incisal level of the upper central incisors
31	ECM	Ectomalare	The most lateral point on the outer surface of the alveolar margins
32	ENM	Endomalare	The most medial point on the inner surface of the alveolar ridge
33	PTM	Palatomaxillare	The midline point of intersection of the palatine and the maxillary bones
34	ZTI	Zygotemporale inferior	The most inferior point on the zygomaticotemporal suture
35	ZTS	Zygotemporale superior	The most superior point on the zygomaticotemporal suture
36	POR	Porion	The most superior point on the margin of the external auditory meatus
37	EAM (A)	Ext auditory meatus	The most anterior point on the margin of the external auditory meatus
38	EAM (P)	Ext auditory meatus	The most posterior point on the margin of the external auditory meatus
39	EMI	External auditory meatus inferior	The most inferior point on the margin of the external auditory meatus
40	AP	Anterior pterion	The most anterior point on the sphenoparietal suture/ the intersection of the parietal, sphenoid and frontal bones
41	MAS	Mastoidale	The most inferolateral point on the mastoid process
42	AST	Asterion	The junction of the lambdoid, parietomastoid and occipitomastoid sutures
43	BR	Bregma	The midline junction of the coronal and sagittal sutures
44	IN	Inferior Nuchal	The most inferior midpoint on the inferior nuchal line
45	L	Lambda	The midline junction of the sagittal and lambdoid sutures, taken in the midline
46	HOR	Hormion	The midpoint junction of the posterior aspect of the vomer and sphenoid bone
47	O	Opisthion	The midpoint on the posterior border of the foramen magnum
48	BA	Basion	The midpoint on the anterior border of the foramen magnum
49	FML	Foramen magnum lateral	The most lateral point on the margin of the foramen magnum, posterior to occipital condyle
50	OCA (L)	Occipitocondyle lateral	The most lateral inferior point on the occipital condyle

51	OCA (A)	Occipitocondyle anterior	The most anteroinferior point on the occipital condyle
52	I	Inion	A point at the base of the external occipital protuberance
53	ENDOBA	Sphenobasion	The midline point on the sphenooccipital suture
54	MFL	Lateral mandibular fossa	The most lateral point on the mandibular fossa
55	MFM	Medial mandibular fossa	The most medial point on the mandibular fossa
56	P3M	Mesial P3	The most mesial point on P3
57	P3D	Distal P3	The most distal point on P3
58	P4D	Distal P4	The most distal point on P4/The most mesial point on M1
61	M3D	Distal M3	The most distal point on M3
62	ENDOBA (lat)	Sphenobasion (lat)	The most lateral, inferior point on the sphenooccipital synchondrosis

Table 4.2. Mandibular landmarks used in this study (adapted from Schroeder, 2015; Von Cramon-Taubadel, N. and Smith, 2012).

	Landmark Abbreviation	Landmark	Landmark Description
1	MMN	Mid-mandibular notch (Sigmoid notch)	The most inferior aspect on the mid-mandibular notch
2	COR	Coronoid process	The most superior aspect on the coronoid process
3	AJUNC	Inferior anterior ramus	The junction of the anterior border of the ramus and alveolus; The most anterior point on the ascending ramus in line with the alveolus
4	GON	Gonian	The point of maximum curvature on the posterior-inferior border where the posterior ramus and the corpus intersect
5	MEN	Mental foramen	The most anteroinferior edge of the mental foramen
6	INFR	Infradentale	The most central point on the mandibular alveolus
7	LAT	Lateral mandibular condyle	The most superolateral point on the mandibular condyle
8	MC	Medial mandibular condyle	The most mediosuperior point on the mandibular condyle
9	MFO	Mandibular foramen	The most posteroinferior aspect on the mandibular foramen
10	MSPIN	Superior mental spine	The most superior aspect on the mental spine
11	ALVB	Alveolar border of body	The most superior point on the alveolus directly above the mental foramen
12	IBB	Inferior border of body	The most inferior point on the mandibular corpus directly below the mental foramen
13	POG	Pogonian	The most anterior projection of bone on the mental symphysis
14	RAM POS	Ramus posterior	The most posterior point on the ascending ramus in line with the alveolus
15	GNA	Gnathion	The most inferior midline point on the mandibular symphysis
16	MBO	Mandibular orale	The most superior midline point on the lingual surface of the alveolus
17	CP3	Canine/P3	The most lateral point on the alveolus between the canine and P3
18	P3M	Mesial P3	The most mesial point on P3
19	P3D	Distal P3	The most distal point on P3
20	P4D	Distal P4	The most distal point on P4/The most mesial point on M1
21	M1D	Distal M1	The most distal point on M1/The most mesial point on M2
22	M2D	Distal M2	The most distal point on M2/The most mesial point on M3
23	M3D	Distal M3	The most distal point on M3
24	ALVS	Alveolus	The most superior,posterior point on the alveolus

Table 4.3. Densified Right palatal and dentition landmarks used in this study (adapted from Von Cramon-Taubadel, N. and Smith, 2012).

	Landmark Abbreviation	Landmark	Landmark Description
1	IDS	Infradentale superius (alveolare)	The upper alveolar point; the apex of the septum between the upper central incisors
2	OL	Orale	The point where a line drawn tangent to the inner margin of the sockets of the two middle incisors of the upper jaw and projected onto the hard palate intersects the midsagittal plane
3	INC	Incisivon	The most posteroinferior point on the border of the incisive foramen
4	PTM	Palatomaxillare	The midline point of intersection of the palatine and the maxillary bones
5	ALV	Alveolon	The intersection of the interpalatal suture and a line tangent to the posterior margins of the alveolar processes
6	M3DL	Distal/Lingual M3	The most distal point on the inner lingual surface of the alveolar ridge on M3
7	M2DL	Distal/Lingual M2	The most medial point on the inner surface of the alveolar ridge between M3 and M2
8	M1DL	Distal/Lingual M1	The most medial point on the inner surface of the alveolar ridge between M2 and M1
9	P4DL	Distal/Lingual P4	The most medial point on the inner surface of the alveolar ridge between M1 and P4
10	P3DL	Distal/Lingual P3	The most medial point on the inner surface of the alveolar ridge between P4 and P3
11	CP3L	Canine/P3 (Lingual)	The most medial point on the alveolus between the canine and P3
12	CLIL	Canine/Lateral Incisor (Lingual)	The most medial point on the alveolus between the canine and the lateral incisor
13	LICIL	Lateral Incisor/Central Incisor (Lingual)	The most medial point on the alveolus between the lateral and central incisors
14	M3DB	Distal/Buccal M3	The most distal point on the outer buccal surface of the alveolar ridge on M3
15	M2DB	Distal/Buccal M2	The most lateral point on the outer surface of the alveolar ridge between M3 and M2
16	M1DB	Distal/Buccal M1	The most lateral point on the outer surface of the alveolar ridge between M2 and M1
17	P4DB	Distal/Buccal P4	The most lateral point on the outer surface of the alveolar ridge between M1 and P4
18	P3DB	Distal/Buccal P3	The most lateral point on the outer surface of the alveolar ridge between P4 and P3
19	CP3B	Canine/P3 (Buccal)	The most lateral point on the alveolus between the canine and P3

20	CLIB	Canine/Lateral Incisor (Buccal)	The most lateral point on the alveolus between the canine and the lateral incisor
21	LICIB	Lateral Incisor/Central Incisor (Buccal)	The most lateral point on the alveolus between the lateral and central incisors

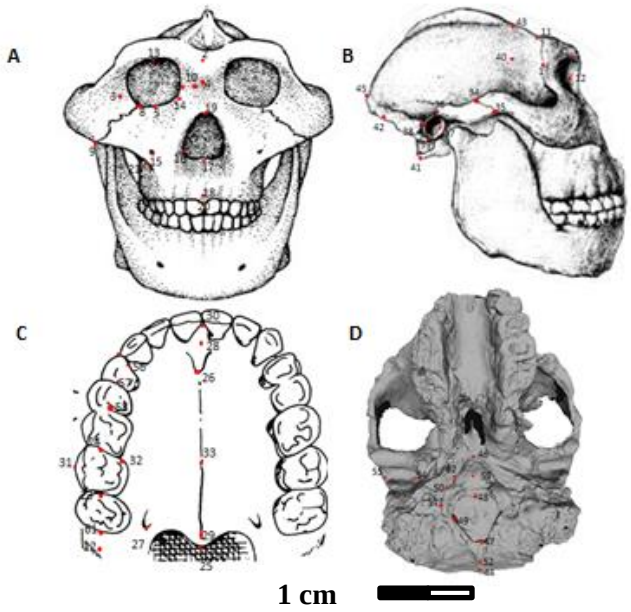

Figure 4.1 A. Craniofacial landmark data frontal view of a *Paranthropus* cranium (adapted from McCollum, 1999). **B**. Craniofacial landmark data lateral view of a *Paranthropus* cranium. **C.** *Paranthropus* craniodental landmark data (adapted from http://bigpictures.club/resize.php?img=http://www.ibri.org/Books/Pun_Evolution/Figures/Fig2-18.gif, 2015). **D**. *Paranthropus* craniofacial landmark data shown on SK 23. Basicranial view**.**

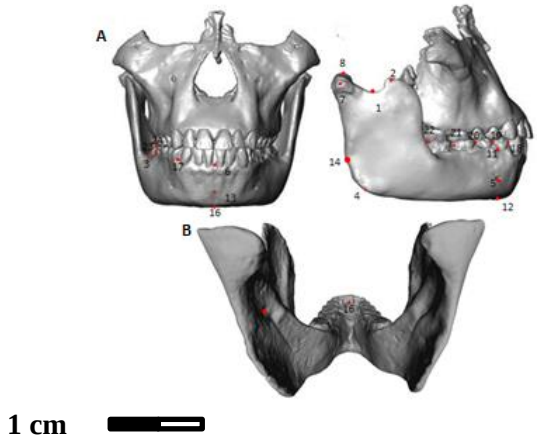

Figure 4.2 A. *Paranthropus* mandibular landmark data frontal and lateral views of a *Paranthropus* cranium (adapted from Benazzi et al., 2013). **B.** *Paranthropus* mandibular landmark data posterior view of SK 23 mandible.

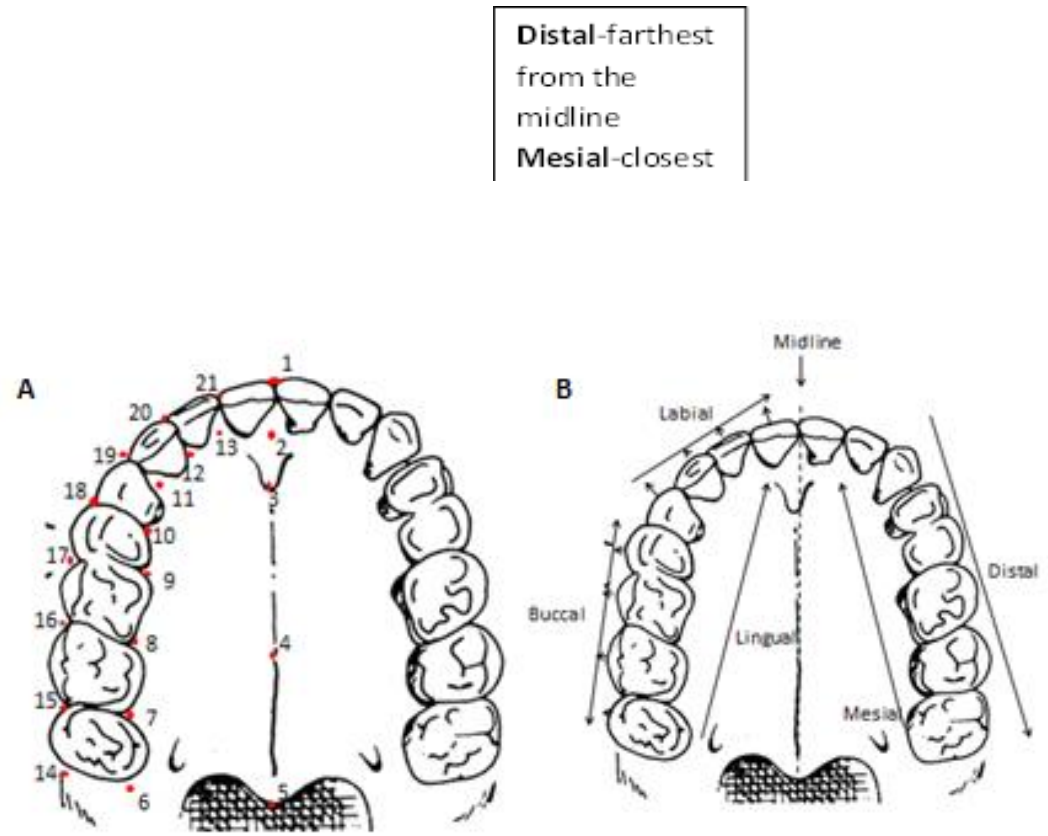

Figure 4.3. A. *Paranthropus* Densified Palatal and Dentition landmark data (adapted from http://bigpictures.club/resize.php?img=http://www.ibri.org/Books/Pun_Evolution/Figures/Fig2-18.gif, 2015). **B**. Palate and tooth profile showing orientation (adapted from Scott & II Turner 1997; Schroeder, 2015; http://bigpictures.club/resize.php?img=http://www.ibri.org/Books/Pun_Evolution/Figures/Fig2-18.gif , 2015).

Calculating Interlandmark Distances

Using landmarks described in **Tables 4.1**, **4.2** and **4.3,** inter-landmark distances were chosen to maximize shape information without redundancy (Ackermann, 2002; see **Tables 4.4**, **4.5**, **4.6**, **4.7**). Thirty-eight craniodental distances, 17 mandibular distances, and 16 densified right palatal inter-landmark distances were calculated. The densified palatal landmarks were broken down into seven tooth regions (complexes), i.e. inter-landmark distances that encompassed the shape and morphology of the: central incisor; lateral incisor, canine, third premolar, fourth premolar; and first to third molars (**Table 4.8**). **Figures 4.1-4.3** illustrate cranial, mandibular and densified palatal landmarks**.** Distances were calculated using this equation:

$$d = \sqrt{(x_2 - x_1)^2 + (y_2 - y_1)^2 + (z_2 - z_1)^2}$$

where (x_1, y_1, z_1) defines the position of landmark one and (x_2, y_2, z_2) defines the position of landmark two. Preservation dictated which landmarks and inter-landmark distances for fossil specimens could be taken. Inter-landmark distances were calculated for both left and right sides (bilateral) and averaged. If only one side (unilateral) was present, only those unilateral inter-landmark distances were used (Schroeder, 2007; 2015). Bilateral inter-landmark distances were collected for all comparative extant specimens and subsequently both sides averaged.

Table 4.4. Craniodental inter-landmark distances used in this study (adapted from Ackermann, 1998, 2009; Schroeder, 2007, 2015). Distances are Left/Right averaged, if one side was missing that side was used. [L] Indicates only the left side.

Measurement No.	Interlandmark Distance
1	ANS-PRO
2	ALR-ANS
3	P3D-P4D
4	M2D-M1D
5	M1D-P4D
5	M2D-M3D
7	ENM-OL
8	ZS-ZI
9	ZI-IOF
10	OR-ZI
11	ZTS-ZTI
12	ZI-FMT
13	GLA-NA
14	DAC-ALR
15	DAC-FMT
16	NA-FMT
17	MF-GLA
18	NA-MF
19	PRO-ZTI
20	DAC-NA
21	ZTI-MFL
22	ZTI-EMI
23	OPH-GLA
24	POR-MAS
25	MFL -MFM
26	BA-HOR
27	HOR-MFL
28	OCA (A)-BA
29	AST-BA [L]
30	EMI-OCA (A)
31	MFM-EMI
32	EMI-HOR
33	EAM (A)-EAM (P)
34	MFL-EMI
35	POR-MFL
36	POR-MFM
37	AST-POR [L]
38	MFL-AST

Table 4.5. Mandibular inter-landmark distances used in this study (adapted from Schroeder, 2015). Distances are Left/Right averaged, if one side was missing that side was used. [L] indicates left; [R] indicates right sides.

Measurement No.	Interlandmark Distance
1	MEN-RAM POS
2	AJUNC-RAM POS
3	AJUNC-GON
4	ALVS-GON
5	RAM POS-GON
6	MEN-GON
7	MEN-ALVB
8	MEN-IBB
9	P3D-P4D
10	P4D-M1D
11	M1D-M2D
12	M2D-M3D
13	ALVB-M2D
14	P3D [L]-P3D[R]
15	P4D [L]-P4D[R]
16	M1D [L]-M1D[R]
17	MEN [L]-MEN [R]

Table 4.6. Densified Right dental and palatal inter-landmark distances used in this study. L indicates lingual and B indicates buccal/labial.

Positions	Interlandmark make-up
Lingual	M3DL-M2DL
	M2DL-M1DL
	M1DL-P4DL
	P4DL-P3DL
	P3DL-CP3L
	CP3L-CLIL
	CLIL-LICIL
	LICIL-OL
Buccal	M3DB-M2DB
	M2DB-M1DB
	M1DB-P4DB
	P4DB-P3DB
	P3DB-CP3B
	CP3B-CLIB
	CLIB-LICIB
	LICIB-IDS
Center	ALV-M3DL
	ALV-M3DB
	PTM-M2DL
	PTM-M2DB
	INC-P3DL
	INC-P3DB
	M3DB-M3DL
	M2DL-M2DB
	M1DL-M1DB
	P4DL-P4DB
	P3DL-P3DB
	CP3L-CP3B
	CLIL-CLIB
	LICIL-LICIB
Diagonal	M3DB-M2DL
	M3DL-M2DB
	M2DB-M1DL
	M2DL-M1DB
	M1DB-P4DL
	M1DL-P4DB
	P4DB-P3DL
	P4DL-P3DB
	P3DB-CP3L

P3DL-CP3B

CP3B-CLIL

CP3L-CLIB

CLIB-LICIL

LICIL-LICIB

CILIL-IDS

CILIB-OL

Table 4.7. Densified Right dental and palatal inter-landmark distances used in this study continued.

Measurement No.	Interlandmark Distance
1	IDS-OL
2	IDS-INC
3	IDS-PTM
4	IDS-ALV
5	OL-INC
6	OL-PTM
7	OL-ALV
8	INC-PTM
9	INC-ALV
10	PTM-ALV
11	ALV-M3DL
12	ALV-M3DB
13	PTM-M2DL
14	PTM-M2DB
15	INC-P3DL
16	INC-P3DB

Table 4.8. Densified Right dental regions (Complexes) of inter-landmark distances used in this study.

Tooth Complex	Interlandmark Distances
M3	M3DL-M2DL
	M3DB-M2DB
	M3DB-M3DL
	M3DB-M2DL
	M3DL-M2DB
M2	M2DL-M1DL
	M2DB-M1DB
	M2DL-M2DB
	M2DB-M1DL
	M2DL-M1DB
M1	M1DL-P4DL
	M1DB-P4DB
	M1DL-M1DB
	M1DB-P4DL
	M1DL-P4DB
P4	P4DL-P3DL
	P4DB-P3DB
	P4DL-P4DB
	P4DB-P3DL
	P4DL-P3DB
P3	P3DL-CP3L
	P3DB-CP3B
	P3DL-P3DB
	P3DB-CP3L
	P3DL-CP3B
C	CP3L-CLIL
	CP3B-CLIB
	CP3L-CP3B
	CP3B-CLIL
	CP3L-CLIB
LI	CLIL-LICIL
	CLIB-LICIB
	CLIL-CLIB
	CLIB-LICIL
	LICIL-LICIB
CI	LICIL-OL
	LICIB-IDS
	LICIL-LICIB
	CILIL-IDS
	CILIB-OL

Data Analysis

To investigate variation in the genus *Paranthropus,* various analytical methods were adopted. Mahalanobis' distances were calculated and Principal Coordinates Analyses (PCoA) used to evaluate and visualise patterns and magnitude of variation. Geometric morphometric approaches were used to superimpose landmark data and evaluate and visualize shape, and size-related shape change. Lastly, Lande's (1977, 1979, 1983) quantitative evolutionary theory was used to test the null hypothesis of genetic drift and reconstruct selection vectors where appropriate.

Paleoanthropological studies are often plagued by: (1) fossil distortion, damage and fragmentation; (2) very small sample sizes (Ackermann, 2009). To mitigate these issues, studies often design analyses to strike a balance between the number of variables and the number of samples. Previous studies (e.g. Ackermann, 1998; Schroeder, 2015) on hominin craniofacial remains analyses have done this by either maximising the number of individuals and having a smaller number of shared variables or maximising the number of variables with a reduced of number specimens. However, this can be problematic when the methods used require large samples, such as with estimates of variance and covariance (Ackermann, 2002, 2009).

In light of the above, several analyses were constructed. These analyses were separated into cranial, mandibular and densified palatal regions. Within these three main regions, various sub-sets were created either to maximise the number of variables and/or individuals. This study also structured analyses into regions to further understand shape variation in shared regions. Because of small sample sizes in the fossil taxa, three comparative extant samples (*Gorilla gorilla*, *Pan troglodytes* and *Homo sapiens*) were used as analogues/models to estimate within-taxon variation in the fossil sample. This assumes that fossils and extant groups have similar patterns of variation (Ackermann, 2009). Because we know this isn't true (though patterns of variation are similar), three extant taxa were used. In this way, we ensure a variety of possible models of variation. **Table 4.9** describes all constructed and executed analyses. In all analyses inter-landmark distances were converted into vectors within Excel for use in the various multivariate statistical approaches.

Table 4.9. Sub-sets of analyses and inter-landmark distances in this study (adapted from Ackermann, 1998; Schroeder 2015).

			Comparative Sample (N)			
Analysis	**Regions**	**Fossil Specimens**	***G. gorilla***	***P. troglodytes***	***H. sapiens***	**Inter-landmark Distance**
Cranial Analysis 1	Midface-Maxilla	OH 5, SK 46, SK 79, SK 83, DNH 7, Sts 52, Sts 71	49	48	45	ANS-PRO, ALR-ANS, P3D-P4D, P4D-M1D, M1D-M2D, M2D-M3D, ENM-OL
Cranial Analysis 2	Zygomatic	KNM ER 732, OH 5, SK 48, DNH 7, Sts 5, Sts 71	49	46	50	ZS-ZI, ZI-IOF, OR-ZI, ZTS-ZTI, ZI-FMT
Cranial Analysis 3	Zygomatic-Upper face	KNM-ER 406, SK 48. Sts 5, Sts 71	50	45	50	GLA-NA, DAC-ALR, ZTS-ZTI, DAC-FMT, NA-FMT, MF-FLA, NA-MF, PRO-ZTI, DAC-NA, ZTI-MFL, ZTI-EMI
Cranial Analysis 4	Upper face-Temporal	KNM-ER 732, DNH 7, Sts 5	49	46	50	OPH-GLA, ZS-ZI, ZI-IOF, OR-ZI, ZTS-ZTI, ZI-FMT, POR-MAS
Cranial Analysis 5	Basicranium	KNM-WT 17000, KNM-ER 406, Sts 5	47	46	50	MFL-MFM, BA-HOR, HOR-MFL, OCA (A)-BA, AST-BA [L], EMI-OCA (A), MFM-EMI, EMI-HOR
Cranial Analysis 6	Temporal	KNM-WT 17000, KNM-ER 406, SK 48, DNH 7, Sts 5	50	50	50	EAM (A)-EAM (P), EMI-POR, MFL-EMI, POR-MFL, POR-MFM, AST-POR [L], MFM-AST
Mandibular Analysis 1	Ramus	KNM-ER 729, SK 12, SK 23, SK 34 (left), SK 34 (right)	50	43	50	MEN-RAM POS, AJUNC-RAM POS, AJUNC-GON, ALVS-GON, RAM POS- GON, MEN-GON
Mandibular Analysis 2	Corpus	KNM-ER 403, KNM-ER 729, KNM-ER 3230, SK 12, SK 23. SK 34 (LEFT), SK 34 (RIGHT), SK 81, SK 876, SKW 5, DNH 7, DNH 8	50	42	49	MEN-ALVB, MEN- IBB, P3D-P4D, P4D-M1D, M1D-M2D, M2D-M3D, ALVB-M2D
Mandibular Analysis	Center	KNM-ER 729, KNM-ER 3230, SK 23, SK 81, SKW 5, DNH 7, DNH 8	50	41	50	P3D- P3D [R], P4D- P4D [R], M1D -M1D [R], MEN-MEN[R]

3

Densified Analysis 1	Center	SK 48, SK 79, OH 5	45	41	50	IDS-OL, IDS-INC, IDS-PTM, IDS-ALV, OL-INC, OL-PTM, OL-ALV, INC-PTM, INC-ALV, PTM-ALV, ALV-M3DL, ALV-M3DB, PTM-M2DL, PTM-M2DB, INC-P3DL, INC-P3DB
Densified Analysis 2	Complex 1 - M3	SK 48, SK 79, OH 5	45	41	50	M3DL-M2DL, M3DB-M2DB, M3DB-M3DL, M3DB-M2DL, M3DL-M2DB
Densified Analysis 3	Complex 2 - M2	SK 48, SK 79, OH 5	45	41	50	M2DL-M1DL, M2DB-M1DB, M2DL-M2DB, M2DB-M1DL, M2DL-M1DB
Densified Analysis 4	Complex 3- M1	SK 48, SK 79, OH 5	45	41	50	M1DL-P4DL, M1DB-P4DB, M1DL-M1DB, M1DB-P4DL, M1DL-P4DB
Densified Analysis 5	Complex 4- P4	SK 48, SK 79, OH 5	45	41	50	P4DL-P3DL, P4DB-P3DB, P4DL-P4DB, P4DB-P3DL, P4DL-P3DB
Densified Analysis 6	Complex 5- P3	SK 48, SK 79, OH 5	45	41	50	P3DL-CP3L, P3DB-CP3B, P3DL-P3DB, P3DB-CP3L, P3DL-CP3B
Densified Analysis 7	Complex 6 - C	SK 48, SK 79, OH 5	45	41	50	CP3L-CLIL, CP3B-CLIB, CP3L-CP3B, CP3B-CLIL, CP3L-CLIB
Densified Analysis 8	Complex 7 - LI	SK 48, SK 79, OH 5	45	41	50	CLIL-LICIL, CLIB-LICIB, CLIL-CLIB, CLIB-LICIL, LICIL-LICIB
Densified Analysis 9	Complex 8 - CI	SK 48, SK 79, OH 5	45	41	50	LICIL-OL, LICIB-IDS, LICIL-LICIB, CILIL-IDS, CILIB-OL

Table 4.10. Summary of geometric morphometric Analyses 1-5. See **Table 4.1**, **Table 4.2** and **Table 4.8** for landmark descriptions.

			Comparative Sample (N)			PC analysis results after Procrustes fit	Regression results
Analysis	**Landmarks**	**Fossils**	***P. troglodytes***	***G. gorilla***	***H. sapiens***	**PC (% Variance)**	**Correlation (r2)**
1	IDS, OL, INC, PTM, ALV, M3DL, M2DL, M1DL, P4DL, P3DL, CP3L, CLIL, LICIL, M3DB, M2DB, M1DB, P4DB, P3DB, CP3B, CLIB, LICIB	SK 48, SK 79, OH 5	41	45	50	PC 1 = 45.97%; PC2 = 9.96%	0.2995
2	MEN, ALVB, IBB, P3D, P4D, M1D, M2D, M3D	SK 23, SKW 5, KNM-ER 729	40	50	49	PC 1= 55.93%; PC 2 = 11.84%	-0.6287
3	ALR, ANS, PRO, OL, ENM, P3D, M1D, M2D, M3D	DNH 8, SK 83, OH 5	46	46	37	PC 1 = 44.54%; PC2 = 16.31%	0,4209
4	ZTS, ZTI, GLA, NA, ALR, PRO, MFL	SK 48, KNM-ER 406, Sts 5	32	49	43	PC 1= 60.88%; PC 2 = 10.96%	0,3660
5	ZTS, ZTI, ZS, ZI, OR , IOF	SK 48, Sts 5	28	49	43	PC 1= 44.72%; PC 2= 15.92%	-0,3340

Calculating Mahalanobis' Distances

Mahalanobis' distance statistic (D^2) was performed and used to assess differences between fossils in the context of extant variation (Harvati, 2003; Harvati et al. 2005). The Mahalanobis' distance equation is denoted as follows:

$$D^2 = (x_1 - x_2)' V^{-1} (x_1 - x_2),$$

Where D^2 equals the Mahalanobis' distance between specimen 1 and specimen 2, x_1 is the vector of traits (variables/inter landmark distances) for specimen 1, x_2 is the vector of traits (variables/inter landmark distances) for specimen 2 and V^{-1} is the inverse of the V/CV matrix of the extant specimens (Ackermann, 2003, 2009; Schroeder, 2007, 2015).

The Mahalanobis' distance statistic was calculated in MATHEMATICA ™ v 10.2 (Ackermann, 1998); code for the programme was written by R.R Ackermann (2003). For each analysis, all possible pairwise distances between specimens were calculated. This is done using each of the three extant V/CV matrices. This allows us to examine how the use of these different V/CV matrices affects the understanding of inter-individual variation in *Paranthropus*.

All possible pairwise Mahalanobis' distances were also calculated for each extant (*G. gorilla, P. troglodytes and H. sapiens*) species to determine significance between individuals in the fossil sample. This included using V/CV matrices from the same species (e.g. chimp pairwise distances calculated in a chimp V/CV matrix) and each of the other extant species (e.g. chimp pairwise distances calculated in a gorilla V/CV matrix (Ackermann, 2002, 2003, 2009; Schroeder, 2007, 2015). The V/CV combinations amounted to nine different models for each analysis: human data with a human V/CV matrix (human-human), gorilla data with a gorilla V/CV matrix (gorilla-gorilla), chimpanzee data with a chimpanzee V/CV matrix (chimp-chimp), human data with a gorilla V/CV matrix (human-gorilla), human data with a chimpanzee V/CV matrix (human-chimp), gorilla data with a human V/CV matrix (gorilla-human), chimpanzee data with a human V/CV matrix (chimp-human), gorilla data with a chimpanzee V/CV matrix (gorilla-chimp) and chimpanzee data with a gorilla V/CV matrix (chimp-gorilla). Subsequently, D^2 values were sorted from smallest to largest number and the 95^{th} percentile determined. By taking this approach, we build into the model and significance

tests the reality that species V/CV differs slightly and that using the variation from a different species to calculate these Mahalanobis' distances can inflate the values (see Ackermann 2005; Schroeder 2015).

Principal Coordinate Analyses (PCoA) were conducted using pairwise Mahalanobis' distances (calculated in MATHEMATICA^{TM} v10.2) to visualize relationships between fossil specimens in each analysis. PCoA illustrate individual differences by graphically depicting inter-individual dissimilarities. Each axis represents an eigenvalue which equates to the amount of variation "captured" by that axis. The first axis represents the largest amount of variation and the second axis represents the second greatest variation in any given data set (Buttigieg and Ramette, 2014). One can tell if individuals are similar (clustering) or dissimilar from each other by looking at locations of individual specimens on the PCoA plot.

Geometric Morphometrics

Five analyses which best represented morphological regions on the cranium and specifically the palate were constructed using MorphoJ v 1.05 (Klingenberg, 2011). General Procrustes Analysis (GPA) is a technique used to superimpose three (and two)–dimensional landmark data (Webster and Sheets, 2010). This geometric morphometrics technique enables us to evaluate morphological variation in terms of shape change including shape change related to size (Klingenberg, 2002; 2011) in the genus *Paranthropus*.

Landmark configurations (x, y, z coordinates) were scaled and translated to the same centroid size. These configurations were then rotated to minimise the mean shape and the sum of squared distances between configurations (Klingenberg, 2002). The new translated coordinates are termed Procrustes coordinates (mean configuration) and retain the original shape information for each specimen (Klingenberg, 2002). The red dots indicate the centroid size, the blue dots are the transformed configurations (mean) and the black dots are all the observations (specimens) in the given dataset. Procrustes coordinates were used to formulate a V/CV matrix in order to generate Principal Component Analyses (PCAs) for each given sub-set. This superimposition technique employed landmark coordinates to examine shape and shape related to size – intra and inter-specific shape variation within and between *Paranthropus* - using extant species V/CV matrices as analogues (Ackermann, 1998; Baab et al., 2012; Slice, 2007). PCAs graphically represent shape differences (variation) between groups of specimens. Within what can be called a "Morphospace" objects are represented by

points where closeness represents similarity and the further these points are the less similar (Baab et al., 2012; Klingenberg, 2011). The first principal component represents the largest amount of shape variation - PC 1 is the most taxonomically informative-, the second principal component represents the second most amount of shape variation (Manly, 1986). Wireframe graphs were constructed using differences between the averaged mean shape and original landmark coordinates allowed for the visualisation of shape change along each respective principal component.

Correlating size and shape (shape related to size), otherwise known as allometry, in geometric morphometrics is done through a multivariate regression analysis of shape, using regression scores from principal component scores (y axis) and logged centroid size (x axis) (Bookstein, 1991; Klingenberg, 2002, 2011). Permutation tests (10 000 runs) were used to evaluate significance for the correlation between size and shape (Klingenberg, 2002; Klingenberg and McIntyre, 1998).

Analysis 1 used only the right side (asymmetrical coordinates) however, in analyses 2-5 landmark coordinates for both sides were used to account for object symmetry where the axis of symmetry passes through the object (Klingenberg, 2002). Each analysis will be presented separately to visualize these changes in relation to their region etc. See **Table 4.10** and **Appendix B** for summary.

Genetic Drift: Testing of the Null Hypothesis

Hypotheses of genetic drift (random divergence) posit that morphological change in the hominin lineage is not only the result of adaptive evolutionary forces but non-adaptive (neutral, chance) forces (Ackermann and Cheverud, 2004). Tests developed from Lande's (Lande, 1977, 1979, 1980) quantitative evolutionary theory are used to analyse the relative roles of genetic drift and selection within *Paranthropus* (Ackermann and Cheverud, 2004). We test the neutral model of evolution using the following equation:

$$B_t = G(t / N_e),$$

where B_t is the between population (sample) V/CV matrix, t is the number of generations G is the additive genetic V/CV matrix with N_e as the given population size (Ackermann and Cheverud, 2004). G can be substituted with the phenotypic within group V/CV matrix (W) following Cheverud (1988), who tested the proportionality of the matrices and found that the matrices are directly proportional to each other (Ackermann, 2002; Schroeder, 2015) because t and N_e are constants, we are left with the following equation:

$$(B \propto W).$$

This study follows Ackermann and Cheverud's (2002, 2004) approach where within-group covariance matrices are converted to reduced uncorrelated principal components (Ackermann and Cheverud, 2004). Logged between-group eigenvalues (B), calculated as the variance among group mean differences between fossil populations, are regressed (LSR) onto logged within-group eigenvalues (W), obtained from principal components calculated from the extant covariance matrices substituted as models for within-population variability. A proportional relationship ($B \propto W$) fails to reject the null hypothesis of drift (Ackermann and Cheverud, 2004). In addition, if populations have diversified through random evolutionary processes then the regression slope will not differ significantly from a slope of 1.0 (at a 0.05 significance level-using a t-test), indicating that the pattern of variance within and between these groups is comparable. A non-proportional relationship or rejection of drift occurs if the p-value is less than 0.05. This indicates that the morphology being analysed is too variable for divergence to have occurred through random forces alone and non-random forces, such as directional selection, are likely to be at work (Ackermann and Cheverud, 2004). Extant model V/CV (phenotypic) matrices were used as analogues to estimate fossil within-group variation.

(Ackermann 2002, 2003, 2009; Schroeder, 2015) using R studio (R v 3.2.4 Revised). (See **Appendix D** for code written by Lauren Schroeder, 2015). It is important to highlight that failing to reject drift does not eradicate the chance non-adaptive forces were acting, however implies that any effects of these non-random processes cannot be separated from divergence due to drift. Additionally, the small size renders the test weak and makes it challenging to reject drift when comparing a small number of species. As seen in the results, considerable deviation from a slope of 1.00, will probably lead to selection. Otherwise, this test is considered as a conservative one (Schroeder, 2015).

Reconstructing Selection

If the null hypothesis of drift is rejected, and selection has been proven to be the acting driving force between the divergence of two populations/taxa, Lande's evolutionary theory (1983) also provides a means for reconstructing the type of selection required to cause groups to diversify. Selection vectors are reconstructed to evaluate the pattern and magnitude of selection that acts to differentiate populations. This methodological approach is determined by the following relationship:

$$\beta = W^{-1}\left[z_i - z_j \right],$$

where β is the differential selection gradient/vector summed over generations, W^{-1} is the inverse of the within-species V/CV matrix, and $\left[z_i - z_j \right]$ is the difference in means between species i and j, in this case the fossil species being compared. Once more (routinely), V/CV matrices from extant population (s) are used as analogues to estimate fossil within-group variation (Ackermann, 2002, 2003, 2009). Selection (directional) can be either positive or negative. The magnitude of selection is reliant on estimated extant model V/CV matrices, and interpretation of results should be evaluated with the utmost caution as extant models may change the interpretation of results (Ackermann, 2003). All analyses were performed using R v3.2.4 revised (See **Appendix D** for code written by Lauren Schroeder, 2015).

CHAPTER FIVE

RESULTS

Mahalanobis' Distances

Mahalanobis' generalised distance statistic was used to evaluate morphological distances between *Paranthropus* fossil specimens for eighteen subsets. Extant V/CV matrices are used as analogues as an estimate for within-fossil variation. Principal Coordinate Analyses (PCoA) were calculated using pairwise Mahalonobis' distances, to graphically present relationships among the fossils and inter-individual morphological dissimilarities in each analysis. Details of each analysis (variables, specimens, comparative material) are given in **Table 4.9**.

Cranial Analyses:

Tables 5.1.1-5.1.18 present pairwise Mahalanobis' distances for all given cranial analyses. Matrices are symmetrical, therefore identical above and below the diagonal row; only the bottom left section of the matrix will be shown in this study. **Tables 5.2.1-5.2.6** present significance values at the 95% level for all cranial analyses given at the end of each subset. **Table 5.3.1** provides the legend for specimens in the PCoA plots. PCoA plots (see **Figure 5.1-5.18**) are presented after each Mahalanobis' distance table.

Cranial Analysis 1: Midface-Maxilla

Analysed variables, specimens, and comparative samples for this and subsequent analyses are listed in **Table 4.9**.

Mahalanobis' distances between fossils groups based on a *Homo sapiens* model of variation are illustrated in **Table 5.1.1** and **Figure 5.1.** OH 5 is significantly different from all the other specimens. SK 46, and SK 83 are also significantly different from each other. **Figure 5.1**

depicts DNH 7, OH 5, SK 46 and SK 79 as outliers from the rest of the specimens. SK 83 and Sts 52 form a cluster.

Performing the same analysis using a *P.troglodytes* model of variation, results are slightly different. DNH 7 has the largest distance value (from OH 5) (**Table 5.1.2**) and is significantly different from all other specimens except SK46. OH 5 is again significantly different from all other specimens. A number of the Swartkrans specimens are significantly different from each other. In the PCoA OH 5, Sts 52 and Sts 71 are separate from the other individuals as illustrated in **Figure 5.2**. DNH 7 and SK 46 form a cluster

Table 5.1.3 illustrates Mahalanobis' distances between fossil specimens based on a *G. gorilla* V/CV matrix. OH 5 is significantly different from all other specimens except SK 79. SK 83 is also significantly different from SK 46 and SK 79. In **Figure 5.3** DNH 7 and SK 46 are outliers separated from the rest of the specimens. OH 5 and SK 79 form clusters including SK 83 and Sts 52 indicating similar morphology.

Table 5.1.1. Matrix of pairwise Mahalanobis' distances for Cranial Analysis 1 generated using a *H. sapiens* variance-covariance matrix. Non-bolded, non-italicized values indicate distances that are not significant using any models. Bolded values indicate distances that are statistically significant using all models. Non-bolded, italicized values indicate distances that are significant using some, but not all models; super-scripted numbers indicate the models for which these distances are significant (1 = significant using human data and human variance-covariance matrix, 2 = significant using human data and chimpanzee variance-covariance matrix, 3 = significant using human data and gorilla variance-covariance matrix, 4 = significant using chimpanzee data and chimpanzee variance-covariance matrix, 5 = significant using chimpanzee data and human variance-covariance matrix, 6 = significant using chimpanzee data and gorilla variance-covariance matrix, 7 = significant using gorilla data and gorilla variance-covariance matrix, 8 = significant using gorilla data and chimpanzee variance-covariance matrix, 9 = significant using gorilla data and human variance-covariance matrix).

	OH 5	**SK 46**	**SK 79**	**SK 83**	**DNH 7**	**Sts 52**	**Sts 71**
OH 5	0						
SK 46	*39.23* [5,7]	0					
SK 79	*41.93* [4,5,6,7]	0.59	0				
SK 83	*26.39* [5]	13.87	17.87	0			
DNH 7	*48.18* [1,4,5,6,7]	1.79	3.32	12.31	0		
Sts 52	*25.33* [5]	17.06	*22.11* [5]	0.68	15.52	0	
Sts 71	*28.49* [5]	11.89	16.51	1.29	10.69	1.18	0

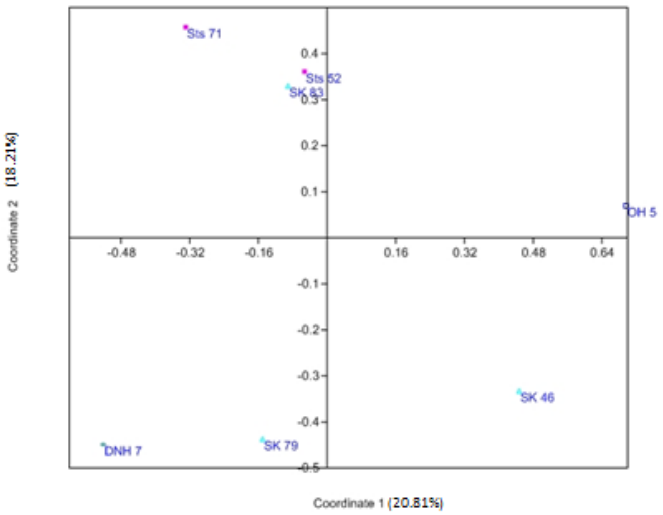

Figure 5.1. Principal coordinate plot of distances among fossils for Cranial Analysis 1 using a *H. sapiens* variance-covariance matrix.

Table 5.1.2. Matrix of pairwise Mahalanobis' distances for Cranial Analysis 1 generated using a *P. troglodytes* variance-covariance matrix. Non-bolded, non-italicized values indicate distances that are not significant using any model. Bolded values indicate distances that are statistically significant using all models. Non-bolded, italicized values indicate distances that are significant using some, but not all models; super-scripted numbers indicate the models for which these distances are significant; values 1-9 as listed in the caption for **Table 5.1.1**.

	OH 5	**SK 46**	**SK 79**	**SK 83**	**DNH 7**	**Sts 52**	**Sts 71**
OH 5	0						
SK 46	*91.11* [1,4,5,6,7]	0					
SK 79	*77.75* [1,4,5,6,7]	7.53	0				
SK 83	*48.30* [5,6,7]	*29.44* [5]	*31.40* [5]	0			
DNH 7	*111.03* [**1,4,5,6,7**]	14.16	*26.22* [5]	*28.10* [5]	0		
Sts 52	*54.70* [1,4,5,6,7]	*33.30* [5]	*48.00* [1,4,5,6,7]	10.47	*38.30* [5]	0	
Sts 71	*62.54* [1,4,5,6,7]	19.60	*31.79* [5]	19.24	*40.31* [5,6,7]	9.48	0

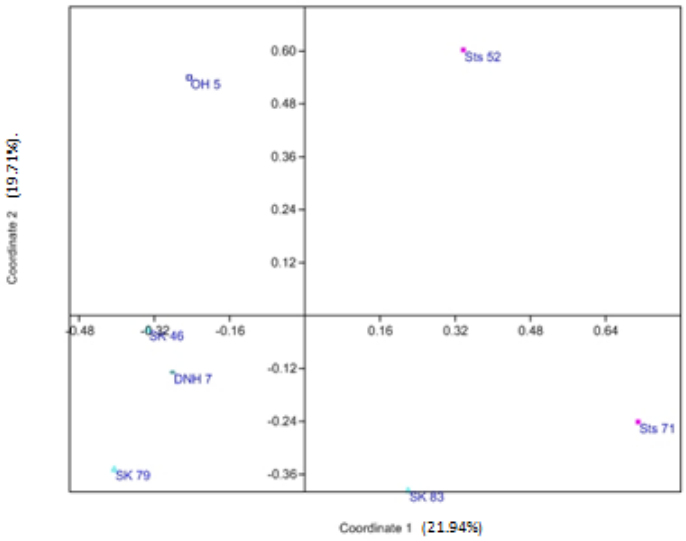

Figure 5.2. Principal coordinate plot of distances among fossils for Cranial Analysis 1 using a *P. troglodytes* variance-covariance matrix.

Table 5.1.3. Matrix of pairwise Mahalanobis' distances for Cranial Analysis 1 generated using a *G. gorilla* variance-covariance matrix. Non-bolded, non-italicized values indicate distances that are not significant using any model. Bolded values indicate distances that are statistically significant using all models. Non-bolded, italicized values indicate distances that are significant using some, but not all models; super-scripted numbers indicate the models for which these distances are significant; values 1-9 as listed in the caption for **Table 5.1.1**.

	OH 5	**SK 46**	**SK 79**	**SK 83**	**DNH 7**	**Sts 52**	**Sts 71**
OH 5	0						
SK 46	*29.07* [5]	0					
SK 79	16.83	2.41	0				
SK 83	*34.16* [5]	*25.35* [5]	*22.24* [5]	0			
DNH 7	*35.98* [5]	9.35	11.51	14.11	0		
Sts 52	*37.01* [5]	17.42	18.98	5.91	10.01	0	
Sts 71	*45.28*[5,6,7]	16.55	19.71	12.82	20.00	5.53	0

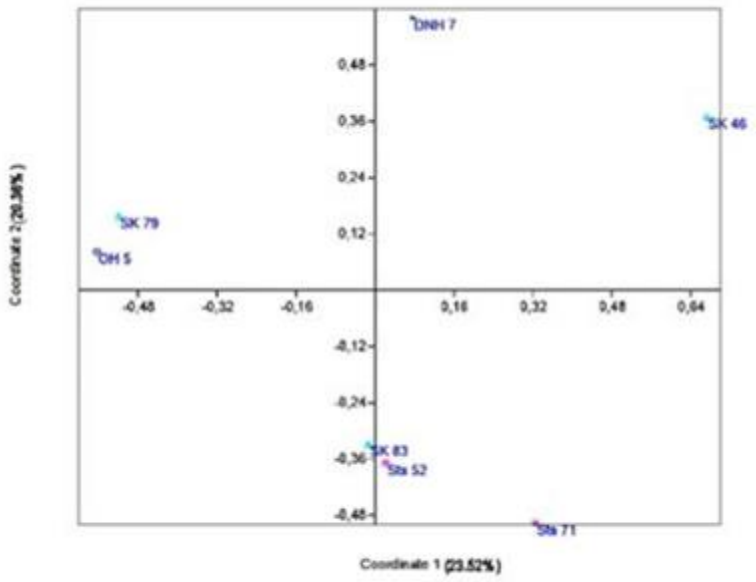

Figure 5.3. Principal coordinate plot of distances among fossils for Cranial Analysis 1 using a *G. gorilla* variance-covariance matrix.

Table 5.2.1. Significance values: Mahalanobis' Distance values for determining significance in fossil specimens for Cranial Analysis 1**.**

Human Human	Human Chimp	Human Gorilla	Chimp Chimp	Chimp Human	Chimp Gorilla	Gorilla Gorilla	Gorilla Chimp	Gorilla Human
47.70	5289.96	3625.44	45.57	21.75	40.25	38.79	654.7	195.33
1	2	3	4	5	6	7	8	9

Table 5.3.1. Legend for Principal Coordinate Graphs (adapted from Schroeder, 2007).

Site name	Site Abbreviation	Country	Symbol
Drimolen	DNH	South Africa	⬭ Oval
Swartkrans	SK	South Africa	△ Triangle
Sterkfontein	Sts	South Africa	■ Filled Square
Koobi Fora	KNM-ER	Kenya	◇ Diamond
West Turkana	KNM-WT	Kenya	✚ Cross
Olduvai Gorge	OH	Tanzania	□ Square

Cranial Analysis 2: Zygomatic

The results of significance tests for the Mahalanobis' distances using a *H. sapiens* are shown in **Table 5.1.4.** Sts 5 (comparative *A. africanus*) has the largest value, indicating that it is significantly different from OH 5 under all models. All other individuals also differ significantly from each other, under various extant V/CV models/tests. **Figure 5.4** shows how these individuals are distinct from each other with no clear clustering.

Table 5.1.5 shows the pairwise Mahalanobis' distances for **Cranial Analysis 2** using a *P. troglodytes* V/CV matrix. Most of the individuals are significantly different from each other, with OH 5 being the most different. DNH 7 is most similar to SK48 and KNM-ER 732. In **Figure 5.5** OH 5, Sts 5 and Sts 71 are distinctly separate from the cluster formed by KNM ER 732, DNH 7 and SK 48.

Using a *G. gorilla* model of variation for **Cranial Analysis 2** to examine Mahalanobis' distances (**Table 5.1.6**), OH 5 is again distinct from all other specimens. There appear to be affiliations between DNH 7 and Sts 71, and between KNM-ER 732 and a number of the South African specimens. In **Figure 5.6** OH 5, KNM-ER 732 and Sts 5 are outliers. DNH 7, SK 48 and Sts 71 form a loose cluster separated from the other observations.

Table 5.1.4. Matrix of pairwise Mahalanobis' distances for Cranial Analysis 2 generated using a *H. sapiens* variance-covariance matrix. Non-bolded, non-italicized values indicate distances that are not significant using any model. Bolded values indicate distances that are statistically significant using all models. Non-bolded, italicized values indicate distances that are significant using some, but not all models; super-scripted numbers indicate the models for which these distances are significant; values 1-9 as listed in the caption for **Table 5.1.1**.

	KNM-ER 732	**OH 5**	**SK 48**	**DNH 7**	**Sts 5**	**Sts 71**
KNM-ER 732	0					
OH 5	*100.71* [1,2,3,4,7,8,9]	0				
SK 48	*20.76* [3]	*105.63* [1,2,3,4,7,8,9]	0			
DNH 7	*30.42* [1,2,3,7]	*59.38* [1,2,3,4,7,8]	*45.74* [1,2,3,4,7]	0		
Sts 5	*45.34* [1,2,3,4,7]	**239.74**	*55.49* [1,2,3,4,7,8]	*86.99* [1,2,3,4,7,8,9]	0	
Sts 71	*17.09* [3]	*144.52* [1,2,3,4,7,8,9]	*38.9* [1,2,3,4,7]	*31.78* [1,2,3,4,7]	*19.26* [3]	0

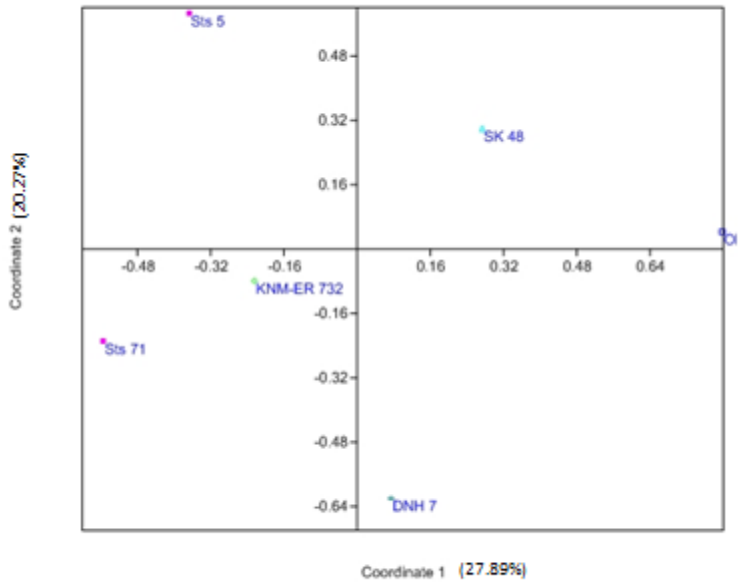

Figure 5.4. Principal coordinate plot of distances among fossils for Cranial Analysis 2 using a *H. sapiens* variance-covariance matrix.

Table 5.1.5. Matrix of pairwise Mahalanobis' distances for Cranial Analysis 2 generated using a *P. troglodytes* variance-covariance matrix. Non-bolded, non-italicized values indicate distances that are not significant using any model. Bolded values indicate distances that are statistically significant using all models. Non-bolded, italicized values indicate distances that are significant using some, but not all models; super-scripted numbers indicate the models for which these distances are significant; values 1-9 as listed in the caption for **Table 5.1.1**.

	KNM-ER 732	**OH 5**	**SK 48**	**DNH 7**	**Sts 5**	**Sts 71**
KNM-ER 732	0					
OH 5	*72.86* [1,2,3,4,7,8]	0				
SK 48	13.89	*50.24* [1,2,3,4,7]	0			
DNH 7	*17.11* [3]	*61.43* [1,2,3,4,7,8]	*23.77* [2,3,7]	0		
Sts 5	*44.49* [1,2,3,4,7]	*181.57* [1,2,3,4,7,8,9]	*61.59* [1,2,3,4,7,8]	*47.4* [1,2,3,4,7]	0	
Sts 71	*23.39* [2,3,7]	*120.36* [1,2,3,4,7,8,9]	*40.86* [1,2,3,4,7]	12.95	12.83	0

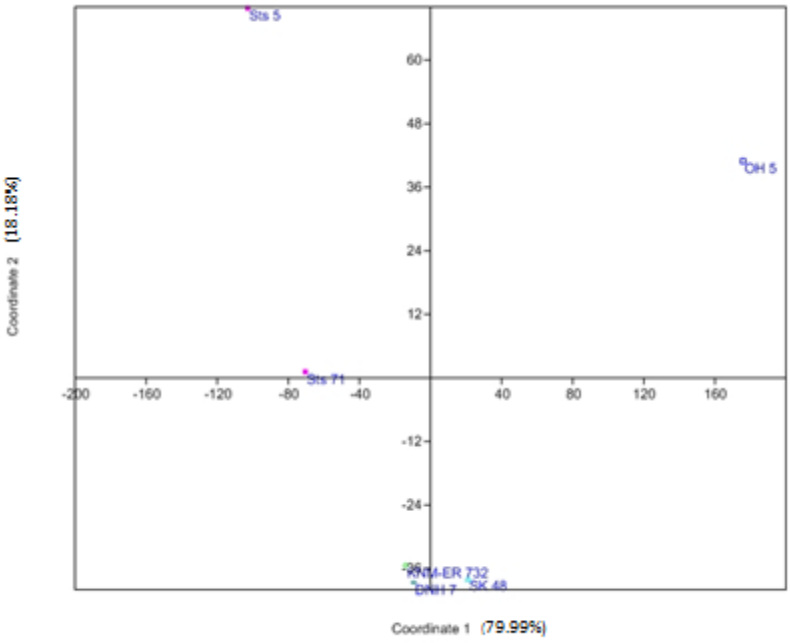

Figure 5.5. Principal coordinate plot of distances among fossils for Cranial Analysis 2 using a *P. troglodytes* variance-covariance matrix.

Table 5.1.6. Matrix of pairwise Mahalanobis' distances for Cranial Analysis 2 generated using a *G. gorilla* variance-covariance matrix. Non-bolded, non-italicized values indicate distances that are not significant using any model. Bolded values indicate distances that are statistically significant using all models. Non-bolded, italicized values indicate distances that are significant using some, but not all models; super-scripted numbers indicate the models for which these distances are significant; values 1-9 as listed in the caption for **Table 5.1.1**.

	KNM-ER 732	**OH 5**	**SK 48**	**DNH 7**	**Sts 5**	**Sts 71**
KNM-ER 732	0					
OH 5	*28.23* [1,2,3,7]	0				
SK 48	11.38	*50.07* [1,2,3,4,7]	0			
DNH 7	13.29	*27.51* [1,2,3,7]	*18.28* [3]	0		
Sts 5	*31.33* [1,2,3,7]	*102.67* [1,2,3,4,7,8,9]	*20.94* [3]	*35.12* [1,2,3,4,7]	0	
Sts 71	12.51	*52.66* [1,2,3,4,7]	14.25	8.09	11.95	0

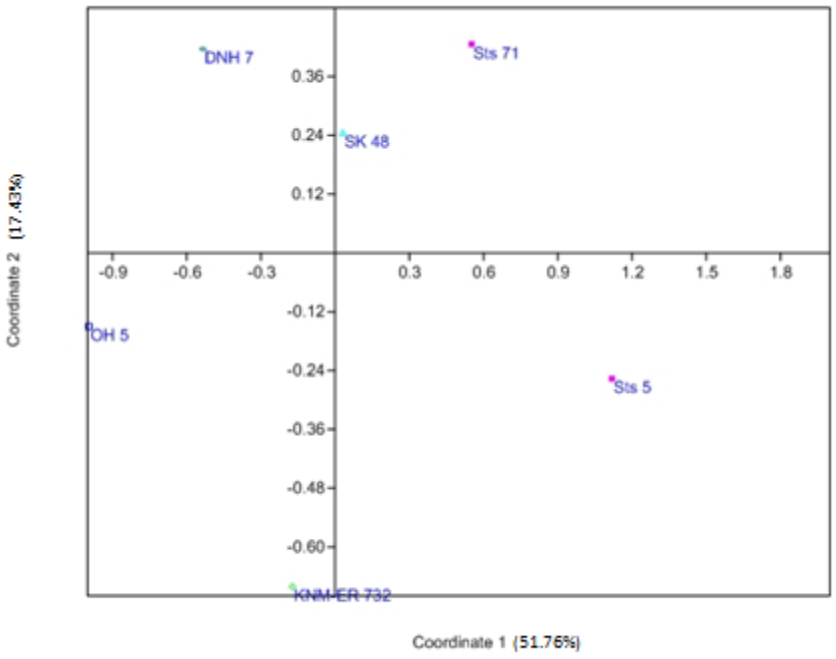

Figure 5.6. Principal coordinate plot of distances among fossils for Cranial Analysis 2 using a *G. gorilla* variance-covariance matrix.

Table 5.2.2. Significance values: Mahalanobis' Distance values for determining significance in fossil specimens for Cranial Analysis 2.

Human Human	Human Chimp	Human Gorilla	Chimp Chimp	Chimp Human	Chimp Gorilla	Gorilla Gorilla	Gorilla Chimp	Gorilla Human
27.39	21.32	15.62	31.59	826.10	188.00	23.25	53.72	85.61
1	2	3	4	5	6	7	8	9

Cranial Analysis 3: Zygomatic-Upper face

Table 5.1.7 shows Mahalanobis' distances and results of significance testing using a *H. sapiens* V/CV matrix and **Figure 5.7** show the results of the PCoA. All specimens are significantly different from each other under this model. Sts 71 has the largest distance (from KNM-ER 406), followed by SK 48 (from Sts 71). Fossil specimens are distinct from each other and are separate illustrated in **Figure 5.7.**

The results using a *P. troglodytes* V/CV matrix are depicted in **Table 5.1.8** and the graph of the PCoA is shown in **Figure 5.8.** The results are comparable to what was seen for the human model.

Table 5.1.9 displays the results of significance testing for Mahalanobis' distances using a *G. gorilla* V/CV matrix. These results are illustrated in **Figure 5.9.** Although the magnitude of the distances is less, the pattern is similar to the other two analyses, with Sts 71 once again most distant from KNMER 406. The plot displays a similar trend to the *P. troglodytes* model. SK 48 and Sts 5 are distinct from each other and Sts 71 and KNM-ER 406 are closest.

Table 5.1.7. Matrix of pairwise Mahalanobis' distances for Cranial Analysis 3 generated using a *H. sapiens* variance-covariance matrix Non-bolded, non-italicized values indicate distances that are not significant using any model. Bolded values indicate distances that are statistically significant using all models. Non-bolded, italicized values indicate distances that are significant using some, but not all models; super-scripted numbers indicate the models for which these distances are significant; values 1-9 as listed in the caption for **Table 5.1.1**.

	KNM-ER 406	**SK 48**	**Sts 5**	**Sts 71**
KNM-ER 406	0			
SK 48	*100.1* [1,2,3,4,6,7]	0		
Sts 5	*91.29* [1,2,3,4,6,7]	*87.03* [1,2,3,4,6,7]	0	
Sts 71	*192.62* [1,2,3,4,5,6,7]	*117.16* [1,2,3,4,6,7]	*43.06* [3,4,7]	0

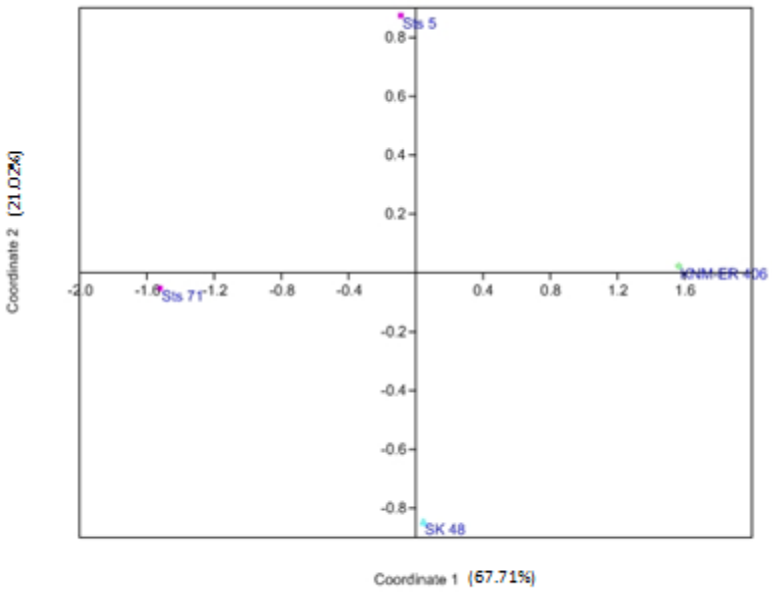

Figure 5.7. Principal coordinate plot of distances among fossils for Cranial Analysis 3 using a *H. sapiens* variance-covariance matrix.

Table 5.1.8. Matrix of pairwise Mahalanobis' distances for Cranial Analysis 3 generated using a *P. troglodytes* variance-covariance matrix. Non-bolded, non-italicized values indicate distances that are not significant using any model. Bolded values indicate distances that are statistically significant using all models. Non-bolded, italicized values indicate distances that are significant using some, but not all models; super-scripted numbers indicate the models for which these distances are significant; values 1-9 as listed in the caption for **Table 5.1.1**.

	KNM-ER 406	**SK 48**	**Sts 5**	**Sts 71**
KNM-ER 406	0			
SK 48	*113.28* [1,2,3,4,6,7]	0		
Sts 5	*120.47* [1,2,3,4,6,7]	*67.61* [1,2,3,7]	0	
Sts 71	*218.72* [1,2,3,4,6,7,8]	*124.92* [1,2,3,4,6,7]	34	0

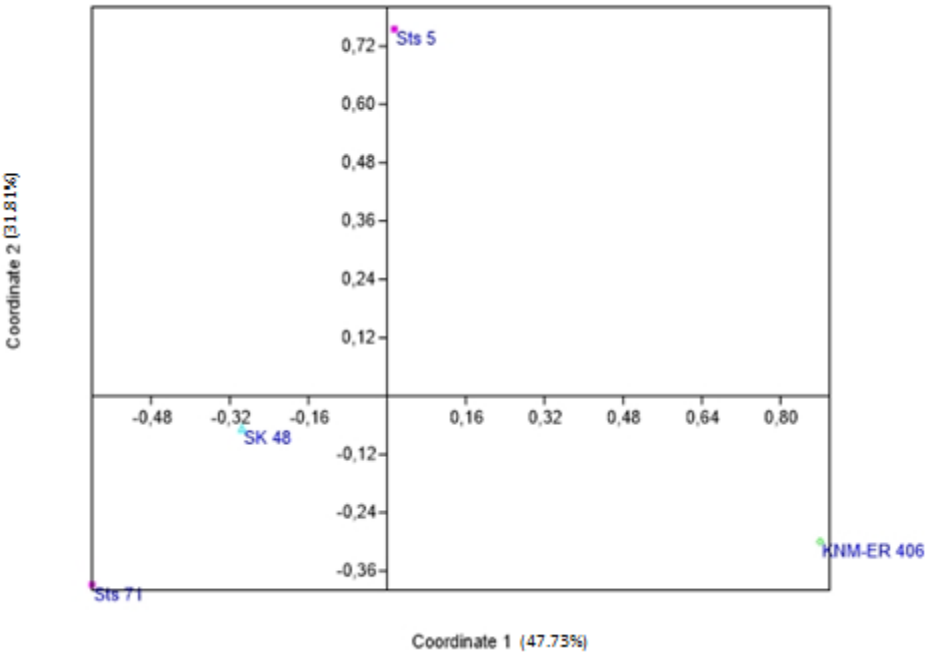

Figure 5.8. Principal coordinate plot of distances among fossils for Cranial Analysis 3 using a *P. troglodytes* variance-covariance matrix.

Table 5.1.9. Matrix of pairwise Mahalanobis' distances for Cranial Analysis 3 generated using a *G. gorilla* variance-covariance matrix Non-bolded, non-italicized values indicate distances that are not significant using any model. Bolded values indicate distances that are statistically significant using all models. Non-bolded, italicized values indicate distances that are significant using some, but not all models; super-scripted numbers indicate the models for which these distances are significant; values 1-9 as listed in the caption for **Table 5.1.1**.

	KNM-ER 406	**SK 48**	**Sts 5**	**Sts 71**
KNM-ER 406	0			
SK 48	*66.76* [1,3,4,7]	0		
Sts 5	*45.41* [1,3,4,7]	34.78	0	
Sts 71	*107.37* [1,2,3,4,7]	*54.71* [1,3,4,7]	23.06	0

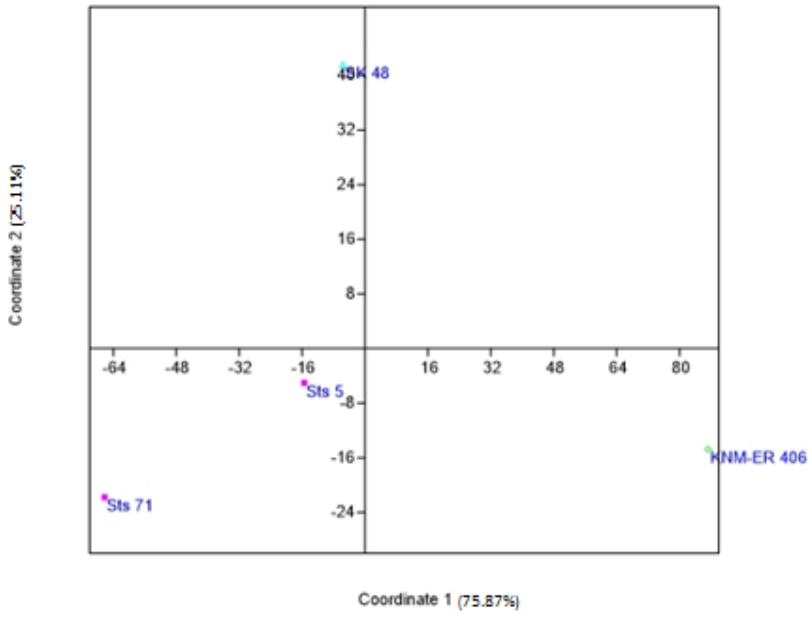

Figure 5.9. Principal coordinate plot of distances among fossils for Cranial Analysis 3 using a *G. gorilla* variance-covariance matrix.

Table 5.2.3. Significance values: Mahalanobis' Distance values for determining significance in fossil specimens for Cranial Analysis 3.

Human Human	Human Chimp	Human Gorilla	Chimp Chimp	Chimp Human	Chimp Gorilla	Gorilla Gorilla	Gorilla Chimp	Gorilla Human
44.33	76.46	36.17	39.37	302.64	73.62	40.85	194.28	230.32
1	2	3	4	5	6	7	8	9

Cranial Analysis 4: Upperface-Temporal

The results of significance testing for Mahalanobis' distances for **Cranial Analysis 4** using a *H. sapiens* V/CV matrix are depicted in **Table 5.1.10**, and **Figure 5.10** (PCoA). DNH 7 and Sts 5 are the most distant from each other.

Table 5.1.11 and **Figure 5.11** show the results of the significance tests for the Mahalanobis' distances and the PCoA plot, respectively, for **Cranial Analysis 4** using a *P. troglodytes* V/CV matrix. In this analysis the distance values are comparable, with KNM-ER 732 and Sts 5 being the most distinct. Similar to the *H. sapiens* model, specimens are quite clearly separate from each other in the PCoA plot.

Table 5.1.12 shows the results of significance tests of the Mahalanobis' distance for **Cranial Analysis 4** using a *G. gorilla* V/CV matrix, and **Figure 5.12** displays the results of the PCoA for this analysis. These results are consistent with the other analyses.

Table 5.1.10. Matrix of pairwise Mahalanobis' distances for Cranial Analysis 4 generated using a *H. sapiens* variance-covariance matrix. Non-bolded, non-italicized values indicate distances that are not significant using any model. Bolded values indicate distances that are statistically significant using all models. Non-bolded, italicized values indicate distances that are significant using some, but not all models; super-scripted numbers indicate the models for which these distances are significant; values 1-9 as listed in the caption for **Table 5.1.1**.

	KNM-ER 732	**DNH 7**	**Sts 5**
KNM-ER 732	0		
DNH 7	*54.30* [1,2,3,4,7]	0	
Sts 5	*56.83* [1,2,3,4,7]	*92.43* [1,2,3,4,7]	0

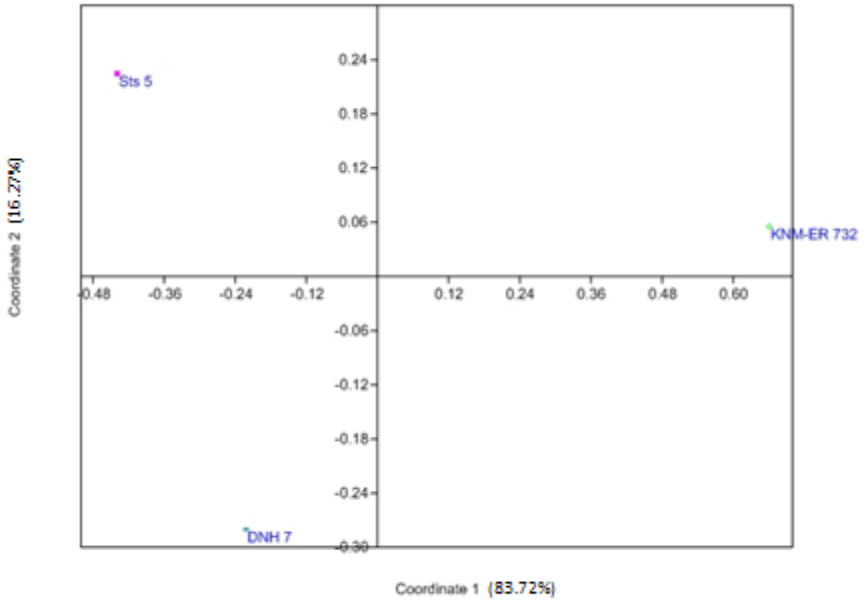

Figure 5.10. Principal coordinate plot of distances among fossils for Cranial Analysis 4 using a *H. sapiens* variance-covariance matrix.

Table 5.1.11. Matrix of pairwise Mahalanobis' distances for Cranial Analysis 4 generated using a *P. troglodytes* variance-covariance matrix. Non-bolded, non-italicized values indicate distances that are not significant using any model. Bolded values indicate distances that are statistically significant using all models. Non-bolded, italicized values indicate distances that are significant using some, but not all models; super-scripted numbers indicate the models for which these distances are significant; values 1-9 as listed in the caption for **Table 5.1.1**.

	KNM-ER 732	**DNH 7**	**Sts 5**
KNM-ER 732	0		
DNH 7	*32.18* [2,3,7]	0	
Sts 5	*58.37* [1,2,3,4,7]	*48.97* [1,2,3,4,7]	0

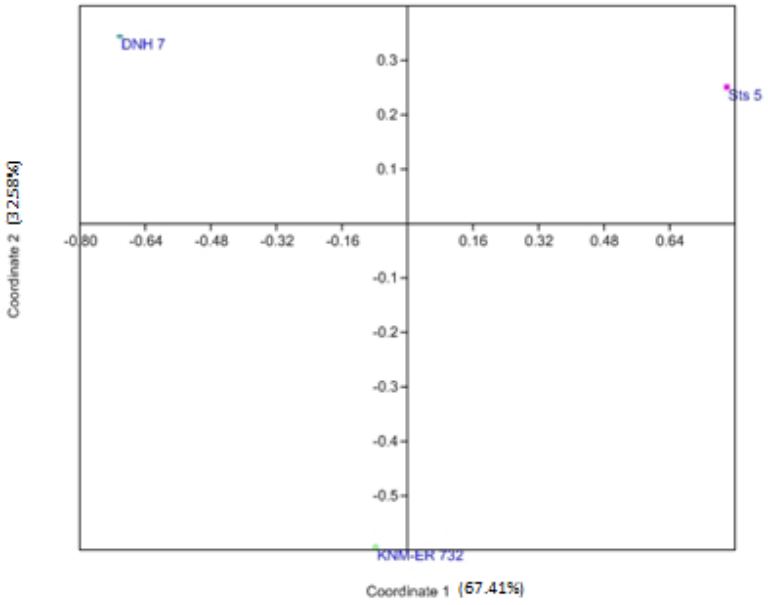

Figure 5.11. Principal coordinate plot of distances among fossils for Cranial Analysis 4 using a *P. troglodytes* variance-covariance matrix.

Table 5.1.12. Matrix of pairwise Mahalanobis' distances for Cranial Analysis 4 generated using a *G. gorilla* variance-covariance matrix. Non-bolded, non-italicized values indicate distances that are not significant using any model. Bolded values indicate distances that are statistically significant using all models. Non-bolded, italicized values indicate distances that are significant using some, but not all models; super-scripted numbers indicate the models for which these distances are significant; values 1-9 as listed in the caption for **Table 5.1.1**.

	KNM-ER 732	**DNH 7**	**Sts 5**
KNM-ER 732	0		
DNH 7	*33.34* [1,2,3,7]	0	
Sts 5	*48.18* [1,2,3,4,7]	*44.21* [1,2,3,4,7]	0

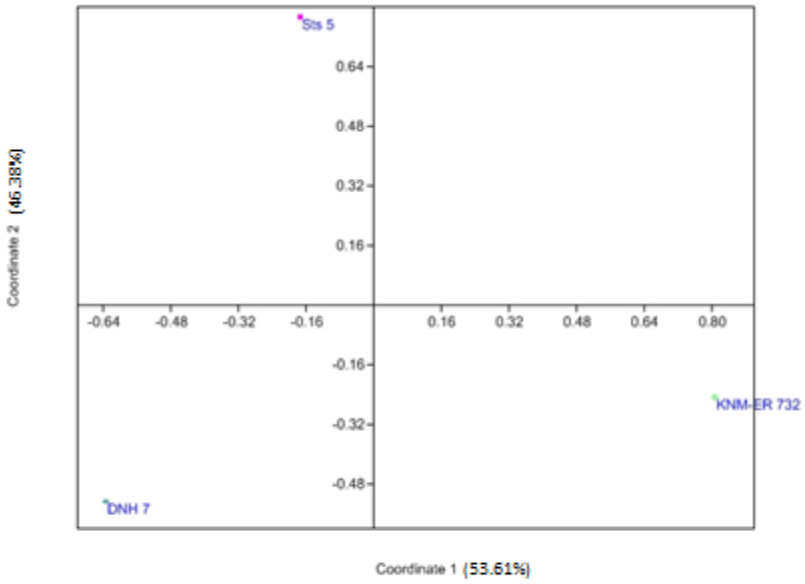

Figure 5.12. Principal coordinate plot of distances among fossils for Cranial Analysis 4 using a *G. gorilla* variance-covariance matrix.

Table 5.2.4. Significance values: Mahalanobis' Distance values for determining significance in fossil specimens for Cranial Analysis 4.

Human Human	Human Chimp	Human Gorilla	Chimp Chimp	Chimp Human	Chimp Gorilla	Gorilla Gorilla	Gorilla Chimp	Gorilla Human
32.98	29.39	27.69	34.13	946.46	210.42	29.72	99.89	161.19
1	2	3	4	5	6	7	8	9

Cranial Analysis 5: Basicranium

Mahalanobis' distances and results of significance tests for **Cranial Analysis 5**, using a *H. sapiens* V/CV matrix, are in **Table 5.1.13.** Sts 5 and KNM-ER 406 are most distinct. **Figure 5.13** illustrates KNM-WT 17 000, KNM-ER 406 and Sts 5 widely separated from each other.

Table 5.1.14 and **Figure 5.14** show the results of **Cranial Analysis 5** using a *P. troglodytes* V/CV matrix. The pattern is similar to the previous analysis.

Table 5.1.15 shows the results of significance tests for the Mahalanobis' distances for **Cranial Analysis 5** using a *G. gorilla* V/CV matrix, and **Figure 5.15** shows the results of the PCoA for this analysis**.** Results display the same trend exhibited in the other two models. Albeit with slightly smaller distance values.

.

Table 5.1.13. Matrix of pairwise Mahalanobis' distances for Cranial Analysis 5 generated using a *H. sapiens* variance-covariance matrix Non-bolded, non-italicized values indicate distances that are not significant using any model. Bolded values indicate distances that are statistically significant using all models. Non-bolded, italicized values indicate distances that are significant using some, but not all models; super-scripted numbers indicate the models for which these distances are significant; values 1-9 as listed in the caption for **Table 5.1.1**.

	KNM-WT 17000	**KNM-ER 406**	**Sts 5**
KNM-WT 17000	0		
KNM-ER 406	*33.04* [1,3,6]	0	
Sts 5	*87.57* [1,2,3,4,5,6,7]	*130.69* [1,2,3,4,5,6,7]	0

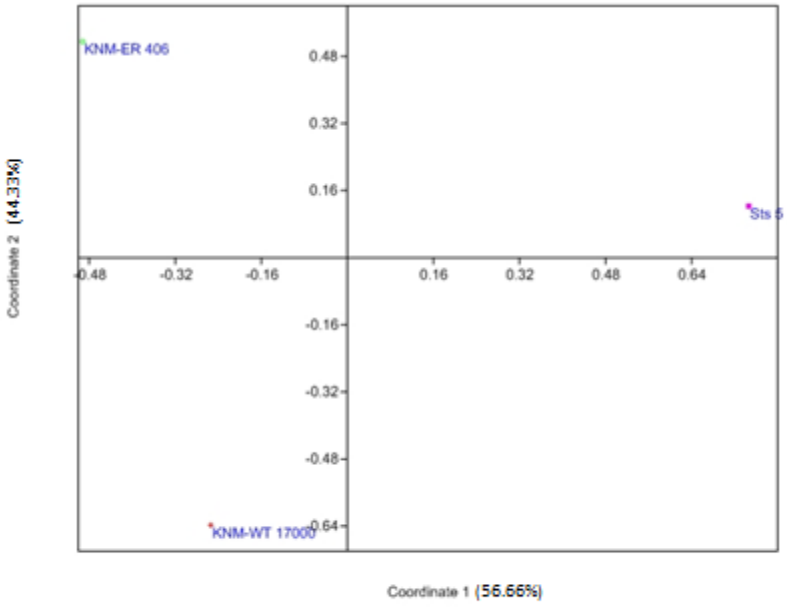

Figure 5.13. Principal coordinate plot of distances among fossils for Cranial Analysis 5 using a *H. sapiens* variance-covariance matrix.

Table 5.1.14. Matrix of pairwise Mahalanobis' distances for Cranial Analysis 5 generated using a *P. troglodytes* variance-covariance matrix. Non-bolded, non-italicized values indicate distances that are not significant using any model. Bolded values indicate distances that are statistically significant using all models. Non-bolded, italicized values indicate distances that are significant using some, but not all models; super-scripted numbers indicate the models for which these distances are significant; values 1-9 as listed in the caption for **Table 5.1.1**.

	KNM-WT 17000	**KNM-ER 406**	**Sts 5**
KNM-WT 17000	0		
KNM-ER 406	*45.47* [1,3,4,6]	0	
Sts 5	*82.26* [1,2,3,4,5,6,7]	*139.29* [1,2,3,4,5,6,7,9]	0

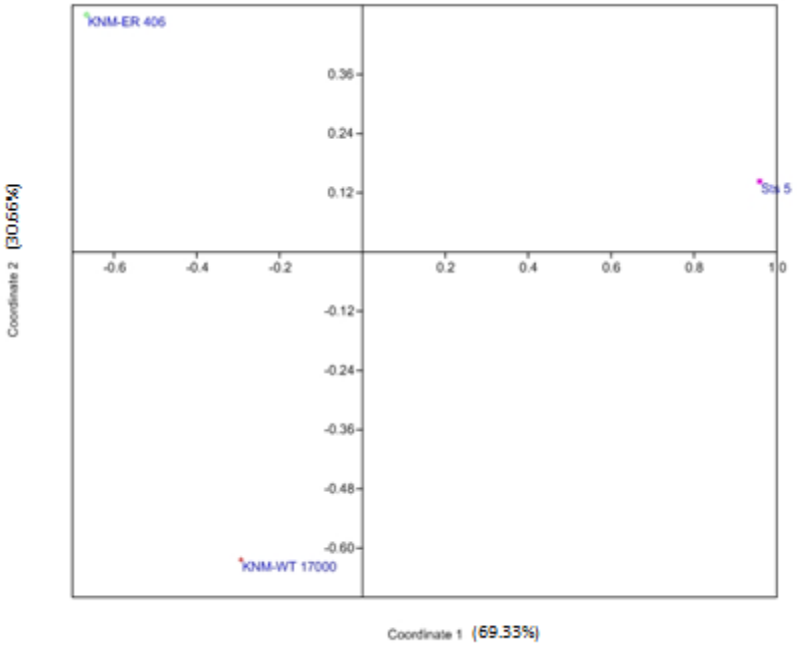

Figure 5.14. Principal coordinate plot of distances among fossils for Cranial Analysis 5 using a *P. troglodytes* variance-covariance matrix.

Table 5.1.15. Matrix of pairwise Mahalanobis' distances for Cranial Analysis 5 generated using a *G. gorilla* variance-covariance matrix. Non-bolded, non-italicized values indicate distances that are not significant using any model. Bolded values indicate distances that are statistically significant using all models. Non-bolded, italicized values indicate distances that are significant using some, but not all models; super-scripted numbers indicate the models for which these distances are significant; values 1-9 as listed in the caption for **Table 5.1.1**.

	KNM-WT 17000	**KNM-ER 406**	**Sts 5**
KNM-WT 17000	0		
KNM-ER 406	*25.34* [6]	0	
Sts 5	*39.75* [1,3,4,6]	*84.79* [1,2,3,4,5,6,7]	0

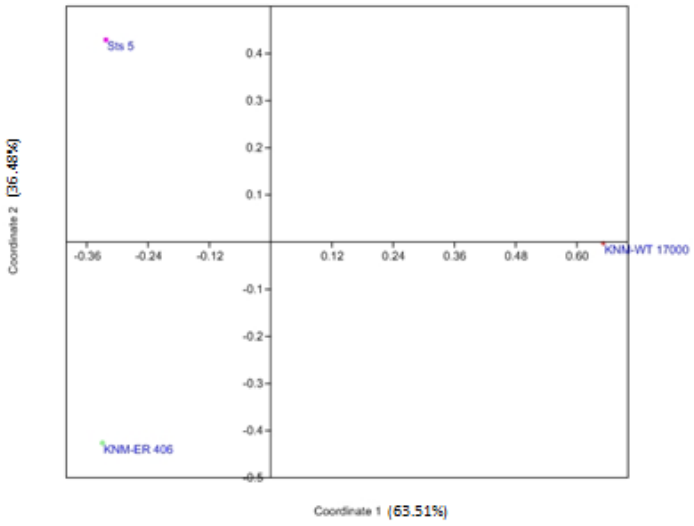

Figure 5.15. Principal coordinate plot of distances among fossils for Cranial Analysis 5 using a *G. gorilla* variance-covariance matrix.

Table 5.2.5. Significance values: Mahalanobis' Distance values for determining significance in fossil specimens for Cranial Analysis 5.

Human Human	Human Chimp	Human Gorilla	Chimp Chimp	Chimp Human	Chimp Gorilla	Gorilla Gorilla	Gorilla Chimp	Gorilla Human
31.74	55.14	27.61	34.24	48.93	20.67	45.79	227.93	142.84
1	2	3	4	5	6	7	8	9

Cranial Analysis 6: Temporal

Results of significance testing of the Mahalanobis' distances for **Cranial Analysis 6** using a *H. sapiens* V/CV matrix are depicted in **Table 5.1.16.** DNH 7 is significant for all models/tests. SK 48 is significantly different from DNH 7 followed in value by Sts 5. SK 48 stands out as being extremely distant, relative to all the other specimens, but all of the specimens are significantly different from each other. **Figure 5.16**, which shows the results of the PCoA analysis for subset 6 using a *H. sapiens* V/CV. All specimens are distinct and separate from each other. Sts 5 is almost completely off the chart followed by SK 48.

The results of the significance tests for the Mahalanobis' distance for **Cranial Analysis 6** using the *P. troglodytes* V/CV matrix are shown in **Table 5.1.17. Figure 5.17** shows the results of the PCoA analysis. The results are similar to the human V/CV results above.

Table 5.1.18 displays the results of significance tests for the Mahalanobis' distances for **Cranial Analysis 6** using a *G. gorilla* V/VC matrix, and **Figure 5.18** shows the results from the PCoA for this analysis. Once again, SK 48 is quite distinct from all other specimens, in contrast to DNH 7 which is most similar to the other specimens (except SK 48). This trend is similar to that was seen in the other analyses. SK 48, DNH 7 and KNM WT 17000 are separate from the KNM ER 406 and Sts 5 cluster.

Table 5.1.16. Matrix of pairwise Mahalanobis' distances for Cranial Analysis 6 generated using a *H. sapiens* variance-covariance matrix. Non-bolded, non-italicized values indicate distances that are not significant using any model. Bolded values indicate distances that are statistically significant using all models. Non-bolded, italicized values indicate distances that are significant using some, but not all models; super-scripted numbers indicate the models for which these distances are significant; values 1-9 as listed in the caption for **Table 5.1.1**.

	KNM-WT 17000	**KNM-ER 406**	**SK 48**	**DNH 7**	**Sts 5**
KNM-WT 17000	0				
KNM-ER 406	*32.53* [4]	*0*			
SK 48	*478.96* [1,2,3,4,5,6,7,9]	*478.7* [1,2,3,4,5,6,7,9]	0		
DNH 7	*43.15* [1,2,3,6]	*76.86* [1,3,4,5,6,7]	**707.1**	0	
Sts 5	*50.73* [1,3,4,6,7]	*58.47* [1,3,4,5,6,7]	510.54 [1,2,3,4,5,6,7,9]	*36.66* [1,3,4]	0

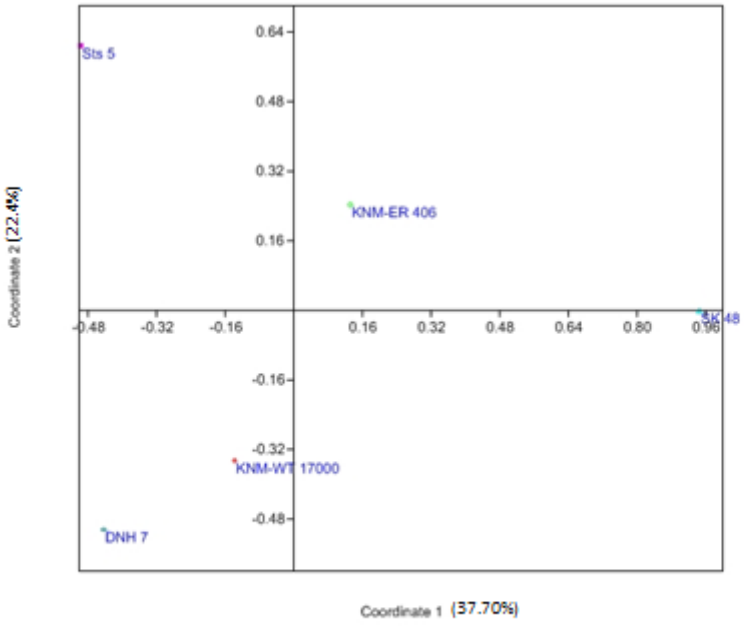

Figure 5.16. Principal coordinate plot of distances among fossils for Cranial Analysis 6 using a *H. sapiens* variance-covariance matrix.

Table 5.1.17. Matrix of pairwise Mahalanobis' distances for Cranial Analysis 6 generated using a *P. troglodytes* variance-covariance matrix Non-bolded, non-italicized values indicate distances that are not significant using any model. Bolded values indicate distances that are statistically significant using all models. Non-bolded, italicized values indicate distances that are significant using some, but not all models; super-scripted numbers indicate the models for which these distances are significant; values 1-9 as listed in the caption for **Table 5.1.1**.

	KNM-WT 17000	**KNM-ER 406**	**SK 48**	**DNH 7**	**Sts 5**
KNM-WT 17000	0				
KNM-ER 406	*57.63* [1,2,3,5,6,7]	0			
SK 48	*405.33* [1,2,3,4,5,6,7,9]	*442.95* [1,2,3,4,5,6,7,9]	0		
DNH 7	*95.05* [1,3,4,5,6,7]	*82.2* [1,3,4,5,6,7]	*371* [1,2,3,4,5,6,7,9]	0	
Sts 5	*116.96* [1,2,3,4,5,6]	*60.32* [1,3,4,5,6,7]	*331.21* [1,2,3,4,5,6,7,9]	22.04	0

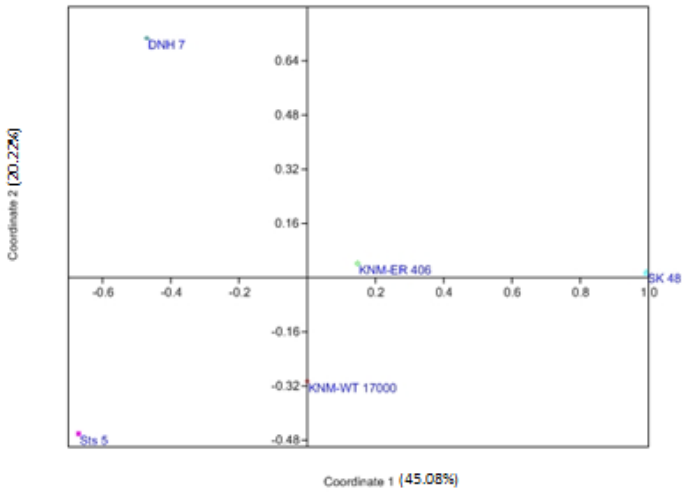

Figure 5.17. Principal coordinate plot of distances among fossils for Cranial Analysis 6 using a *P. troglodytes* variance-covariance matrix.

Table 5.1.18. Matrix of pairwise Mahalanobis' distances for Cranial Analysis 6 generated using a *G. gorilla* variance-covariance matrix. Non-bolded, non-italicized values indicate distances that are not significant using any model. Bolded values indicate distances that are statistically significant using all models. Non-bolded, italicized values indicate distances that are significant using some, but not all models; super-scripted numbers indicate the models for which these distances are significant; values 1-9 as listed in the caption for **Table 5.1.1**.

	KNM-WT 17000	**KNM-ER 406**	**SK 48**	**DNH 7**	**Sts 5**
KNM-WT 17000	0				
KNM-ER 406	25.42	0			
SK 48	*324.1* [1,2,3,4,5,6,7,9]	*392.74* [1,2,3,4,5,6,7,9]	0		
DNH 7	19.44	19.58	*432.35* [1,2,3,4,5,6,7,9]	0	
Sts 5	*33.58* [1,3,4]	27.52	*310.84* [1,2,3,4,5,6,7,9]	22.298	0

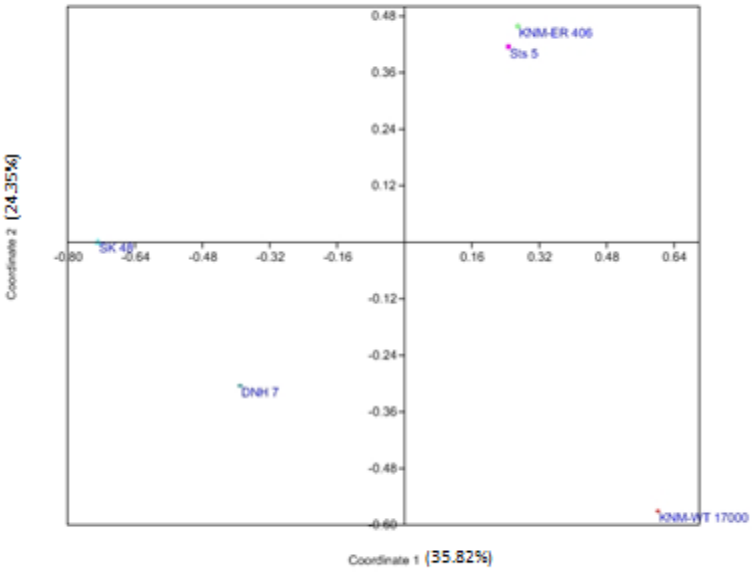

Figure 5.18. Principal coordinate plot of distances among fossils for Cranial Analysis 6 using a *G. gorilla* variance-covariance matrix.

Table 5.2.6. Significance values: Mahalanobis' Distance values for determining significance in fossil specimens for Cranial Analysis 6.

Human Human	Human Chimp	Human Gorilla	Chimp Chimp	Chimp Human	Chimp Gorilla	Gorilla Gorilla	Gorilla Chimp	Gorilla Human
33.16	128.85	31.09	29.82	52.07	35.01	46.45	610.07	134.90
1	2	3	4	5	6	7	8	9

Mandibular Analyses:

Tables 5.1.19-5.1.27 illustrate pairwise Mahalanobis' distances. **Tables 5.2.7-5.2.9** show significance values at the 95% level for all mandibular analyses at the end of each subset. **Table 5.3.1** provides the legend for specimens in the PCoA plots. PCoA plots (see **Figure 5.19-5.27**) are presented after each Mahalanobis' distance table.

Mandibular Analysis 1: Ramus

Results of significance testing of the Mahalanobis' distances for **Mandibular Analysis 1** using a *H. sapiens* V/CV matrix are presented in **Table 5.1.19** which shows that all specimens are significantly different from each other, except SK 34 LEFT and SK 23. Moreover, DNH 7 and SK 34 RIGHT are significantly different from other specimens (KNM-ER 729 and SK 12, and SK 23, respectively) irrespective of the model used to assess significance across all extant model combinations. **Figure 5.19** visually confirms SK 34 RIGHT as an outlier separate from all the other specimens including KNM-ER 729. SK 12 and SK 23 form a cluster, as do DNH 7 and SK 34 LEFT.

Table 5.1.20 shows the pairwise Mahalanobis' distances between fossils based on a *P. troglodytes* V/CV matrix. KNM-ER 729 and SK 12 are significantly different from all other specimens. The remaining specimens also differ from each other significantly in various ways. **Figure 5.20** shows that most of the specimens are separated, with DNH 7 closest to SK 34 RIGHT.

When the same analysis is done using a *G. gorilla* model of variation, the results differ to a certain extent (**Table 5.1.21**), although the general pattern is similar. Interestingly, in the previous analyses SK 34 RIGHT and SK 34 LEFT differed significantly from each other, suggesting that distortion plays a role, that the model being used as a substitute for variation is poor, or that the variables used are not good taxonomic indicators. This analysis supports the middle option, and suggests that the gorilla may be a better model for variation in the mandible, as it does not consider the difference between SK 34 RIGHT and LEFT as significant. Indeed, as can be seen in **Figure 5.21** SK 34 RIGHT and SK 34 RIGHT form a tight cluster.SK 23 and KNM-ER are depicted as outliers in the graph.

Table 5.1.19. Matrix of pairwise Mahalanobis' distances for Mandibular Analysis 1 generated using a *H. sapiens* variance-covariance matrix. Non-bolded, non-italicized values indicate distances that are not significant using any model. Bolded values indicate distances that are statistically significant using all models. Non-bolded, italicized values indicate distances that are significant using some, but not all models; super-scripted numbers indicate the models for which these distances are significant; values 1-9 as listed in the caption for **Table 5.1.1**.

	KNM-ER 729	**SK 12**	**SK 23**	**SK 34 left**	**SK 34 right**	**DNH 7**
KNM-ER 729	0					
SK 12	*57.61* [1,3,4,7]	0				
SK 23	*46.51* [1,4,7]	*106.32* [1,3,4,6,7,8]	0			
SK 34 left	*110.41* [1,3,4,6,7,8]	*166.54* [1,2,3,4,6,7,8,9]	14.84	0		
SK 34 right	*123.72* [1,2,3,4,6,7,8]	**183.28**	*40.20* [1,4,7]	*28.83* [1,4]	0	
DNH 7	**209.73**	**337.88**	*79,36* [1,3,4,6,7]	*53.07* [1,4,7]	*39.48* [1,4,7]	0

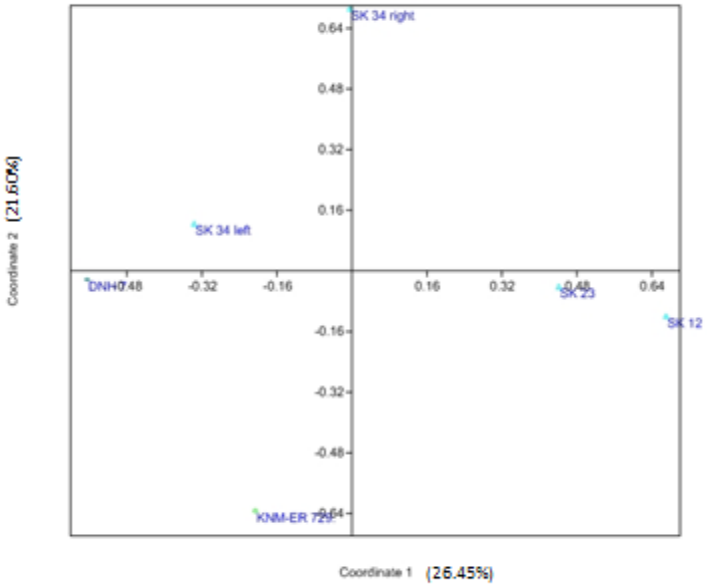

Figure 5.19. Principal coordinate plot of distances among fossils for Mandibular Analysis 1 using a *H. sapiens* variance-covariance matrix.

Table 5.1.20. Matrix of pairwise Mahalanobis' distances for Mandibular Analysis 1 generated using a *P. troglodytes* variance-covariance matrix. Non-bolded, non-italicized values indicate distances that are not significant using any model. Bolded values indicate distances that are statistically significant using all models. Non-bolded, italicized values indicate distances that are significant using some, but not all models; super-scripted numbers indicate the models for which these distances are significant; values 1-9 as listed in the caption for **Table 5.1.1**.

	KNM-ER 729	**SK 12**	**SK 23**	**SK 34 left**	**SK 34 right**	**DNH 7**
KNM-ER 729	0					
SK 12	*125.57* [1,2,3,4,6,7,8]	0				
SK 23	*67.76* [1,3,4,6,7]	*51.94* [1,3,7]	0			
SK 34 left	*125.73* [1,2,3,4,6,7,8]	*70.89* [1,3,4,6,7]	12.4	0		
SK 34 right	*135.99* [1,2,3,4,6,7,8]	*111.96* [1,3,4,6,7,8]	*40.14* [1,4,7]	*33.15* [1,4,7]	0	
DNH 7	*75.71* [1,3,4,6,7]	*112.68* [1,3,4,6,7,8]	21.33	*27.99* [1,4]	20.07	0

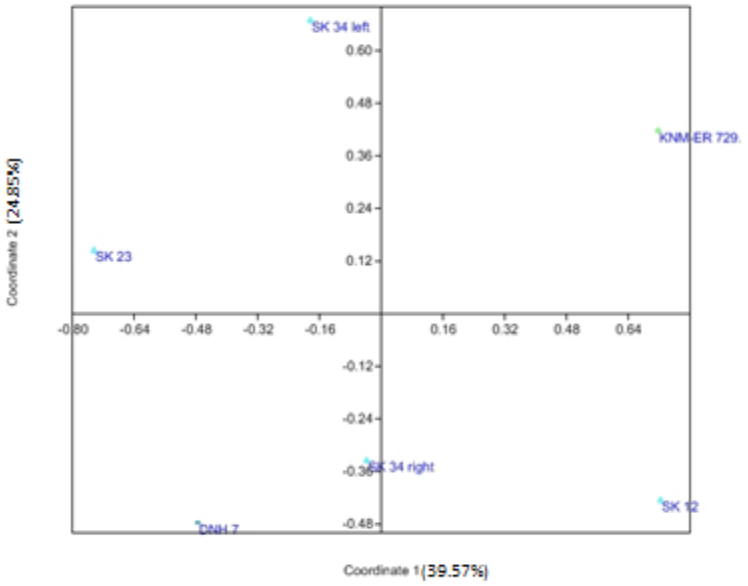

Figure 5.20. Principal coordinate plot of distances among fossils for Mandibular Analysis 1 using a *P. troglodytes* variance-covariance matrix.

Table 5.1.21. Matrix of pairwise Mahalanobis' distances for Mandibular Analysis 1 generated using a *G. gorilla* variance-covariance matrix. Non-bolded, non-italicized values indicate distances that are not significant using any model. Bolded values indicate distances that are statistically significant using all models. Non-bolded, italicized values indicate distances that are significant using some, but not all models; super-scripted numbers indicate the models for which these distances are significant; values 1-9 as listed in the caption for **Table 5.1.1**.

	KNM-ER 729	**SK 12**	**SK 23**	**SK 34 left**	**SK 34 right**	**DNH 7**
KNM-ER 729	0					
SK 12	*38.00* [1,4,7]	0				
SK 23	23.01	*53.07* [1,4,7]	0			
SK 34 left	*40.56* [1,4,7]	*74.61* [1,3,4,6,7]	5.12	0		
SK 34 right	*47.37* [1,4,7]	*95.28* [1,3,4,6,7]	17.55	19.56	0	
DNH 7	*42.29* [1,4,7]	*88.32* [1,3,4,6,7]	6.99	7.7	14.18	0

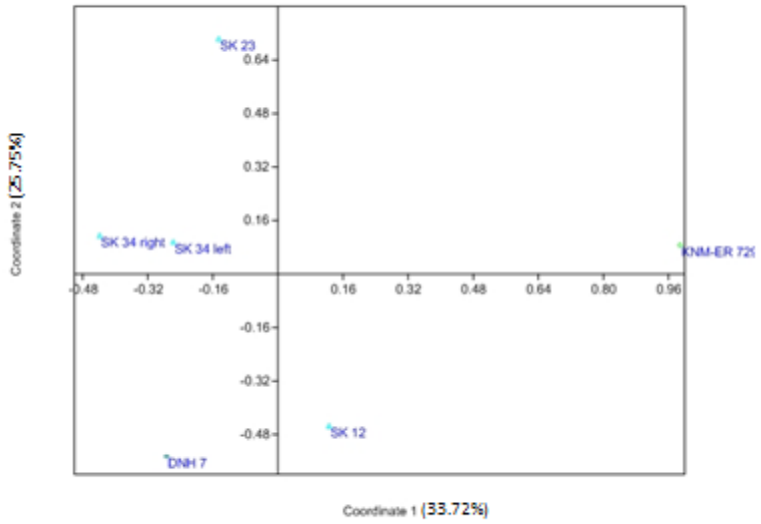

Figure 5.21. Principal coordinate plot of distances among fossils for Mandibular Analysis 1 using a *G. gorilla* variance-covariance matrix.

Table 5.2.7. Significance values: Mahalanobis' Distance values for determining significance in fossil specimens for Mandibular Analysis 1.

Human Human	Human Chimp	Human Gorilla	Chimp Chimp	Chimp Human	Chimp Gorilla	Gorilla Gorilla	Gorilla Chimp	Gorilla Human
27.24	121.48	53.47	23.54	166.90	59.29	30.22	101.27	143.15
1	2	3	4	5	6	7	8	9

Mandibular Analysis 2: Corpus

Mahalanobis' distances between fossil specimens based on a *Homo sapiens* model of variation are illustrated in **Table 5.1.22** and **Figure 5.22.** This analysis largely distinguished DNH 7 and DNH 8 from all the other specimens, regardless of the model that is used to test significance. This result is also shown in **Figure 5.22**, as DNH 8 and DNH 7 are separated from the rest of the specimens. **Figure 5.22** also shows SK 34 LEFT and SK 81 separated (generally) from the other specimens. SK 23 and SK 876 are in such close proximity that it is difficult to separate them in the graph. Both SK 23 and SK 876 form a cluster with SK 34 RIGHT, SK 12 and SKW 5. Within the same plot, KNM-ER 729 and KNM-ER 403 form a cluster where KNM-ER 3230 forms a loose cluster with these two specimens. These two clusters are located quite close to each other.

Table 5.1.23 shows the pairwise Mahalanobis' distances for **Mandibular Analysis 2** using a *P. troglodytes* V/CV matrix. Again, DNH 8 and DNH 7 (to a lesser degree), are significantly different from all other specimens. The East African specimens KMN-ER 729 and 3230 are also significantly different from most or all of the other specimens., and KMN-ER 403 somewhat less so. **Figure 5.23** which displays the results of PCoA for Analysis 2 using a *P. troglodytes* V/CV shows both DNH 8 and SK 81 as outliers.

Using a *G. gorilla* model of variation for **Mandibular Analysis 2** to examine Mahalanobis' distances (**Table 5.1.24)** again DNH 8 is significantly different from all other specimens, regardless of the model that is used. As in the other analyses, DNH 7 is also distinct form all other specimens. This result is also shown in the PCoA (**Figure 5.24**), in which DNH 8 is an outlier. DNH 7 and SK 34 LEFT are separated from the other specimens. East African specimens form relatively tighter clusters than South African specimens that are distributed across the plot in a generally more spread out fashion.

Table 5.1.22. Matrix of pairwise Mahalanobis' distances for Mandibular Analysis 2 generated using a *H. sapiens* variance-covariance matrix. Non-bolded, non-italicized values indicate distances that are not significant using any model. Bolded values indicate distances that are statistically significant using all models. Non-bolded, italicized values indicate distances that are significant using some, but not all models; super-scripted numbers indicate the models for which these distances are significant; values 1-9 as listed in the caption for **Table 5.1.1**

	KNM-ER 403	KNM-ER 729	KNM-ER 3230	SK 12	SK 23.	SK 34 left	SK 34 right	SK 81	SK 876	SKW 5	DNH 7	DNH 8
KNM-ER 403	0											
KNM-ER 729	*35,15* [4]	0										
KNM-ER 3230	31.99	2.8	0									
SK 12	8.93	*33,27* [4]	32.51	0								
SK 23.	2.56	27.16	24.42	4.76	0							
SK 34 LEFT	12.38	12.64	15.92	12.99	8.61	0						
SK 34 RIGHT	*35,86* [4]	17.51	28.3	*35,53* [4]	32.82	8.32	0					
SK 81	13.72	16.39	17	7.56	7.7	9.09	26.84	0				
SK 876	*37,30* [4]	*42,34* [4]	*36,05* [4]	17.68	22.27	30.86	*60,66* [1,4,6,7]	21.78	0			
SKW 5	7.07	*42,05* [4]	*37,02* [4]	3.04	5.45	20.65	*50,171* [1,4]	10.34	23.57	0		
DNH 7	*75,11* [1,4,6,7]	*124,07* [1,3,4,5,6,7]	*107,30* [1,3,4,5,6,7]	*84,29* [1,4,5,6,7]	*79,20* [1,4,6,7]	*82,48* [1,4,6,7]	*109,02* [1,3,4,5,6,7]	*105,47* [1,3,4,5,6,7]	*94,10* [1,3,4,5,6,7]	*78,16* [1,4,6,7]	0	
DNH 8	*75,95* [1,4,6,7]	*155,18* [1,2,3,4,5,6,7,8]	*151,96* [1,2,3,4,5,6,7]	*88,09* [1,3,4,5,6,7]	*97,50* [1,3,4,5,6,7]	*119,89* [1,3,4,5,6,7]	*142,69* [1,3,4,5,6,7]	*104,95* [1,3,4,5,6,7]	**159.79**	*77,25* [1,4,6,7]	**180.41**	0

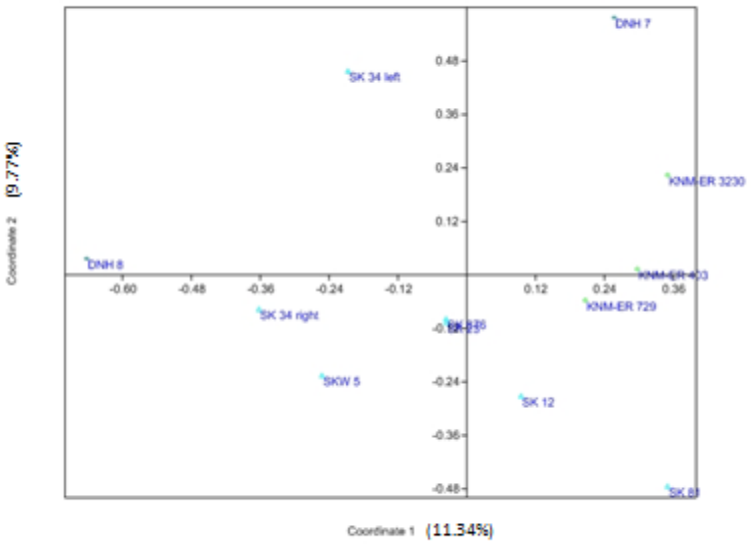

Figure 5.22. Principal coordinate plot of distances among fossils for Mandibular Analysis 2 using a *H. sapiens* variance-covariance matrix.

Table 5.1.23. Matrix of pairwise Mahalanobis' distances for Mandibular Analysis 2 generated using a *P. troglodytes* variance-covariance matrix. Non-bolded, non-italicized values indicate distances that are not significant using any model. Bolded values indicate distances that are statistically significant using all models. Non-bolded, italicized values indicate distances that are significant using some, but not all models; super-scripted numbers indicate the models for which these distances are significant; values 1-9 as listed in the caption for **Table 5.1.1**.

	KNM-ER 403	KNM-ER 729	KNM-ER 3230	SK 12	SK 23.	SK 34 left	SK 34 right	SK 81	SK 876	SKW 5	DNH 7	DNH 8
KNM-ER 403	0											
KNM-ER 729	*59.07* [1,4,6,7]	0										
KNM-ER 3230	*61.98* [1,4,6,7]	2.28	0									
SK 12	6.79	*74.93* [1,4,6,7]	*81.02* [1,4,6,7]	0								
SK 23.	5.91	*52.72* [1,4,7]	*58.06* [1,4,6,7]	10.29	0							
SK 34 LEFT	12.02	*35.88* [4]	*42.61* [4]	19.68	5.36	0						
SK 34 RIGHT	22.32	29.46	*38.22* [4]	31.92	20.42	5.88	0					
SK 81	19.72	*77.11* [1,4,6,7]	*78.51* [1,4,6,7]	14.54	20.39	25.88	*39.33* [4]	0				
SK 876	*36.93* [4]	*72,87* [1,4,6,7]	*74,66* [1,4,6,7]	*35,31* [4]	18.89	23.47	*46,66* [4]	19.99	0			
SKW 5	12.52	*101,46* [1,3,4,5,6,7]	*103,86* [1,3,4,5,6,7]	4.23	21.81	*36,56* [4]	*52,45* [1,4,7]	14.62	*45,45* [4]	0		
DNH 7	*65,39* [1,4,6,7]	**174.23**	**173.52**	*73,83* [1,4,6,7]	*75,72* [1,4,6,7]	*79,70* [1,4,6,7]	*92,89* [1,3,4,5,6,7]	*104,48* [1,3,4,5,6,7]	*114,12* [1,3,4,5,6,7]	*71,91* [1,4,6,7]	0	
DNH 8	**455.95**	**613.44**	**592.05**	**451.43**	**554.68**	**574.66**	**553.82**	**441**	**627.8**	**395.51**	**556**	0

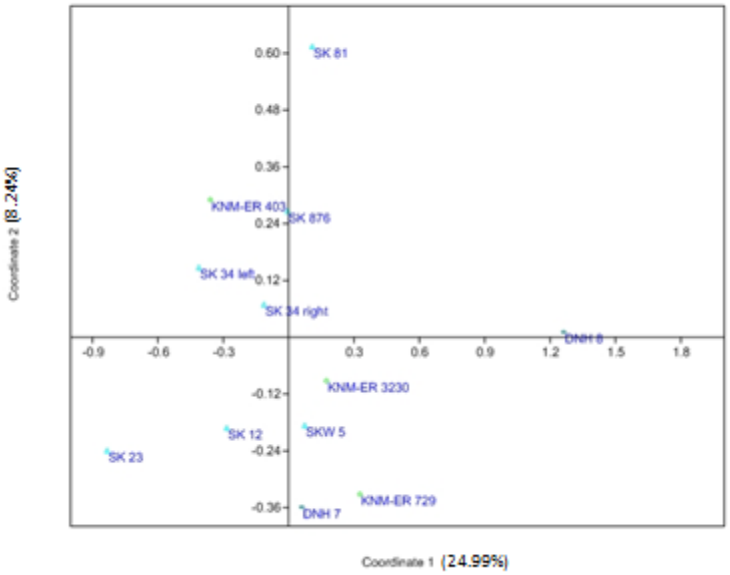

Figure 5.23. Principal coordinate plot of distances among fossils for Mandibular Analysis 2 using a *P. troglodytes* variance-covariance matrix.

Table 5.1.24. Matrix of pairwise Mahalanobis' distances for Mandibular Analysis 2 generated using a *G. gorilla* variance-covariance matrix. Non-bolded, non-italicized values indicate distances that are not significant using any model. Bolded values indicate distances that are statistically significant using all models. Non-bolded, italicized values indicate distances that are significant using some, but not all models; super-scripted numbers indicate the models for which these distances are significant; values 1-9 as listed in the caption for **Table 5.1.1**.

	KNM-ER 403	**KNM-ER 729**	**KNM-ER 3230**	**SK 12**	**SK 23.**	**SK 34 left**	**SK 34 right**	**SK 81**	**SK 876**	**SKW 5**	**DNH 7**	**DNH 8**
KNM-ER 403	0											
KNM-ER 729	31.86	0										
KNM-ER 3230	23.65	3.41	0									
SK 12	10.33	18.76	19.59	0								
SK 23.	3.39	25.76	21.54	5.87	0							
SK 34 LEFT	18.21	11.65	16.59	4.49	10.66	0						
SK 34 RIGHT	*50.29* [1,4,7]	17.08	30.88	22.55	40.93	10.17	0					
SK 81	19.95	16.62	18.21	4.37	12.86	5.47	19.5	0				
SK 876	27.49	26.23	26.16	11.48	14.45	12.38	*34.93* [4]	6.54	0			
SKW 5	5.22	29.31	24.02	3.23	5.01	12.93	*39.72* [4]	8.86	15.82	0		
DNH 7	*44.23* [4]	*81.81* [1,4,6,7]	*74.07* [1,4,6,7]	*41.73* [4]	*48.28* [1,4]	*47.61* [1,4]	*68.78* [1,4,6,7]	*50.37* [1,4,7]	*57.64* [1,4,6,7]	*35.04* [4]	0	
DNH 8	*154.34* [1,2,3,4,5,6,7]	**199.84**	**173.02**	**183.69**	**196.01**	**211.79**	**231.5**	**190.35**	**243.34**	*158.80* [1,2,3,4,5,6,7,8]	**187.53**	0

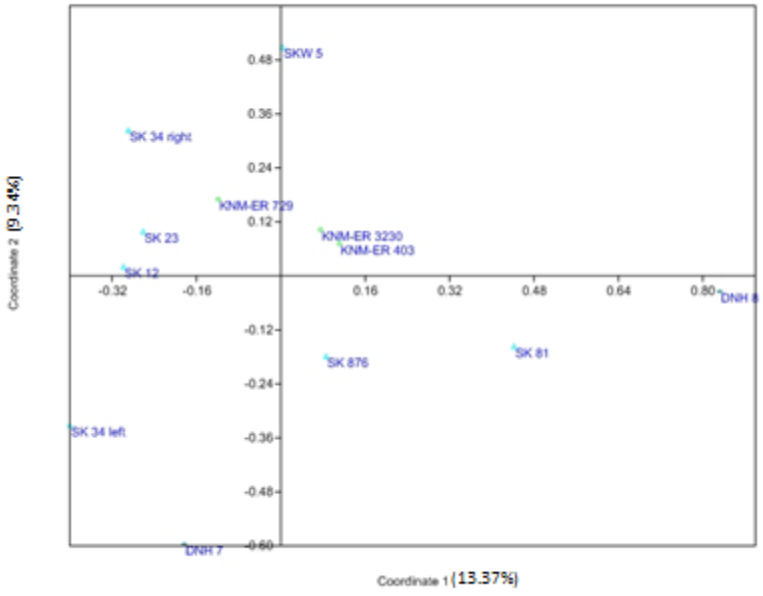

Figure 5.24. Principal coordinate plot of distances among fossils for Mandibular Analysis 2 using a *G. gorilla* variance-covariance matrix.

Table 5.2.8. Significance values: Mahalanobis' Distance values for determining significance in fossil specimens for Mandibular Analysis 2**.**

Human Human	Human Chimp	Human Gorilla	Chimp Chimp	Chimp Human	Chimp Gorilla	Gorilla Gorilla	Gorilla Chimp	Gorilla Human
47.15	144.06	84.46	33.15	83.63	54.72	50.22	155.09	159.09
1	2	3	4	5	6	7	8	9

Mandibular Analysis 3: Midline

Table 5.1.25 shows the Mahalanobis' distances and results of significance testing using a *H. sapiens* V/CV matrix, and **Figure 5.25** depicts the results of the PCoA. These results demonstrate that DNH 8 (and to a lesser extent DNH 7) is most distinct from the other specimens with significant values across all (or most) combinations of extant models. **Figure 5.25** shows that DNH 8 is separated from the cluster formed by KNM-ER 729 and SK 23. DNH 7 is distinct from SK 81 and SKW 5 cluster. KNM-ER 3230 is a clear outlier separated from the other specimens.

Table 5.1.26 displays the results of significance testing for Mahalanobis' distance for **Mandibular Analysis 3** using a *P. troglodytes* V/CV matrix. These results indicate that DNH 8, DNH 7 are again most distinct, including SK 23 but all of the other distances are also significant. **Figure 5.26** (PCoA graph for **Mandibular Analysis 3** using a *P. troglodytes* V/CV) shows that DNH 8, SKW 5 and SK 81 are generally separated from the other specimens. Specimens in this plot are all distinct from each other indicated by their sparse distribution across the graph.

Table 5.1.27 and **Figure 5.27** show the results of the significance tests for the Mahalanobis' distances and the PCoA plot, respectively, using a *G. gorilla* V/CV matrix. **Table 5.1.27** shows DNH 8 is significantly different from all other specimens regardless of the model that is used to assess significance. The overall pattern is similar to the other analyses. The PCoA plot shows that DNH 8 and SKW 5 (to a lesser degree) are separated from the rest of the specimens. DNH 7 and KNM-ER 3230 are in close proximity forming a cluster. SK 81 and KNM-ER 729 form a cluster.

Table 5.1.25. Matrix of pairwise Mahalanobis' distances for Mandibular Analysis 3 generated using a *H. sapiens* variance-covariance matrix. Non-bolded, non-italicized values indicate distances that are not significant using any model. Bolded values indicate distances that are statistically significant using all models. Non-bolded, italicized values indicate distances that are significant using some, but not all models; super-scripted numbers indicate the models for which these distances are significant; values 1-9 as listed in the caption for **Table 5.3.1**.

	KNM-ER 729	**KNM-ER 3230**	**SK 23**	**SK 81**	**SKW 5**	**DNH 7**	**DNH 8**
KNM-ER 729	0						
KNM-ER 3230	5.47	0					
SK 23	*55.06* [1,2,3,4,6,7]	*30.92* [1,4,6]	0				
SK 81	*19.23* [6]	12.17	*13.95* [6]	0			
SKW 5	*28.63* [1,4,6]	9.44	11.35	15.12	0		
DNH 7	*60.63* [1,2,3,4,6,7]	*52.36* [1,2,3,4,6,7]	*83.50* [1,2,3,4,6,7]	*62.32* [1,2,3,4,6,7]	*57.69* [1,2,3,4,6,7]	0	
DNH 8	**305.13**	**229.04**	*139.60* [1,2,3,4,6,7,8,9]	**232.49**	**149.12**	**272.95**	0

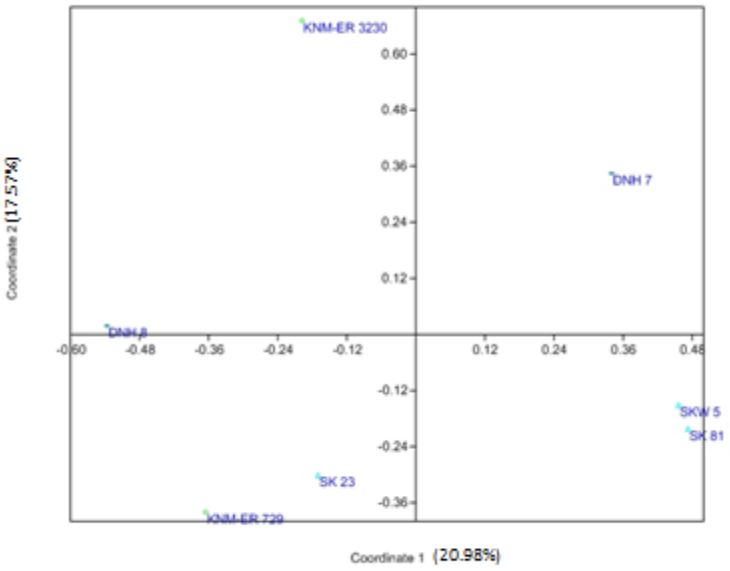

Figure 5.25. Principal coordinate plot of distances among fossils for Mandibular Analysis 3 using a *H. sapiens* variance-covariance matrix.

Table 5.1.26. Matrix of pairwise Mahalanobis' distances for Mandibular Analysis 3 generated using a *P. troglodytes* variance-covariance matrix. Non-bolded, non-italicized values indicate distances that are not significant using any model. Bolded values indicate distances that are statistically significant using all models. Non-bolded, italicized values indicate distances that are significant using some, but not all models; super-scripted numbers indicate the models for which these distances are significant; values 1-9 as listed in the caption for **Table 5.1.1**.

	KNM-ER 729	KNM-ER 3230	SK 23	SK 81	SKW 5	DNH 7	DNH 8
KNM-ER 729	0						
KNM-ER 3230	*13.87* [6]	0					
SK 23	**162.34**	*86.04* [1,2,3,4,6,7]	0				
SK 81	*52.68* [1,2,3,4,6,7]	*20.13* [6]	*35.22* [1,3,4,6]	0			
SKW 5	*83.57* [1,2,3,4,6,7]	*29.49* [1,4,6]	*20.34* [6]	*18.17* [6]	0		
DNH 7	**248.1**	**180.34**	**149.74**	**150.74**	*131.34* [1,2,3,4,6,7,8,9]	0	
DNH 8	**761.02**	**569.59**	**258.41**	**474.21**	**342.3**	**433.15**	0

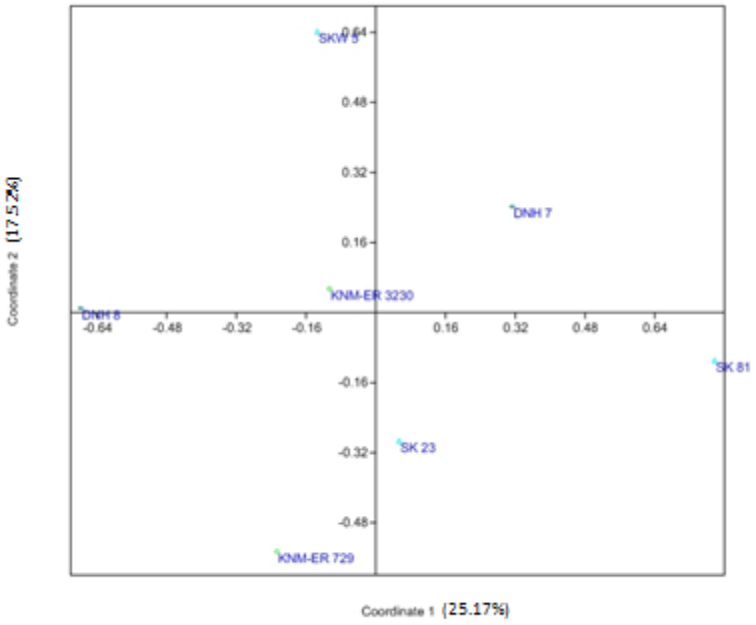

Figure 5.26. Principal coordinate plot of distances among fossils for Mandibular Analysis 3 using a *P. troglodytes* variance-covariance matrix.

Table 5.1.27. Matrix of pairwise Mahalanobis' distances for Mandibular Analysis 3 generated using a *G. gorilla* variance-covariance matrix. Non-bolded, non-italicized values indicate distances that are not significant using any model. Bolded values indicate distances that are statistically significant using all models. Non-bolded, italicized values indicate distances that are significant using some, but not all models; super-scripted numbers indicate the

models for which these distances are significant; values 1-9 as listed in the caption for **Table 5.1.1**.

	KNM-ER 729	KNM-ER 3230	SK 23	SK 81	SKW 5	DNH 7	DNH 8
KNM-ER 729	0						
KNM-ER 3230	9.74	0					
SK 23	*99.19* [1,3,4,6,7,8]	*47.95* [1,2,3,4,5,6,7]	0				
SK 81	*26.52* [1,4,6]	6.19	*24.81* [1,4,6]	0			
SKW 5	*58.17* [1,2,3,4,6,7]	*20.33* [6]	7.32	10.21	0		
DNH 7	*130.90* [1,2,3,4,6,7,8,9]	*85.93* [1,2,3,4,6,7]	*60.92* [1,2,3,4,6,7]	*67.49* [1,2,3,4,6,7]	*55.25* [1,2,3,4,6,7]	0	
DNH 8	**540.35**	**405.03**	**186.03**	**344.23**	**244.55**	**275.75**	0

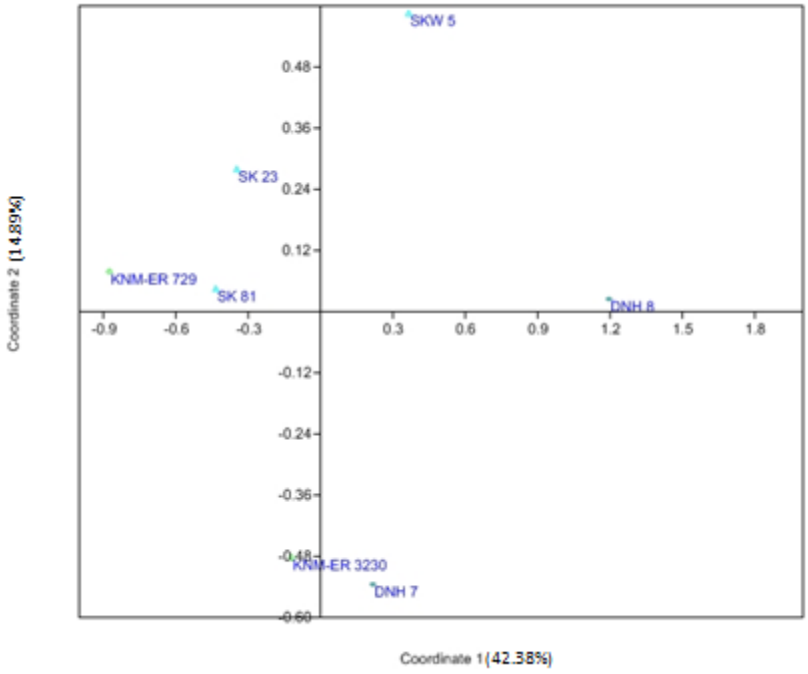

Figure 5.27. Principal coordinate plot of distances among fossils for Mandibular Analysis 3 using a *G. gorilla* variance-covariance matrix.

Table 5.2.9. Significance values: Mahalanobis' Distance values for determining significance in fossil specimens for Mandibular Analysis 3.

Human Human	Human Chimp	Human Gorilla	Chimp Chimp	Chimp Human	Chimp Gorilla	Gorilla Gorilla	Gorilla Chimp	Gorilla Human
22.53	47.45	32.41	22.15	147.78	12.98	42.92	93.38	110.14
1	2	3	4	5	6	7	8	9

Densified analyses:

This section includes three fossil individuals (OH 5, SK 79 and SK 48) with good, shared preservation of the palate. All analyses include five variables with the exception of **Densified Analysis 1** which includes sixteen variables. Matrices and significance values for Densified Analyses 1-9 can be found in **Appendix A. Tables A.1.1–Table A.1.27** present pairwise Mahalanobis's distances. **Tables A.2.1** shows significance values (for all densified analyses) at the 95% level. PCoA plots are not presented, as comparisons are between three individuals and therefore they offer little information (i.e. they are all essentially "triangles").

Densified Analysis 1: Center

The Mahalanobis' distances and results of significance tests under a *H. sapiens* model of V/CV are shown in **Table A.1.1**. (**APPENDIX A**). Under the human model the largest differences is between the East African (OH 5) and South African material. Using a *P. troglodytes* model of variation (**Table A.1.2**), the greatest distance is between the two South African specimens. Under a gorilla model of V/CV (**Table A.1.3**) none of the specimens are significantly different from each other.

Densified Analysis 2: M3 Complex

The Mahalanobis' distances and results of significance tests using a *H. sapiens* are shown in **Table A.1.4. Table A.1.5** shows the pairwise Mahalanobis' distances and significance between fossils based on a *P. troglodytes* V/CV matrix. **Table A.1.6** displays outcomes of significance tests for the Mahalanobis' distances under a *G. gorilla* V/CV matrix. No individuals are significantly different from each other under any assessment of significance

Densified Analysis 3: M2 Complex

Using a *H. sapiens* V/CV matrix (**Table A.1.7)** to investigate Mahalanobis' distances, the difference between OH 5 and SK 48 is the greatest. However, no fossil specimens are significantly different from other fossil specimens. Pairwise Mahalanobis' distances between fossils based on a *P. troglodytes* model of variation are given in **Table A.1.8.** Here the largest distance is again between OH 5 and SK 48, and this time it is significant. **Table A.1.9** shows results of significance testing for Mahalanobis' distance for Analysis 3 using a *G. gorilla* V/CV matrix. Again, the distance between OH 5 is greatest, but no individuals are significantly different from any of the other individuals.

Densified Analysis 4: M1 Complex

Table A.1.10 shows the results of the significance tests for the pairwise Mahalanobis' distances using a *H. sapiens* V/CV matrix. SK 48 is significantly different from SK 79 under one model (Chimp-Human). The results of significance tests of Mahalanobis' distances under a *P. troglodytes* V/CV matrix are in **Table A.1.11.** SK 79 is significantly different from both OH 5 and SK 48. **Table A.1.12** (significance testing of Mahalanobis' distances) shows the results of **Analysis 4** using a *G. gorilla* matrix. Again, SK 79 has the largest, and the only significant, value.

Densified Analysis 5: P4 Complex

Tables A.1.13-A.1.15 show the pairwise Mahalanobis' distances and significance values under the three extant models of V/CV. No fossil specimen is significantly different from any of the other individuals under any model.

Densified Analysis 6: P3 Complex

Tables A.1.16-A.1.18 show the pairwise Mahalanobis' distances and significance values under the three extant models of V/CV. No fossil specimen is significantly different from any of the other individuals under any model.

Densified Analysis 7: C Complex

Tables A.1.19-A.1.21 show the pairwise Mahalanobis' distances and significance values under the three extant models of V/CV. No fossil specimen is significantly different from any of the other individuals under any model.

Densified Analysis 8: LI Complex

Tables A.1.22-A.1.24 show the pairwise Mahalanobis' distances and significance values under the three extant models of V/CV. No fossil specimen is significantly different from any of the other individuals under any model.

Densified Analysis 9: CI Complex

Pairwise Mahalanobis' distances between fossils based on a *Homo sapiens* model of variation are given in **Table A.1.25.** Fossil individuals are not significantly different from each other. When the same analysis is done using a *P. troglodytes* model of variation, the results (**Table A.1.26**) follow the same trend, but in this case SK 79 and SK 48 are significantly different. Under a *G. gorilla* model of variation (**Table A.1.27**) no individuals are significantly different each other.

Geometric Morphometrics

Analysis 1: Densified Palate

General Procrustes Analysis

Figures 5.28 A & B illustrates the shape of the right palate. Landmark configurations for all observations are centered on the mean configurations with no major outliers.

Principal Component Analysis-shape variation

Wireframe graphs depict shape change along PC1 which differs as the palate becomes thinner and elongated; whereas shape change along PC2 broadens and shortens the palate (see **Figure 5.28 C & D,** respectively). **Figure 5.29** illustrates PCA (Principal Component Analysis) for **Analysis 1**. As PC scores become more positive individuals become larger in size. Extant group convex hulls are arranged and separated along PC1 accounting for 45.98% of the shape variation. The scatter plot shows that *H. sapiens* are slightly more variable followed by *P. troglodytes* and *G. gorilla* (which are comparable along with species overlap); however, gorillas and chimps are larger in size as expected. The PCA demonstrates that both *P. boisei* and *P. robustus* are in or near the shape-space of *H. sapiens*. The morphology (shape) of the hard palate is therefore more morphologically similar to *H. sapiens* than to the African apes.

Regression (Allometry) Analysis

Results for the regression scores vs log centroid size are illustrated in **Figure 5.30** (used regression residuals)**.** As seen in the diagram, fossil specimens fall outside the range of the 95% ellipses for all extant species.

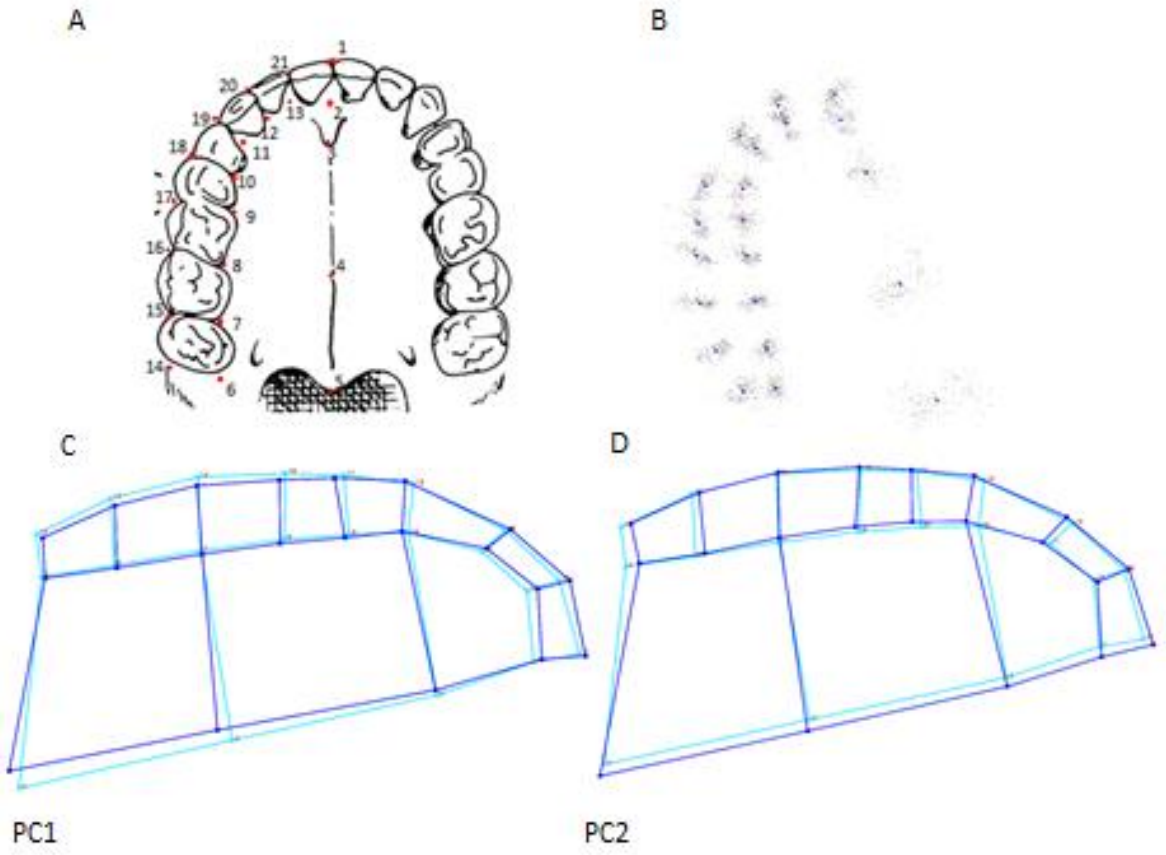

Figure 5.28. **A**. Landmarks for Analysis 1 (see **Table 4.3** for descriptions). **B**. GPA (General Procrustes Analysis) using landmark coordinates from **A** (adapted from Clark, 1970). **C**. Wireframe graphs depicting shape change along PC1 at a transformation factor of 0.05. **D.** Wireframe graphs depicting shape change along PC2 at a transformation factor of 0.05.

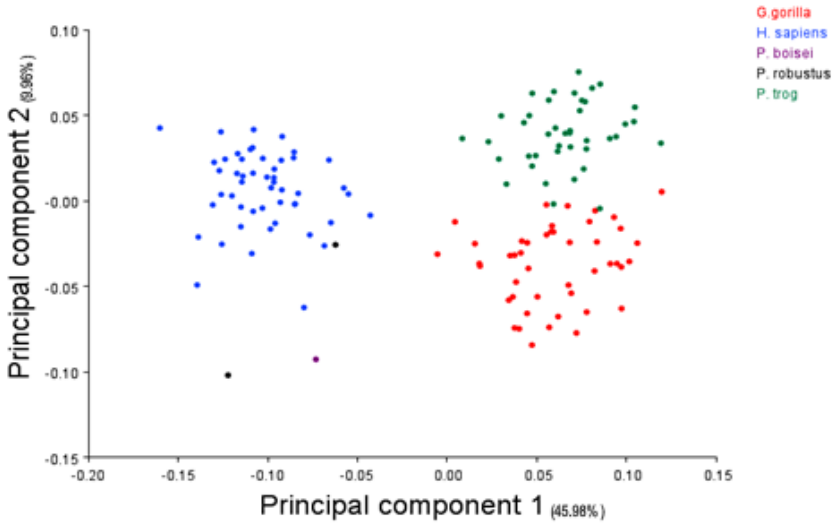

Figure 5.29. Principal component analysis for Analysis 1 using General Procrustes coordinates.

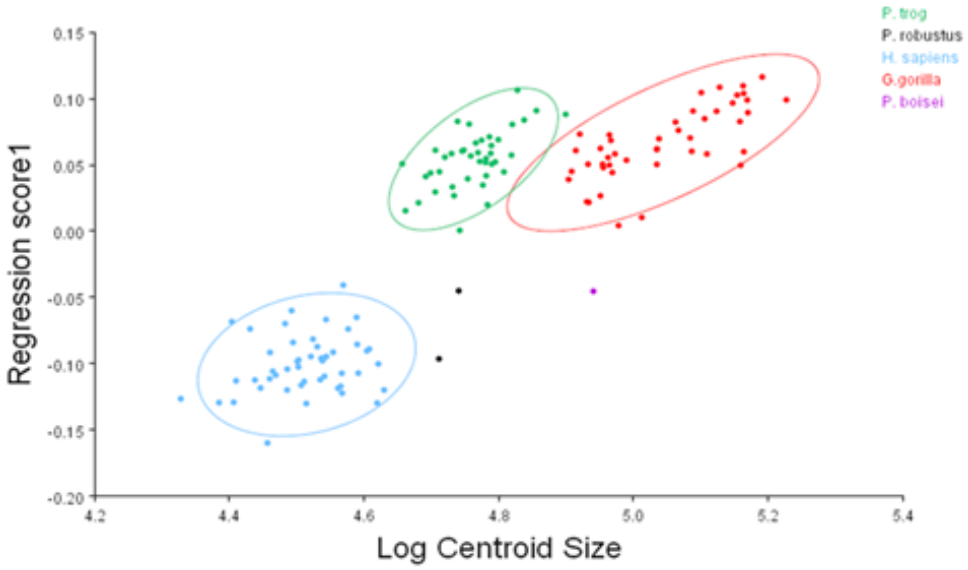

Figure 5.30. Regression plot showing size related shape change of unpooled principal component scores to log centroid size for Analysis 1 at 95% significance.

Analysis 2: Mandible-Corpus

General Procrustes Analysis

GPA analyses are shown in **Figure 5.31** (**B**). Landmark configurations are arranged around the centroid and mean (Procrustes fit) with no extreme outliers. However, it must be noted that observations for M3D, MEN and ALVB are widely dispersed and further from the transformed configuration in comparison to other observations in the dataset.

Principal Component Analysis

. **Figure 5.31** shows shape changes along PC1 (**C**) and along PC2 (**D**). PC1 shape shows slight widening medio-laterally (shown in dark blue) of the mandibles. In **Figure 5.31** (**D**) -PC2- between P4D and P3D moving anteriorly, the mandibular corpus is constricting in shape. However, from P4D moving posteriorly (moving towards the back of the mandible), the mandible appears to be widening. A PC1 against PC2 plot for the mandible can be seen in **Figure 5.32**. The PCA plot shows larger PC scores associated with smaller overall size. Mandibular shape variation within *G. gorilla* individuals (in red) is more dispersed and variable than *P. troglodytes* and *H. sapiens* alveolar bodies. This plot demonstrates that groups separate along PC 1- which accounts for 55.93% of the shape variation– with a shape change that widens and shortens the corpus. The *H. sapiens* convex hull lies close in proximity to the *P. troglodytes* hull showing no overlaps, although there are extreme outliers. The *P. robustus* specimens fall under *G. gorilla* and *P. troglodytes* convex hulls, respectively. *P. boisei* (OH 5) is close in proximity with *P. robustus* however is excluded from a convex hull of any extant group

Regression Analysis

Regression plot results for **Analysis 2** are displayed in **Figure 5.33.** Extant groups fall under their 95% ellipses with overlaps among the chimp and human data (excluding a few outliers within *P. troglodytes* and *G. gorilla*). One *P. robustus* specimen falls under *G. gorilla* (95% ellipses) with the remaining *P. robustus* and *P. boisei* "hovering" in close proximity however, not within the *G. gorilla* convex hull. Specimens are similar in shape (morphologically) to *G. gorilla* specimens.

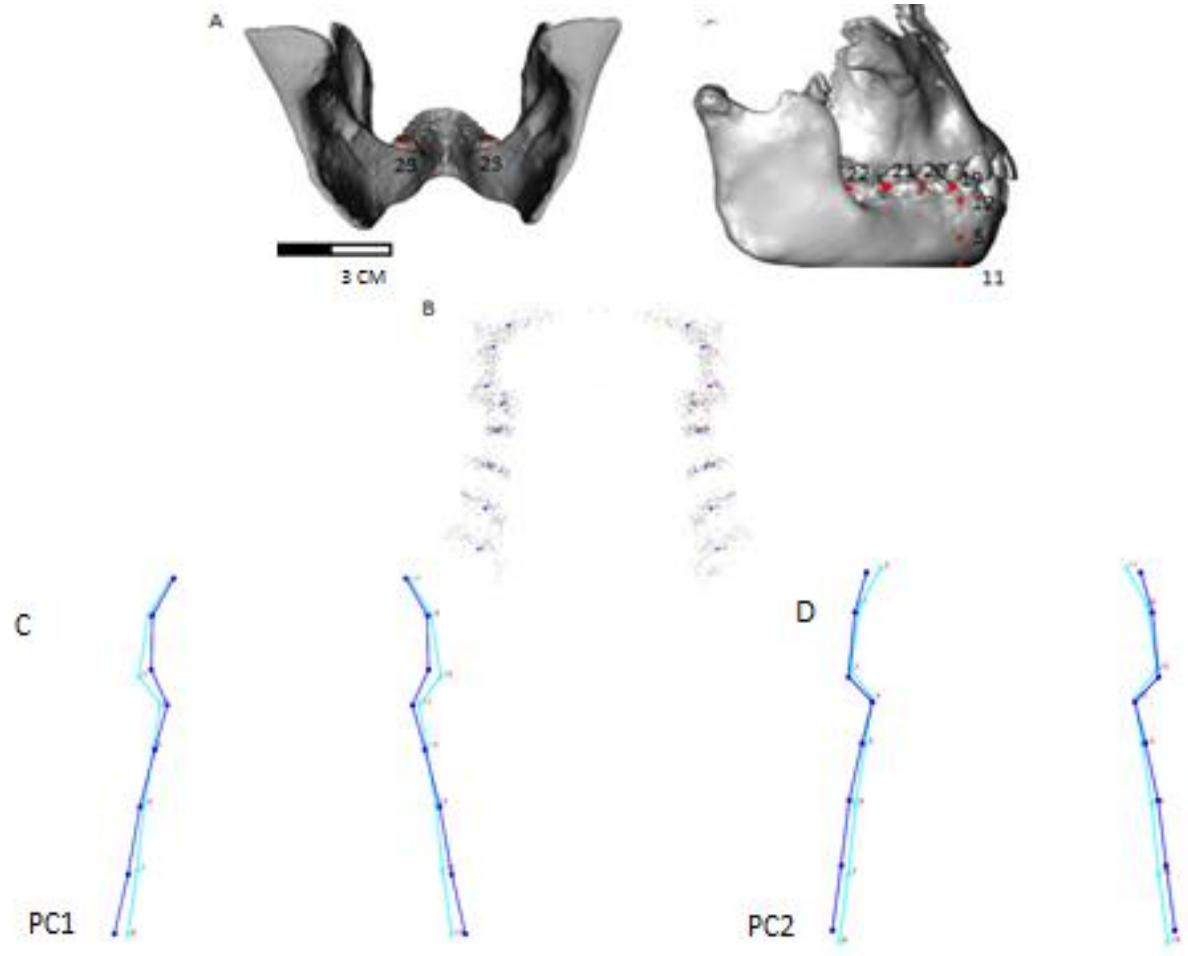

Figure 5.31. **A**. Landmarks (SK 23-top left) for Analysis 2-left side of mandible not shown in figure. **B**. GPA (General Procrustes Analysis) using landmark coordinates from **A** -see **Table 4.2** for descriptions- (adapted from Benazzi et al., 2013). **C**. Wireframe graphs depicting shape change along PC1 at a transformation of 0.05. **D**. Wireframe graphs depicting shape change along PC2 at a transformation of 0.05.

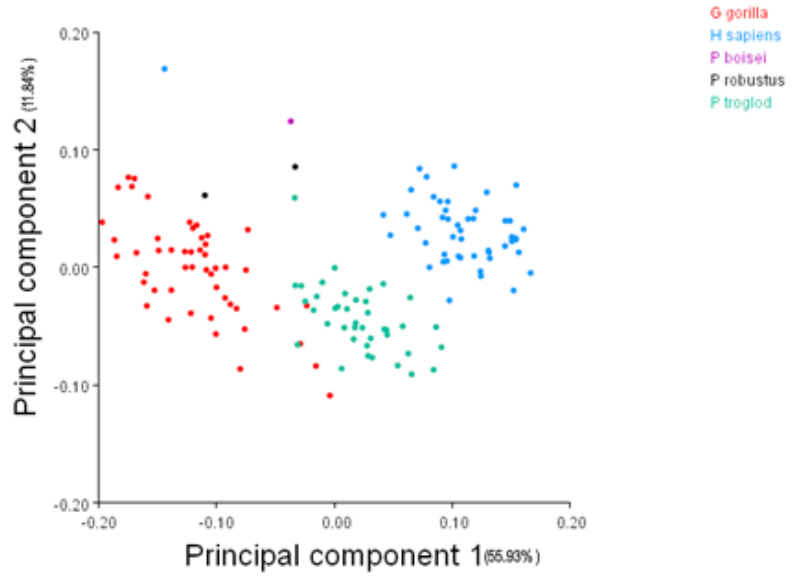

Figure 5.32. Principal component analysis for Analysis 2 using General Procrustes coordinates.

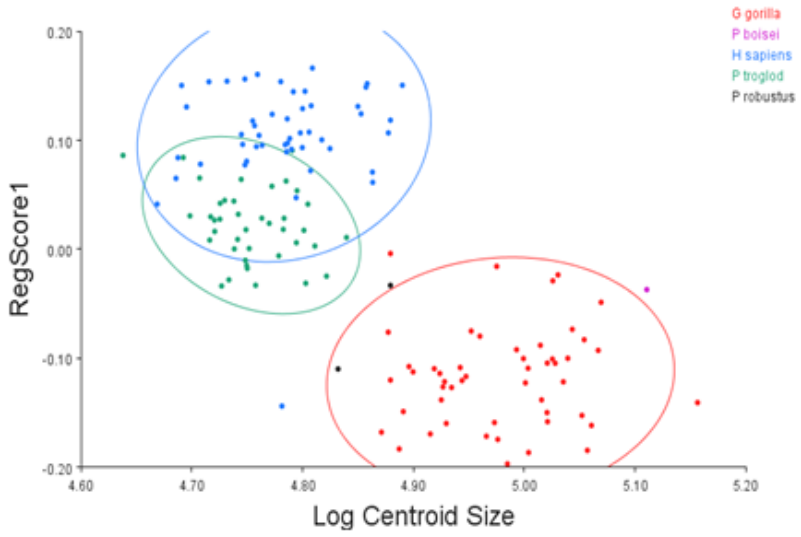

Figure 5.33. Regression plot showing size related shape change of unpooled principal component scores to log centroid size for Analysis 2 at 95% significance.

Analysis 3: Maxilla-Midface

General Procrustes Analysis

Procrustes fit results are displayed in **Figure 5.334** (**B)** along with (**A)** (to give context to placement of landmarks in the GPA). Observations within the dataset are centered on the fit with no extreme outliers. Landmarks such as ANS and OL show an overlap on the GPA –hence the overlapped numbers including observations along a straight line- while PRO landmark observations are arranged along a straight line. No extreme outliers can be seen in this figure, although observations overlap in such a way that they cannot be distinguished as to what landmarks they belong to especially numbers 2, 4 (on the Procrustes fit).

Principal Component Analysis

Shape change along PC1 (**Figure 5.33 C**) and PC2 (**Figure 5.34 D**) exhibit changes in maxillary and dental regions (illustrated in dark blue). Changes along PC1 illustrate (landmarks moving inwards) this region narrowing and elongating in shape -which accounts for 44.4% of the variation- from the mean configuration. PC2 exhibits a change that shortens and broadens this region. PCA plot (PC1 vs PC2) for **Analysis 3** is displayed in **Figure 5.34.** *G. gorilla* and *P. troglodytes* observations from the dataset fall closely together with some overlap. As PC scores increase overall body size decreases. The *H. sapiens* observations form their own convex hull with outliers near the *P. troglodytes* outliers. The overlap of *P. troglodytes* to *H. sapiens* and *G. gorilla* suggests the degree of sexual dimorphism between that of the two species and size variation is not as large as that of the gorillas. The *P. robustus* observations (DNH 8 and SK 83) group together and fall under the *H. sapiens* hull. Whereas, OH 5 (*P. boisei*) falls under the chimp convex hull.

Regression Analysis

Figure 5.35 demonstrates the regression plot (regression score 1 against log centroid size) for **Analysis 3**. Extant samples are grouped in convex hulls at 95% significance along PC1. None of the fossil specimens fall into the 95% ellipses. SK 83 and DNH 8 are close in proximity to *H. sapiens* but OH 5 is closer to the *G. gorilla* convex hull.

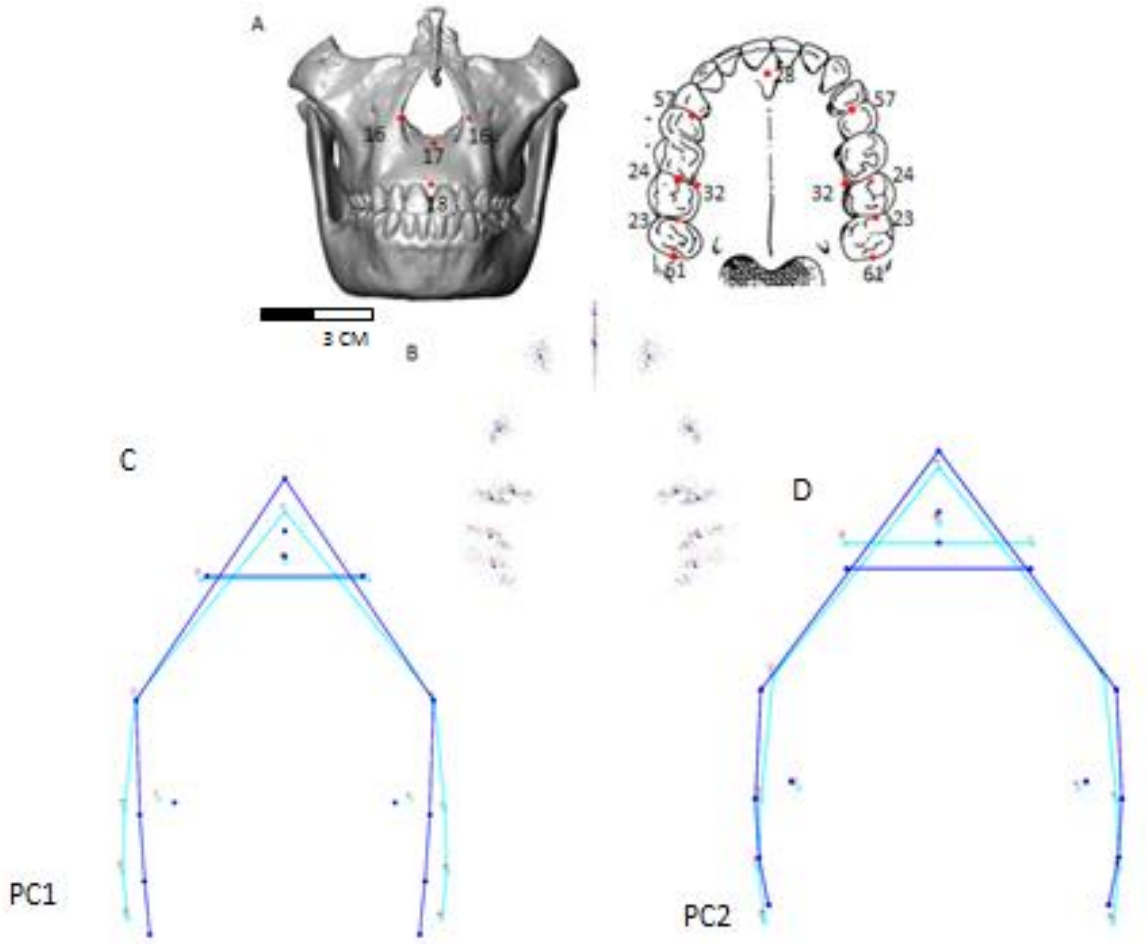

Figure 5.34. A. Landmarks for Analysis 3 (See **Table 4.1** for descriptions). **B**. GPA (General Procrustes Analysis) using landmarks coordinates from **A** (adapted from Benazzi et al., 2013; McCollum, 1999). **C.** Wireframe graphs depicting shape change along PC1 at a transformation of 0.05. **D.** Wireframe graphs depicting shape change along PC2 at a transformation of 0.05.

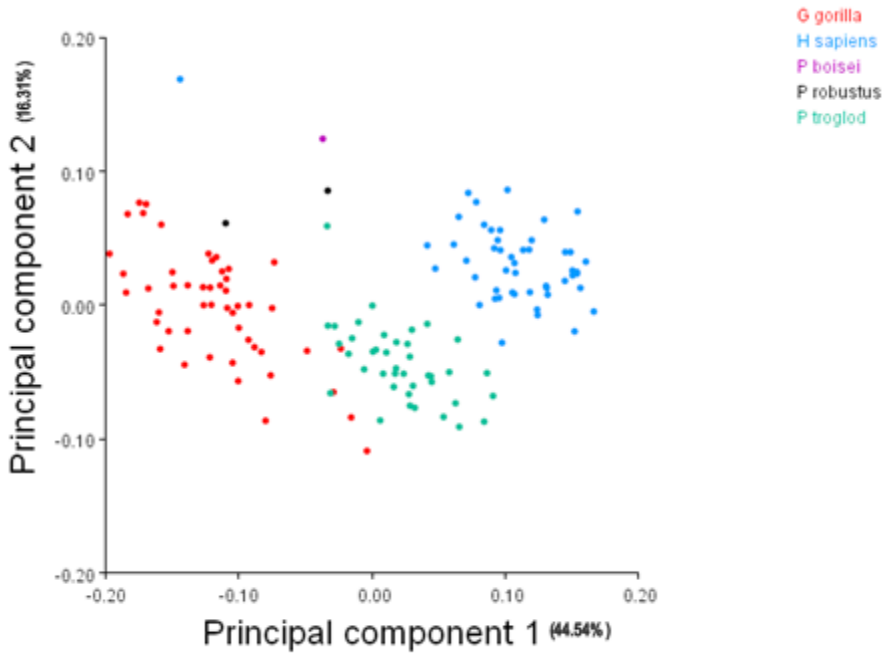

Figure 5.35. Principal component analysis for Analysis 3 using General Procrustes coordinates.

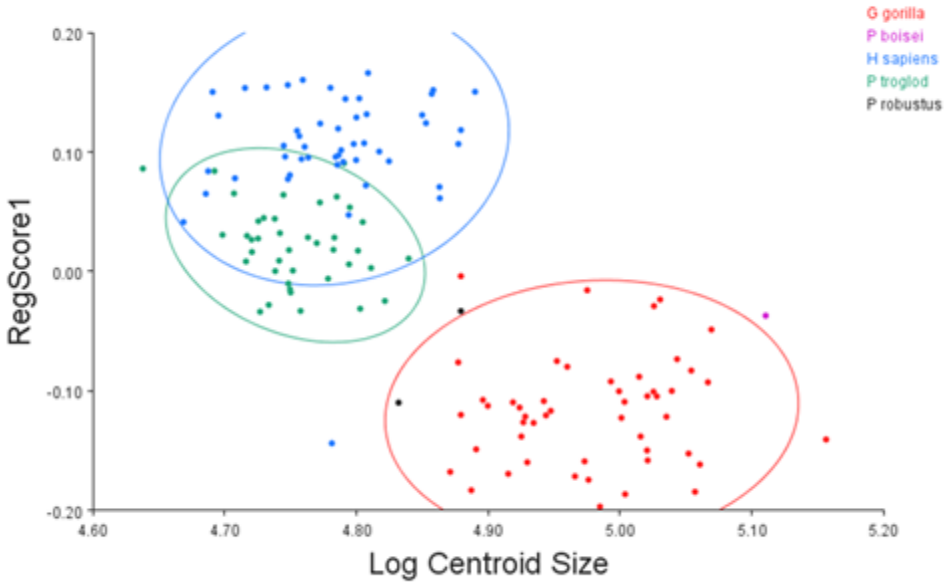

Figure 5.36. Regression plot showing size related shape change of unpooled principal component scores to log centroid size for Analysis 3 at 95% significance.

Analysis 4: Zygomatic-Face-Basicranium

General Procrustes Analysis

Figure 5.37 (A & B) exhibit landmark coordinates used (**A**), and Procrustes fit (**B**) results. **Figure 5.37 B** demonstrates that observations in the dataset center on the mean configurations. For landmarks GLA and NA –since there are so close in proximity- observations appear to overlap and are slightly indistinguishable- nonetheless there are no outliers. ANS coordinates after superimposition are concentrated around the fit, however the trend is different in that observations aren't clustered around but are aligned in a vertical manner.

Principal Component Analysis

Shape change along PC1 (**Figure 5.38 C**) and PC2 (**Figure 5.38 D B**) for **Analysis 4** shows that, PC1 (60.89% of the variance) elongates and constricts the given regions (including ANS). PC2 illustrates shortening and widening of the regions demonstrated in the dark blue color (**Figure 37 C & D**). Shape change occurs along the 1st PC illustrating the zygoma constricting the face, while the rest of the face elongates. PC scores increase as body size increases. Fossil specimens in this graph cluster together but do not fall under the given extant group convex hulls. Not surprisingly, *A. africanus* falls within the *P. troglodytes* convex hull of shape variation. **Figure 5.38** presents GPA analysis in the form of a PCA (PC1 against PC2).

Regression Analysis

Results for **Analysis 4** regression plot (regression score 1 against log centroid size) are depicted in **Figure 5.39**. Extant groups are within the 95% ellipses (excluding 2 *P. troglodytes* samples). *A. africanus* falls under the 95% convex hull *P. troglodytes*. *P. robustus* is near the hull; however, KNM-ER 406 falls outside all extant group ellipses (hulls).

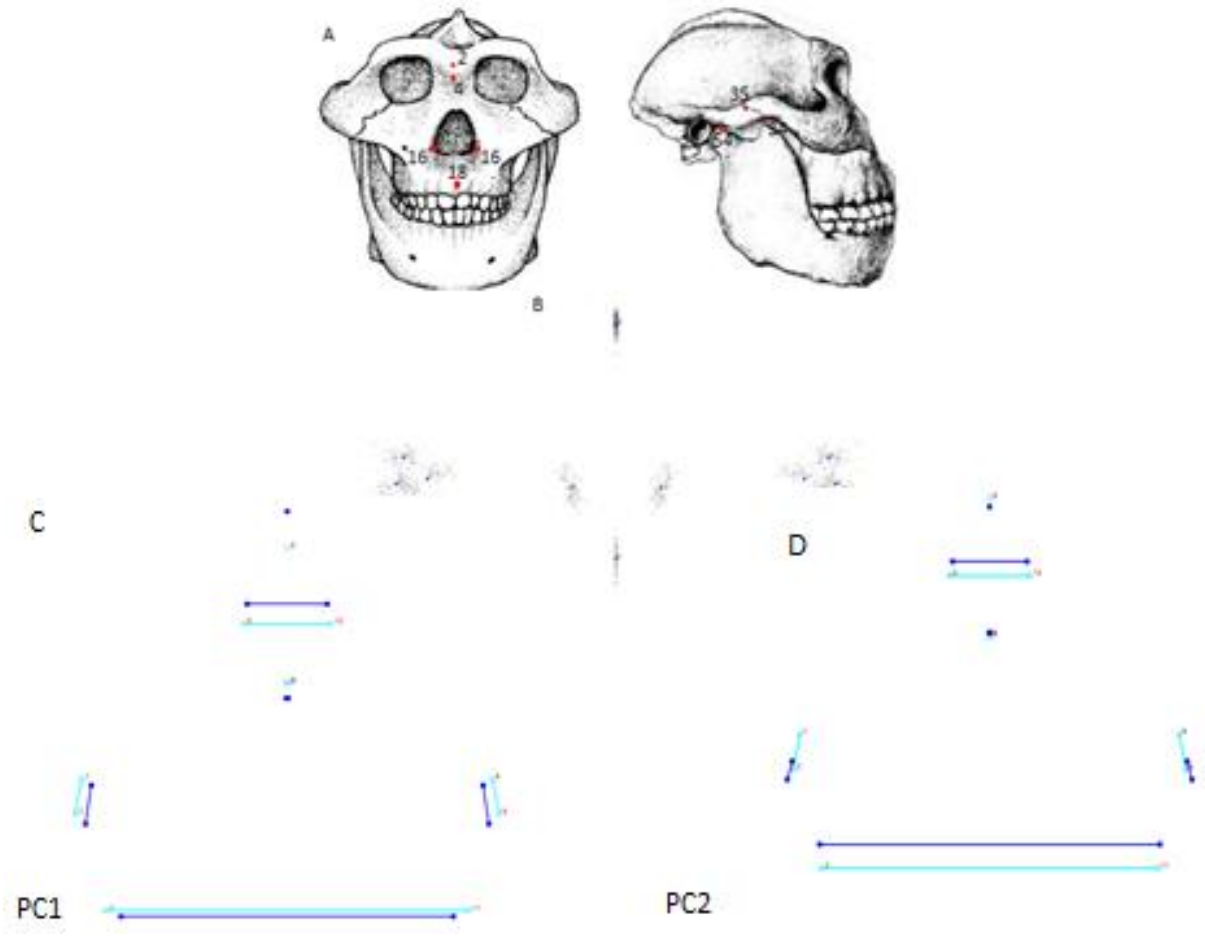

Figure 5.37. **A**. Landmarks for Analysis 4 (See **Table 4.1**). **B**. GPA (General Procrustes Analysis) using landmark coordinates from **A** (adapted from McCollum, 1999). **C.** Wireframe graphs depicting shape change along PC1 at a transformation of 0.05. **D.** Wireframe graphs depicting shape change along PC2 at a transformation of 0.05.

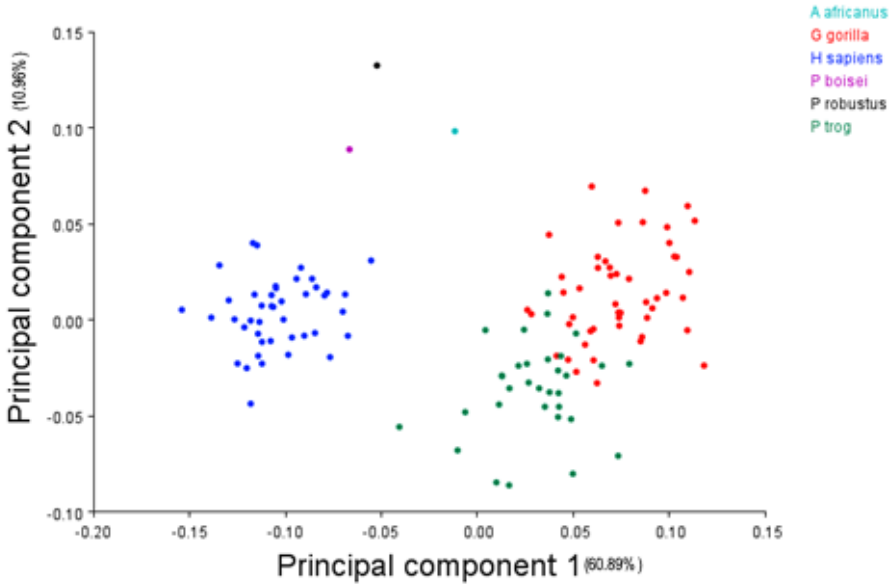

Figure 5.38. Principal component analysis for Analysis 4 using General Procrustes coordinates.

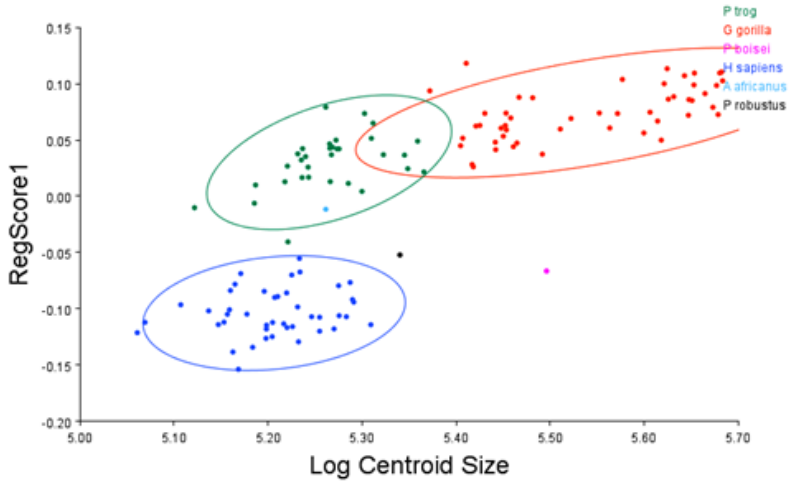

Figure 5.39. Regression plot showing size related shape change of unpooled principal component scores to log centroid size for Analysis 4 at 95% significance.

Analysis 5: Zygomatic-Midface

General Procrustes Analysis

Procrustes fit was performed on landmark coordinates for the Zygomatic-Midface regions. Landmark coordinates –**Figure 5.40 (A)** -used in the analysis together with the results for the GPA are illustrated in **Figure 5.40** (**B**). The dataset indicates that samples are focused around the fit with no extreme outliers.

Principal Component Analysis

Results for shape change (seen in dark blue) along PC1 (**Figure 5.40 C**) indicate a widening and constriction in the facial region and the opposite for the zygoma (slight constriction and elongation). Outcomes for shape change along PC2 (**Figure 5.40 D**) exhibit broadening and slight elongation in the facial region whereas the zygoma shorten in length. PCA for **Analysis 5** is displayed in **Figure 5.41** (PC1 against PC2). PC scores increase as size increases. The scatter plot illustrates that shape change occurs along PC2 whereby the zygoma shorten in size, while the rest of the face broadens (elongates) by widening the zygomaticomaxillary sutures and foramina. Extant species convex hulls group together showing overlap between *P. troglodytes* and *H. sapiens* as well as *P. troglodytes* and *G. gorilla*. Both Sts 5 and SK 48 fall within the *G. gorilla* convex hull.

Regression Analysis

Regression plot for **Analysis 5** (**Figure 5.42**) with 95% ellipses -separating along PC 1- around extant groups shows a different result. *P. troglodytes* overlaps with both *G. gorilla* and *H. sapiens*. Interestingly, a chimp sample is in the center of the *G. gorilla* convex hull. Both Sts 5 and SK 48 fall under the *G. gorilla* convex hull additionally, Sts 5 is within the overlap of *P. troglodytes* and *G. gorilla*.

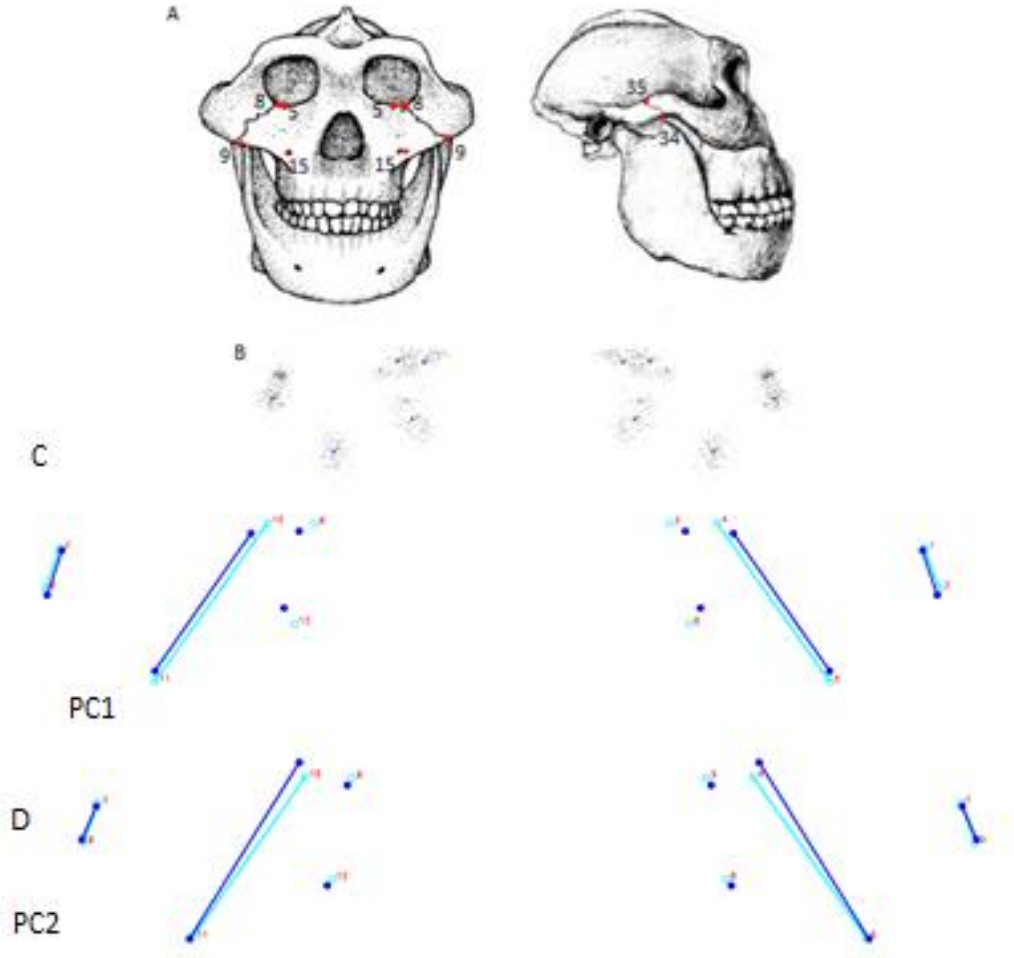

Figure 5.40. A. Landmarks for Analysis 5 (See **Table 4.1**). B. GPA (General Procrustes Analysis) using landmark coordinates from **A** (adapted from McCollum, 1999). **C.** Wireframe graphs depicting shape change along PC1 at a transformation of 0.05. **D.** Wireframe graphs depicting shape change along PC2 at a transformation of 0.05.

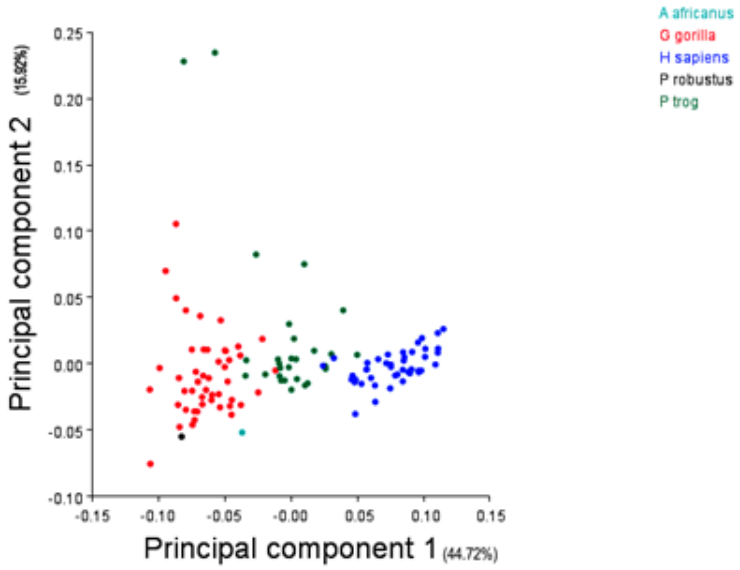

Figure 5.41. Principal component analysis for Analysis 5 using General Procrustes coordinates.

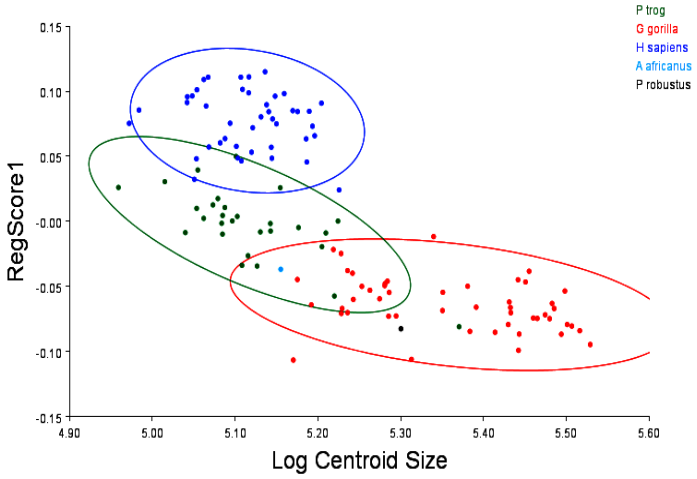

Figure 5.42. Regression plot showing size related shape change of unpooled principal component scores to log centroid size for Analysis 5 at 95% significance.

Genetic Drift: Testing the null hypothesis of drift

Cranial analyses

All six of the cranial analyses listed in **Table 4.9** are tested against the null hypothesis of drift. These results are presented in **Table 5.4.1.**

In **Cranial Analysis 1**, which concentrates on the midface and maxilla regions, all but one of the comparisons (under all extant models) failed to reject drift as an explanation for diversification. However, assuming a human model of within-species variation, the diversification between *A. africanus* and *P. robustus* is consistent with selection acting to diversify these taxa. The slope using the human model is less than 1.0, indicating less between group variation in the first PCs and more in the bottom PCs than expected.

Cranial Analysis 2 concentrated on the zygomatic region. Drift cannot be rejected at the 95% significance level for the any comparisons, under any model.

Cranial Analysis 3 focuses on the zygomatic and upper facial regions. Again, drift cannot be rejected at the 95% significance for any of the comparisons, although a number of comparisons are suggestive, with a p-value between 0.10 and 0.05 under chimp and human models.

Cranial Analysis 4 was constructed to investigate relationships and patterns of variation in three female fossil specimens. Again, all comparisons were consistent with drift, although the *P. robustus-A. africanus* diversification under a human model has a p-value of 0.07.

Cranial Analysis 5 focused on the basicranial region. Among all fossil comparisons variation is consistent with drift regardless of which extant V/CV matrix is used.

Cranial Analysis 6 focuses on the temporal region in the skull using comparisons between all australopith taxa, gracile and robust. Comparisons between *P. aethiopicus* and *P. boisei*, P. *boisei* and *P. robustus*, and *P. boisei* and *A. africanus* show diversification that is consistent with drift irrespective of which extant V/CV matrix is used. Results for the remaining comparisons (*P. aethiopicus – P. robustus, P. aethiopicus – A. africanus, P. robustus – A. africanus*) show variation consistent with drift for under some but not all models. *P. aethiopicus – P. robustus* and *P. aethiopicus – A. africanus* diversification indicates selection acting to diversify the taxa under a chimpanzee model of variation. For *P. robustus – A. africanus* drift is rejected (selection is detected) using the gorilla V/CV matrix. Slopes for all of these rejections of drift are all less than 1.0, indicating that variation between fossil groups is relatively small in the first few PCs relative to the minor PCs.

Mandibular Analyses

All mandibular analyses compare *P. boisei* and *P. robustus* only. **Mandibular Analysis 1** focuses on the ramus portion of the mandible. Results are presented in **Table 5.4.2.** Variation between these specimens is consistent with drift under a chimp and gorilla model of V/CV, but not a human model of V/CV, indicating the effects of selection. The slope for this rejection is <1.0, indicating less between-fossil variation in the first eigenvectors compared to the last eigenvectors.

Mandibular Analysis 2 concentrates on the corpus. Diversification is consistent with drift under human and gorilla V/CV. Under a chimp model of variation drift is rejected. The slope is <1.0 indicating little between-fossil variation in the first PCs and more in the minor PCs.

Mandibular Analysis 3 investigates the midline region. Drift is rejected when a chimp V/CV matrix is utilized, however when either human or gorilla V/CV matrices are used diversification is consistent with drift.

Densified Analyses

Regression results of logged between-fossil group variance to within-fossil group variation testing the deviance from a slope of 1.0 for densified palatal analyses are presented in **Table 5.4.3** (see **Appendix C** for regression plots**)**. The results reveal that the majority of all analyses performed across *P. boisei-P. robustus* comparisons (taxa included in all analyses) cannot reject the null hypothesis of drift. The exception to this is in **Densified Palate Analysis 1**, where drift is rejected under a chimp model of variation, and **Densified Palate Analysis 5** where drift is rejected under a gorilla model of variation. In both of these cases the slopes are < 1.0, showing less between-group variation than expected in the first PCs relative to within group.

Table 5.4.1. Cranial analyses results for logged between-group variance regressed on within-group variance testing for genetic drift.

ANALYSIS	COMPARISON	CONSISTENT WITH DRIFT	MODEL	SLOPE	R2	P-VALUE
CRANIAL ANALYSIS 1						
MIDFACE/MAXILLA						
	P. boisei-P. robustus	YES	HUMAN	0.86	0.55	0.71
	P. boisei-P. robustus	YES	CHIMP	1.37	0.69	0.40
	P. boisei-P. robustus	YES	GORILLA	1.28	0.57	0.60
	P. boisei-A. africanus	YES	HUMAN	0.71	0.44	0.45
	P. boisei-A. africanus	YES	CHIMP	0.59	0.26	0.4
	P. boisei-A. africanus	YES	GORILLA	0.39	0.08	0.36
	A. africanus- P. robustus	NO	HUMAN	-0.27	0.07	**0.04**
	A. africanus- P. robustus	YES	CHIMP	0.90	0.55	0.7
	A. africanus- P. robustus	YES	GORILLA	0.59	0.54	0.16
CRANIAL ANALYSIS 2						
ZYGOMATIC						
	P. boisei-P. robustus	YES	HUMAN	2.04	0.75	0.22

	P. boisei-P. robustus	YES	CHIMP	0.67	0.26	0.66
	P. boisei-P. robustus	YES	GORILLA	0.39	0.06	0.57
	P. boisei-A. africanus	YES	HUMAN	1.13	0.71	0.77
	P. boisei-A. africanus	YES	CHIMP	0.48	0.17	0.45
	P. boisei-A. africanus	MAYBE	GORILLA	0.68	0.9	**0.09**
	A. africanus- P. robustus	YES	HUMAN	1.03	0.17	0.99
	A. africanus- P. robustus	YES	CHIMP	0.26	0.09	0.23
	A. africanus- P. robustus	YES	GORILLA	1.07	0.62	0.90
CRANIAL ANALYSIS 3 ZYGOMATIC-UPPER FACE						
	P. boisei-P. robustus	YES	HUMAN	1.07	0.72	0.75
	P. boisei-P. robustus	MAYBE	CHIMP	0.67	0.61	**0.1**
	P. boisei-P. robustus	YES	GORILLA	0.88	0.43	0.75
	P. boisei-A. africanus	YES	HUMAN	1.38	0.42	0.5
	P. boisei-A. africanus	YES	CHIMP	0.95	0.5	0.86
	P. boisei-A. africanus	YES	GORILLA	0.9	0.53	0.73

	A. africanus- P. robustus	MAYBE	HUMAN	0.66	0.6	**0.09**
	A. africanus- P. robustus	MAYBE	CHIMP	0.56	0.46	**0.06**
	A. africanus- P. robustus	YES	GORILLA	0.88	0.43	0.75
CRANIAL ANALYSIS 4 FEMALES						
	P. boisei- P. robustus	YES	HUMAN	0.61	0.01	0.89
	P. boisei- P. robustus	YES	CHIMP	-0.79	0.06	0.26
	P. boisei- P. robustus	YES	GORILLA	0.24	0.02	0.38
	P. boisei-A. africanus	YES	HUMAN	0.94	0.45	0.92
	P. boisei-A. africanus	YES	CHIMP	0.51	0.02	0.76
	P. boisei-A. africanus	YES	GORILLA	0.37	0.21	0.11
	P. robustus-A. africanus	MAYBE	HUMAN	0.04	0.00	**0.07**
	P. robustus-A. africanus	YES	CHIMP	0.8	0.09	0.87
	P. robustus-A. africanus	YES	GORILLA	0.27	0.07	0.15
CRANIAL ANALYSIS 5 BASICRANIUM						

P. aethiopicus - P. boisei	YES	HUMAN	2.20	0.59	0.15
P. aethiopicus - P. boisei	YES	CHIMP	1.11	0.55	0.79
P. aethiopicus - P. boisei	YES	GORILLA	0.06	0.00	0.26
P. aethiopicus -A .africanus	YES	HUMAN	0.49	0.15	0.32
P. aethiopicus -A. africanus	YES	CHIMP	0.82	0.25	0.78
P. aethiopicus -A. africanus	YES	GORILLA	0.84	0.19	0.82
P. boisei-Africanus	YES	HUMAN	0.91	0.45	0.82
P. boisei-Africanus	YES	CHIMP	1.05	0.62	0.87
P. boisei-Africanus	YES	GORILLA	0.59	0.18	0.46
CRANIAL ANALYSIS 6 TEMPORAL					
P. aethiopicus -P. boisei	YES	HUMAN	1.03	0.59	0.93
P. aethiopicus -P. boisei	YES	CHIMP	0.74	0.28	0.65
P. aethiopicus -P. boisei	YES	GORILLA	0.59	0.56	0.14
P. aethiopicus-P. robustus	YES	HUMAN	0.70	0.25	0.61

P. aethiopicus-P. robustus	NO	CHIMP	0.16	0.04	0.05
P. aethiopicus-P. robustus	YES	GORILLA	0.56	0.43	0.18
P. aethiopicus-A. africanus	YES	HUMAN	0.70	0.56	0.32
P. aethiopicus-A. africanus	NO	CHIMP	0.00	0.00	**0.02**
P. aethiopicus-A. africanus	YES	GORILLA	0.62	0.34	0.37
P. boisei-P. robustus	YES	HUMAN	1.19	0.34	0.80
P. boisei-P. robustus	YES	CHIMP	0.58	0.48	0.18
P. boisei-P. robustus	YES	GORILLA	0.67	0.26	0.54
P. boisei-A. africanus	YES	HUMAN	0.79	0.73	0.37
P. boisei-A. africanus	YES	CHIMP	0.81	0.22	0.79
P. boisei-A. africanus	YES	GORILLA	0.58	0.31	0.32

P. robustus- A. africanus	MAYBE	HUMAN	-0.04	0.00	**0.10**
P. robustus- A. africanus	YES	CHIMP	0.15	0.02	0.18
P. robustus- A. africanus	NO	GORILLA	0.18	0.1	**0.01**

Table 5.4.2. Mandibular analyses results for logged between-group variance regressed on within-group variance testing for genetic drift.

ANALYSIS	COMPARISON	CONSISTENT WITH DRIFT	MODEL	SLOPE	R2	P-VALUE
MANDIBULAR ANALYSIS 1 RAMUS						
	P. boisei - P. robustus	NO	HUMAN	0.28	0.49	**0.01**
	P. boisei - P. robustus	YES	CHIMP	0.35	0.05	0.44
	P. boisei - P. robustus	YES	GORILLA	0.54	0.33	0.29
MANDIBULAR ANALYSIS 2 CORPUS						
	P. boisei - P. robustus	YES	HUMAN	0.87	0.08	0.92
	P. boisei - P. robustus	NO	CHIMP	-0.24	0.04	**0.05**
	P. boisei - P. robustus	YES	GORILLA	0.36	0.07	0.32
MANDIBULAR ANALYSIS 3 MIDLINE						
	P. boisei - P. robustus	YES	HUMAN	0.93	0.89	0.78
	P. boisei - P. robustus	NO	CHIMP	0.14	0.26	**0.03**
	P. boisei - P. robustus	YES	GORILLA	0.61	0.21	0.69

Table 5.4.3. Densified palate analyses results for logged between-group variance regressed on within-group variance testing for genetic drift.

ANALYSIS	COMPARISON	CONSISTENT WITH DRIFT	MODEL	SLOPE	R2	P-VALUE
DENSIFIED PALATE ANALYSIS 1						
MIDLINE						
	P. boisei-P. robustus	YES	HUMAN	0.87	0.55	0.55
	P. boisei-P. robustus	NO	CHIMP	0.54	0.48	**0.01**
	P. boisei-P. robustus	MAYBE	GORILLA	0.69	0.52	**0.10**
DENSIFIED PALATE ANALYSIS 2						
M3 COMPLEX						
	P. boisei-P. robustus	YES	HUMAN	0.5	0.2	0.45
	P. boisei-P. robustus	YES	CHIMP	1.63	0.71	0.37
	P. boisei-P. robustus	YES	GORILLA	0.53	0.48	0.23
DENSIFIED PALATE ANALYSIS 3						
M2 COMPLEX						
	P. boisei-P. robustus	YES	HUMAN	0.7	0.62	0.41
	P. boisei-P. robustus	YES	CHIMP	0.85	0.34	0.84
	P. boisei-P. robustus	YES	GORILLA	0.92	0.56	0.88
DENSIFIED PALATE ANALYSIS 4						
M1 COMPLEX						
	P. boisei-P. robustus	YES	HUMAN	1.85	0.75	0.26
	P. boisei-P. robustus	YES	CHIMP	1.89	0.48	0.46
	P. boisei-P. robustus	YES	GORILLA	0.93	0.95	0.61
DENSIFIED PALATE						

ANALYSIS 5						
P4 COMPLEX						
	P. boisei-P. robustus	YES	HUMAN	0.44	0.20	0.35
	P. boisei-P. robustus	YES	CHIMP	1.82	0.49	0.5
	P. boisei-P. robustus	NO	GORILLA	0.89	0.99	**0.03**
DENSIFIED PALATE						
ANALYSIS 6						
P3 COMPLEX						
	P. boisei-P. robustus	YES	HUMAN	0.68	0.17	0.74
	P. boisei-P. robustus	YES	CHIMP	0.70	0.09	0.83
	P. boisei-P. robustus	YES	GORILLA	0.63	0.06	0.81
DENSIFIED PALATE						
ANALYSIS 7						
C COMPLEX						
	P. boisei-P. robustus	YES	HUMAN	0.47	0.17	0.43
	P. boisei-P. robustus	MAYBE	CHIMP	0.47	0.7	**0.06**
	P. boisei-P. robustus	YES	GORILLA	0.65	0.51	0.41
DENSIFIED PALATE						
ANALYSIS 8						
LI COMPLEX						
	P. boisei-P. robustus	YES	HUMAN	0.53	0.45	0.26
	P. boisei-P. robustus	YES	CHIMP	1.7	0.53	0.50
	P. boisei-P. robustus	YES	GORILLA	0.94	0.83	0.83
DENSIFIED PALATE						
ANALYSIS 9						
CI COMPLEX						
	P. boisei-P. robustus	YES	HUMAN	0.6	0.63	0.23
	P. boisei-P. robustus	YES	CHIMP	1.92	0.82	0.16

	P. boisei-P. robustus	YES	GORILLA	0.54	0.24	0.46

Reconstructing Selection

Results showed that in most cases phenotypic diversity seen across the genus *Paranthropus* (as well as *A. africanus*) is consistent with random evolutionary forces such as drift. However, there are nine examples where drift is rejected (See **Table 5.5.1- Table 5.5.3**). For the nine comparisons that were rejected for drift, in order to evaluate the nature (pattern and magnitude) of selection that may have acted to diversify *Paranthropus* from each other and *Paranthropus* (robust australopiths) from *A. africanus* (gracile australopith); selection necessary to create detected differences was reconstructed (shown in **Figures 5.43 – Figure 5.45**). Where vectors do not agree, interpretations are made relative to the appropriate selection vectors – i.e. if drift was rejected under a chimpanzee model, the chimp-derived selection vector is considered most relevant.

Cranial analyses

The first rejection of drift occurs in **Cranial Analysis 1**, the midface –maxilla regions (see **Table 5.5.1**), between *A. africanus* and *P. robustus* using a human variance/covariance matrix (p-value = 0.05). The selection required to produce *P. robustus* midface-maxilla changes from *A. africanus* is moderately positive to weak for maxilla height and overall tooth enlargement and moderately negative to weak for the nasal aperture, palate length and enlargement of the fourth molar. The response to this selection is overall moderate and negative for the majority of the traits in this region, implying a general decrease in overall size. The response is generally consistent with the direction and magnitude of selection.

In **Cranial Analysis 6** rejection of drift occurs in the temporal region (see **Table 5.5.1**) between comparisons of *P. aethiopicus – P. robustus, P aethiopicus – A. africanus* and *P. robustus – P. africanus* respectively. The two former comparisons are rejected under a chimp variance/covariance matrix while the latter is rejected under a gorilla model of variation. The selection required to produce a *P. robustus* temporal from *P. aethiopicus* is strongly negative for the external auditory meatus (height and width), MFL-EMI, POR-MFM and MFL-AST. Selection required is also strongly positive for POR-MFL and AST- POR [L]. Response to this selection is relatively strong and varies between negative and positive for the traits in this temporal region. The response is generally consistent with the direction and magnitude of selection, except for MFL-AST, which responds in the direction opposite to selection.

Selection required to create a *P aethiopicus* temporal change from *A. africanus* is negative for external auditory meatus (EAM) anteroposterior width, POR –MFL, and AST-MFL. It is also positive for EAM superoinferior height and general temporal morphology (MFL-EMI, POR-MFM and AST-POR [L]). Response to selection is strong and positive across a majority of traits, except EAM (A)-EAM (P) and POR-MFL. Although the response is consistent with the direction of selection in many cases, there is one exception, suggesting that some morphological change results from selection acting on correlated anatomical regions.

The selection required to produce a *P. robustus* temporal region from *A. africanus* is strongly negative for external auditory meatus (EAM) anteroposterior width, EMI-POR and MFL-AST, and strongly positive for the

remaining temporal region. The response to selection is mostly negative to neutral, with the exception of POR-MFM which is positive. There is evidence for both direct and correlated selection.

Mandibular analyses

Rejection of drift occurs in all regions – corpus, ramus and midline – for comparisons between *P. boisei* and *P. robustus* (See **Table 5.5.2**). In **Mandibular Analysis 1** rejection occurs using a human model of variation. The selection required to produce a *P. robustus* mandible from *P. boisei* ranges from weak to strongly negative for ramus width and a relatively large portion of mandibular length. Additionally, the selection required is strongly positive for MEN-RAM POS and AJUNC-GON (under a human vector model) increasing the length of the mandible. Though it is worth noting here that there are some substantial differences between vectors under different models (discussion is based on the human one since the rejection of drift occurred under this model). The response to selection is strong and a mixture of both negative and positive; it is generally but not always in the direction of the selection.

The selection required to produce a *P. robustus* corpus from *P. boisei* is weak to negative for superoinferior corpus height and M1 to M2 molar size and shape (see **5.4.2**). This shows a decrease in general molar size, given the strong negative selection. Furthermore, selection required to influence P4 and M2 is positively weak, this indicates limited selection on molar enlargement. The response to selection is relatively strong and majority negative and consistent with the direction of selection.

The selection required to produce a *P. robustus* hard palate from *P. boisei* is negative for the length between left and right M1, positive for PD3-PD3 [R] and weak for the other variables. The response to selection is excessively strong and negative across all variables. This could be indicative of adaptive reduction in size, shape and robustness of the palate relative to the "hyper-robust" species.

Densified analyses

Results for testing drift for this subset are demonstrated in **Table 5.4.3** while reconstructed selection vectors can be seen in **Table 5.5.3**. **Densified Palate Analysis 1** compares *P. boisei* and *P. robustus* and detects selection under a chimp variance/covariance matrix. The magnitude of the selection values driving diversification in the densified region of the hard palate is very large in some cases, and similar to the pattern seen in the previous hard palate analysis. The selection pressures required to produce a *P. robustus* hard palate from *P. boisei* are strongly (stronger than any detection seen previously) negative for length and depth. Strong to moderate positive selection is also detected for depth and width (from the midline to buccal side of teeth) of the region. Interestingly, the responses to the selection pressures are mostly positive, indicating that morphological change is happening in a direction opposite to the force of selection.

Densified Palate Analysis 5 compares *P. boisei* and *P. robustus* with selection detected under a gorilla model of variation. Selective pressures (looking at the gorilla vector) required to produce a *P. robustus* fourth

premolar complex from *P. boisei* is negative for P4DL-P3DB and weak to moderately positive for the remainder of the region. The direction of morphological change is mostly consistent (opposite for one trait) with the selective pressures, indicating an increase in overall tooth dimensions (length and width) in response to selection.

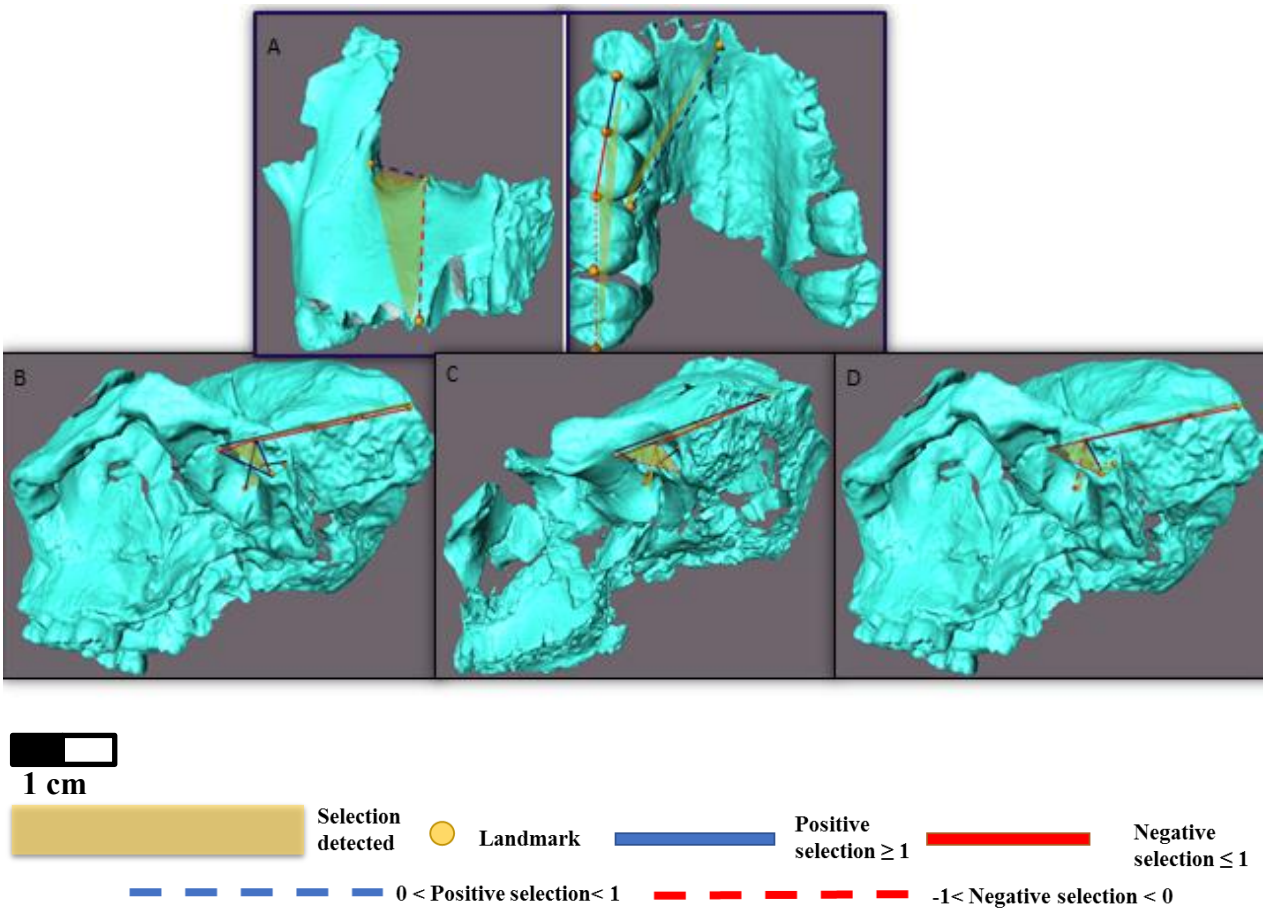

Figure 5.43. Visually represented selection vectors necessary to produce observed differences in Cranial morphology. Landmark definitions are given in **Table 4.1**.

Selection vector values are presented in **Table 5.5.1**. The cranial regions undergoing selection are given in yellow. Positive and negative selection vectors are shown in blue and red respectively. Strongly positive (values ≥ 1) and strongly negative (values ≤ -1) selection are represented by solid lines. Weak to moderate selection (0 > values > 1; -1 < values < 0) are displayed

as dashed lines. (**A**) Cranial Analysis 1 Midface – Maxilla between *A. africanus* and *P. robustus*. (**B**) Cranial Analysis 6- Temporal between *P. aethiopicus* and *P. robustus*. (**C**) Cranial Analysis 6 -Temporal between *P aethiopicus* and *A africanus*. (**D**) Cranial Analysis 6 – Temporal between *P. robustus* and *A. africanus.*

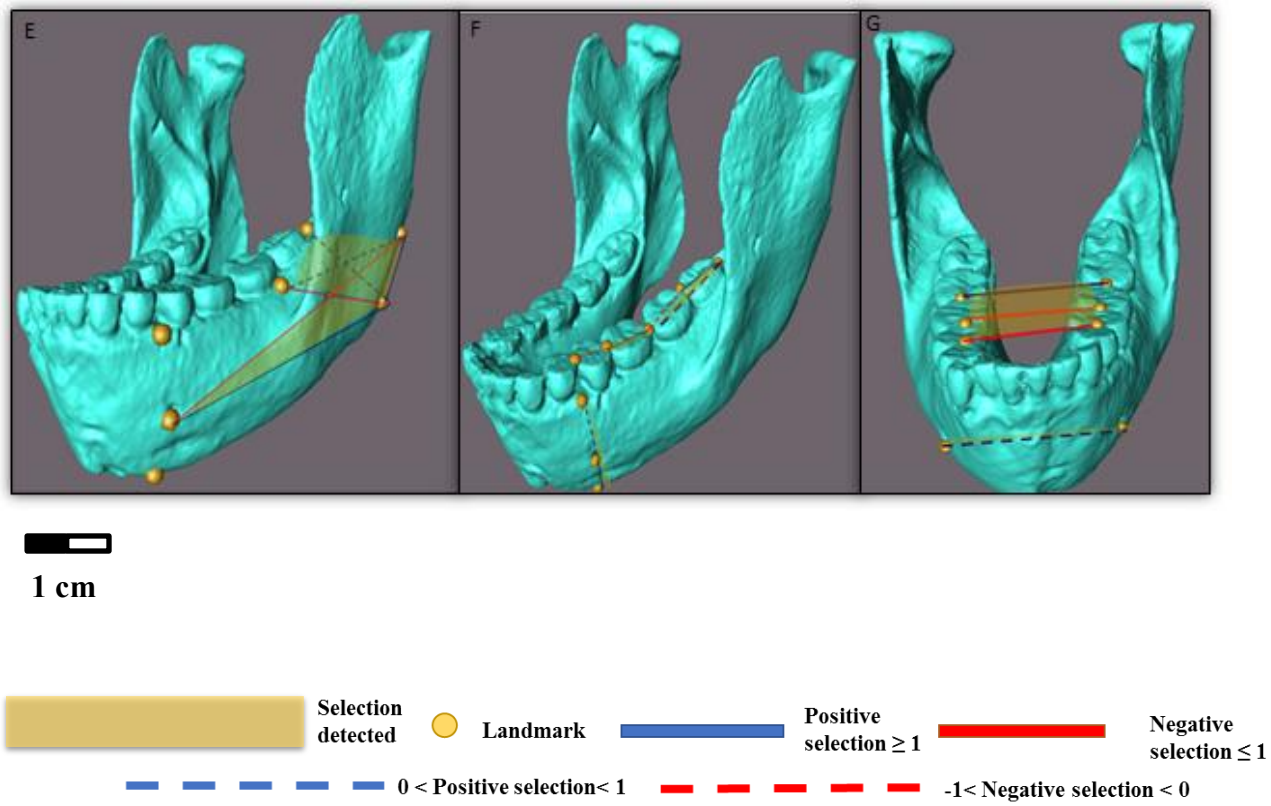

Figure 5.44. Visually represented selection vectors necessary to produce observed differences in Mandibular morphology. Landmark definitions are given in **Table 4.2**.

Selection vector values are presented in **Table 5.5.2**. The mandibular regions undergoing selection are given in yellow. Positive and negative selection vectors are shown in blue and red respectively. Strongly positive (values ≥ 1) and strongly negative (values ≤ -1) selection are represented by solid lines. Weak to moderate selection (0 > values > 1; -1 < values < 0) are displayed

as dashed lines. (**E**) Mandibular Analysis 1- Ramus between *P. boisei* and *P. robustus*. (**F**) Mandibular Analysis 2- Corpus between *P. boisei* and *P. robustus*. (**G**) Mandibular Analysis 3- Midline between *P. boisei* and *P. robustus*.

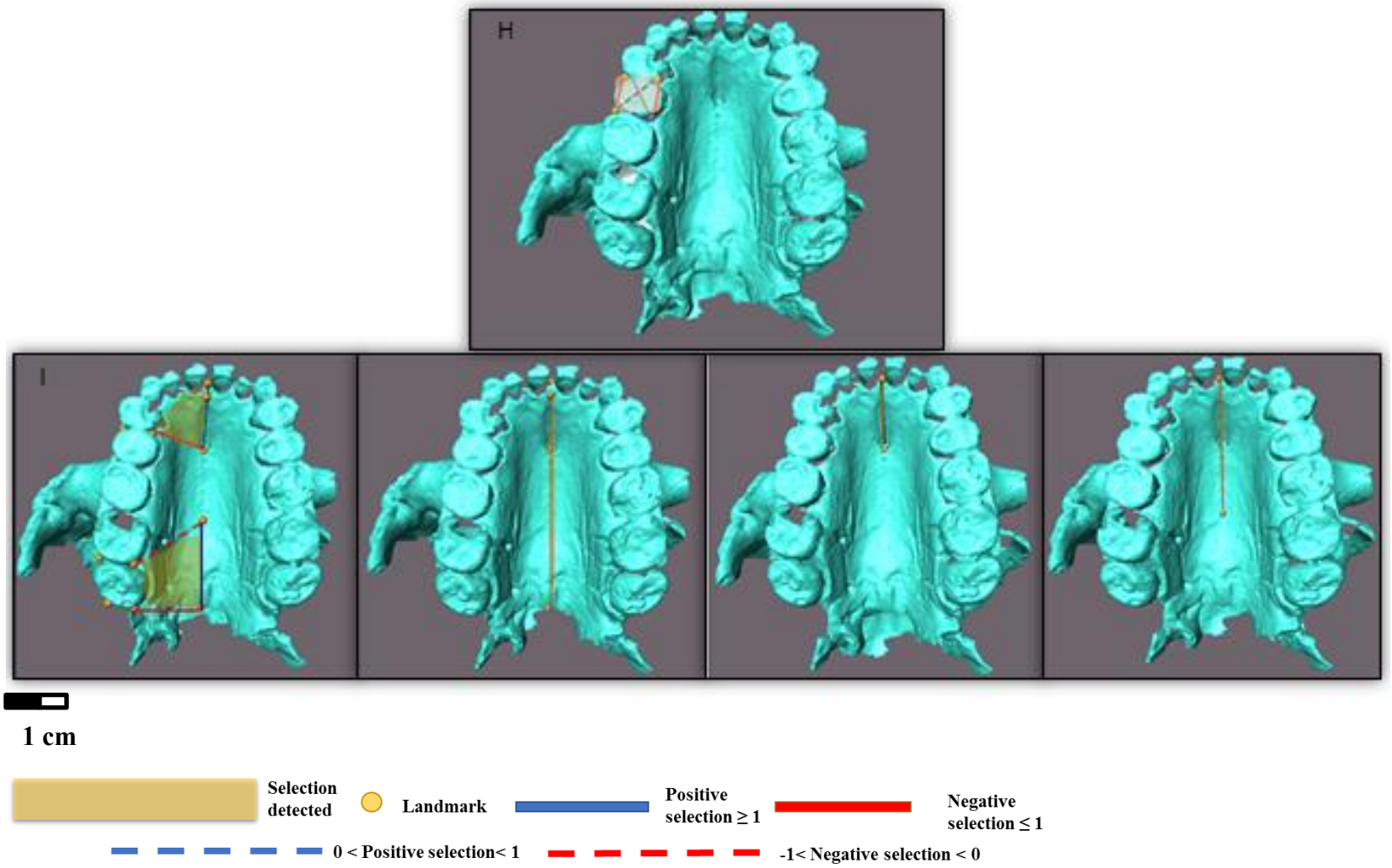

Figure 5.45. Visually represented selection vectors necessary to produce observed differences in

palatal morphology. Landmark definitions are given in **Table 4.3**.

Selection vector values are presented in **Table 5.43.**. The palatal regions undergoing

selection are given in yellow. Positive and negative selection vectors are shown in blue and red

respectively. Strongly positive (values ≥ 1) and strongly negative (values ≤ -1) selection are

represented by solid lines. Weak to moderate selection (0 > values > 1; -1 < values < 0) are displayed

as dashed lines. (**H**) Densified Palate Analysis 5 – P4 Complex between *P. boisei* and *P. robustus*. (**I**) Densified Palate Analysis 1 – Midline between *P. boisei* and *P. robustus*.

Table 5.5.1. Reconstructed differential selection vectors for the cranial regions.

CRANIAL ANALYSIS 1								
MIDFACE-MAXILLA		**ANS-PRO**	**ALR-ANS**	**P3D-P4D**	**M2D-M1D**	**M1D-P4D**	**M2D-M3D**	**ENM-OL**
A. africanus- P. robustus	DIFFERENCE VECTOR	4.3	-4.6	-0.5	-1.47	0.64	-1.56	-5.47
	β_h	0.26	-0.23	**-1.9**	0.00	*1.77*	0.05	-0.79
	β_c	0.70	-0.33	-0.04	**-2.27**	*3.12*	-0.45	**-1.56**
	βg	0.5	-0.61	**-1.67**	-0.98	*1.79*	0.05	-0.02
CRANIAL ANALYSIS 6								
TEMPORAL		**EAM (A)-EAM (P)**	**EMI-POR**	**MFL-EMI**	**POR-MFL**	**POR-MFM**	**AST-POR [L]**	**MFL-AST**
P. aethiopicus-P. robustus	DIFFERENCE VECTOR	**-1.34**	**-8.67**	**-4.03**	*4.85*	**-3.58**	*9.01*	*9.51*
	β_h	0.66	**-2.59**	*2.9*	*12.55*	-0.96	*12.38*	**-12.78**
	β_c	**-5.1**	**-6.39**	**-6.17**	*11.8*	**-2.54**	*3.06*	**-3.3**
	βg	-0.31	-0.83	0.67	**10.23**	-0.87	**9.7**	**-9.83**
TEMPORAL		**EAM (A)-EAM (P)**	**EMI-POR**	**MFL-EMI**	**POR-MFL**	**POR-MFM**	**AST-POR [L]**	**MFL-AST**
P. aethiopicus-A. africanus	DIFFERENCE VECTOR	-3.11	2.35	4.86	-4.96	7.03	7.56	3.89
	β_h	-0.54	**-3.01**	*3.35*	**-4.81**	*3.11*	**-1.31**	*1.03*
	β_c	**-1.15**	2.24	*7.4*	**-7.65**	*4.03*	*1.84*	**-2.22**
	βg	0.34	**-1.69**	*1.88*	**-3.51**	*1.42*	0.12	0.29
TEMPORAL		**EAM (A)-EAM (P)**	**EMI-POR**	**MFL-EMI**	**POR-MFL**	**POR-MFM**	**AST-POR [L]**	**MFL-AST**
P. robustus- A. africanus	DIFFERENCE VECTOR	-4.46	-6.32	0.83	-0.1	3.45	-1.46	-5.63
	β_h	0.12	**-5.61**	*6.2*	*7.74*	*2.15*	*11.07*	**-11.75**
	β_c	**-6.25**	**-4.15**	*1.31*	*4.14*	*1.48*	*4.91*	**-5.52**
	βg	0.04	**-2.53**	*2.57*	*6.72*	0.55	*9.82*	**-9.53**

Table 5.5.2. Reconstructed differential selection vectors for the mandibular regions.

MANDIBULAR ANALYSIS 1								
RAMUS		**MEN-RAM POS**	**JUNC-RAM PO**	**AJUNC-GON**	**ALVS-GON**	**RAM POS-GON**	**MEN-GON**	
P. boisei- P. robustus	DIFFERENCE VECTOR	-9.06	7.2	4.53	-4.4	-19.51	1.56	
	β_h	3.54	-0.58	4.32	-0.77	**-4.53**	**-4.81**	
	β_c	**-5.03**	*5.01*	**-2.83**	-0.56	-0.37	*4.79*	
	βg	-0.79	*1.68*	**-1.26**	-0.04	-0.42	0.59	
MANDIBULAR ANALYSIS 2								
CORPUS		**MEN-ALVB**	**MEN-IBB**	**P3D-P4D**	**P4D-M1D**	**M1D-M2D**	**M2D-M3D**	**ALVB-M2D**
P. boisei- P. robustus	DIFFERENCE VECTOR	-0.88	-7.56	0.44	-0.25	2.05	-2.89	-8.58
	β_h	0.36	-0.41	0.02	0.00	-0.51	**-1.96**	-0.21
	β_c	-0.23	**-1.8**	0.24	**-1.15**	0.88	***-5.89***	-0.81
	βg	-0.02	-0.47	0.98	-0.56	-0.35	-0.95	-0.14
MANDIBULAR ANALYSIS 3								
MIDLINE		**P3D-P3D[R]**	**P4D-P4D[R]**	**M1D-M1D[R]**	**MEN-MEN**			
P. boisei- P. robustus	DIFFERENCE VECTOR	-5.14	-8.51	-21.35	-15.03			
	β_h	*1.31*	-0.16	**-1.84**	-0.23			
	β_c	*1.5*	*2.37*	**-7.57**	-0.09			
	βg	*2.01*	*1.32*	**-5.16**	0.01			

Table 5.5.3. Reconstructed differential selection vectors for the palatal regions.

ISIFIED PALATE ANALYSIS 1									
MIDLINE		**IDS-OL**	**IDS-INC**	**IDS-PTM**	**IDS-ALV**	**OL-INC**	**OL-PTM**	**OL-ALV**	**INC-PTM**
P. boisei-P. robustus	DIFFERENCE VECTOR	0.63	1.41	1.14	-1.65	0.75	0.17	-2.57	-0.13
	βh	**-10.86**	**-7.39**	*11.92*	*5.57*	*5.75*	**-11.94**	**-4.88**	**-1.64**
	βc	**-8.27**	**-47.21**	*58.88*	**-3.37**	*37.93*	**-56.86**	*8.27*	**-11.07**
	βg	*1.07*	**-7.41**	*19.9*	**-12.99**	*8.22*	**-12.61**	*4.9*	**-14.43**
		INC-ALV	**PTM-ALV**	**ALV-M3DL**	**ALV-M3DB**	**PTM-M2DL**	**PTM-M2DB**	**INC-P3DL**	**INC-P3DB**
	DIFFERENCE VECTOR	-2.84	-2.77	3.03	4.01	0.7	2.11	1.85	2.24
	βh	0.03	**-2.23**	0.24	*1.74*	**-1.67**	*1.63*	*1.11*	0.55
	βc	*2.7*	**-8.75**	0.09	*2.19*	**-2.4**	0.85	*1.85*	*2.49*
	βg	*15.07*	**-7.51**	-0.22	0.96	-0.16	-0.18	-0.24	0.54
ISIFIED PALATE ANALYSIS 5									
P4 COMPLEX		P4DL-P3DL	P4DB-P3DB	P4DL-P4DB	P4DB-P3DL	P4DL-P3DB			
P. boisei-P. robustus	DIFFERENCE VECTOR	1.29	1.28	0.03	1.7	0.37			
	βh	*2.06*	*1.78*	**-1.1**	0.36	**-1.22**			
	βc	0.97	*1.21*	**-1.08**	*1.67*	-0.19			
	βg	*1.59*	*1.02*	0.98	0.04	**-2.59**			

CHAPTER 6

DISCUSSION/

CONCLUSION

Past research on the morphology of *Paranthropus* has primarily concentrated on describing cranial morphology and determining phylogenetic relationships, with less focus on understanding intra-specific variation (e.g. Rak, 1983, Kimbel, 2006; Wood 2010, Wood and Schroer, 2017). Moreover, our interpretation of the craniofacial morphology of *Paranthropus* has been contextualized within an adaptive framework, with little consideration of the role that random divergence (i.e. drift) might play in producing diversity. The goal of this research was both to further understand intra-specific variation in the cranium and to explore the evolutionary processes that have shaped craniofacial diversification in this genus. What follows is a summary of the findings in the context of the research objectives, as well as a brief discussion of the limitations of this work and future research goals.

Evaluating Objectives

Objective 1: To understand and quantify inter-individual variation in *Paranthropus.*

- Question 1a: Are there significant differences in craniodental morphology between East and South African *Paranthropus* specimens for the variables being examined?

In a number of analyses, there are significant morphological differences between the East and South African *Paranthropus* specimens. In particular, *P. boisei* and *P. aethiopicus* specimens are shown to be significantly different from South African specimens (*P. robustus*) and from each other (*P. boisei* and *P. aethiopicus*). This result highlights the general consensus and importance of treating these three taxa as individual species (Constantino and Wood, 2007; Grine, 1988;

McCollum, 1999). This can be seen between *P. robustus* and in both *P. boisei* and *P. aethiopicus* in the temporal region, where species are clearly separate and distinct. These include comparisons between. DNH 7 (*P. robustus*) KNM-ER 406 (*P. boisei*) and KNM-WT 17000 (*P. aethiopicus*). In addition, this is indicated between comparison of SK 48 –*P. robustus*- and KNM-ER 406 and KNM-WT 17000. Furthermore, gracile australopith, Sts 5 (*A. africanus*) is also a distinct species from both *P. aethiopicus* and *P. boisei* (to a lesser extent). Several cranial analyses reveal throughout that East African specimens are distinct and separate. It must be noted that due to a small East African sample size particularly one *P. aethiopicus* cranial sample, analyses were limited.

This study corroborates past research (Ackermann, 1988; Hlazo, 2015; Schroeder, 2007) in that these results demonstrate the large degree of intra-specific variation *in P. robustus* and within South African specimens more generally. They also highlight the distinctiveness of the robust australopiths from gracile australopiths (represented by *A. africanus* in this study). These analyses contribute to our understanding of the phylogenetic relationships between paranthropines (e.g. Grine, 1988; Strait et al., 1997; Ward, 1991) in so far as they demonstrate the distinctiveness of the East and South African material in some regions of the cranium. Differences may be attributed to the smaller less derived features such as size of the posterior tooth dentition, palate, size of the mandible and general "robustness" of the cranium and mandible seen in *P. robustus* versus *P. boisei*, and the anterior dentition and general size (of *P. aethiopicus* (Rak, 1983; Walker and Leakey, 1988)

- Question 1b: Does intra-specific variation (to the degree that it can be quantified) in East and South African paranthropine species differ?

Although it is difficult to assess, the results reported here may suggest that there is more intra-specific variation in the South African paranthropines than there is in the East African paranthropines. This is reflected in the fact that, in some analyses (see e.g., **Mandibular Analysis 2**, corpus region), the PCoA plots reveal that East African specimens form relatively tight clusters with little distance between specimens (suggesting a relatively lower level of intra-specific variation in this group), whereas the South African specimens, by contrast, are relatively

dispersed with larger distances between specimens (suggesting a relatively greater level of intra-specific variation in this group). A relatively large degree of dispersion among the South African specimens is also seen in the analyses of the ramus and corpus (**Mandibular Analysis 1-2**) and in the zygomatic and upper face (**Cranial Analysis 3**) as well as in the temporal region (**Cranial Analysis 6**); however, these results are severely hampered by small sample sizes for the East African group (see below).

In general, these results may indicate that there is greater intra-specific variation in *P. robustus* relative to *P. boisei* and that the best evidence for the larger degree of variation in *P. robustus* comes from the mandibular corpus. However, the sample size of East African specimens size is small in all of the analyses (and always smaller than that of the South African specimens); thus, the results reported here may provide neither an accurate representation of the degree of intra-specific variation in the East African sample nor a realistic comparison of the amount of intra-specific variation in the two groups. It is also worth noting that the South African sample includes at least one specimen (DNH 7) which is unambiguously female, whereas the east African sample includes only one female cranium (KNM-ER 732) and no unambiguously female mandibles. Therefore, the larger degree of intraspecific variation in the South African sample may be due to the fact that sexual dimorphism (for mandibles) is included in the sample, but not in the East African sample (without mandibles).

- Question 1c: Do DNH 7 and DNH 8 differ significantly from other *P. robustus* specimens?

Many questions have been raised regarding how the Drimolen material compare to other specimens assigned to the genus *Paranthropus* and, particularly, to those assigned to *P. robustus* (Keyser, 2000). Therefore, the morphological comparisons of the Drimolen material provided here have important implications for interpreting the variation in *Paranthropus*, more generally, and in *P. robustus* more specifically. The results presented here demonstrate that the Drimolen specimens are distinct from other *P. robustus* specimens, particularly in the morphology of the lower region of the face and mandible in both the size and robustness of the corpus height/width and palate. The two Drimolen specimens are also significantly different from each other, which may reflect sexual dimorphism (i.e., since DNH 8 is considered to be a male and DNH 7 is

considered to be a female). These differences are highlighted in the in the mandible and maxilla, particularly in the mandibular corpus (height/width) and palate.

The significant differences seen between the two Drimolen specimens may be attributed to sexual dimorphism. The differences seen between both DNH 7 & DNH 8 in comparison to the other *P. robustus* specimens changes the approach and way of understanding into the taxonomic variability that exists in the South African specimens. Results have shown that variation within the South African specimens is large and needs to be treated differently as the differences might not solely relate to just a greater variability within a species; taxonomy (taxonomic implications) may play a role too. Many researchers, as highlighted by Cofran and Thackeray (2009) in their study, conclude that specimens from Swartkrans and other nearby sites should be subsumed into a single *P. robustus* species. However, researchers such as Schwartz and Tattersall (2005) argue that these two sites carry two different species i.e., *P. robustus* and *P. crassidens.* Nevertheless, researchers have not reached a general consensus on this (Cofran and Thackeray, 2009).

Objective 2: To understand the effects of extant model choice on interpretations of morphological distance.

- Question 2a: Do different extant species provide different estimates of morphological distance among *Paranthropus* individuals*?*

Previous research (e.g. Ackermann, 2003; Hlazo, 2015; Schroeder, 2007, 2015) has shown that using different extant models results in different estimates of morphological distance. This study further contributes to this work by showing that human and chimpanzee models show comparable (similar) trends in the face, zygoma and temporal regions of the cranium (**Cranial Analysis 1**, **Cranial Analysis 2** and **Cranial Analysis 4).** There is a tendency for analyses using gorilla models to show the smallest number of significant differences among specimens and less so for other two extant taxa. As in previous studies (Ackermann, 1998; 2003; Hlazo, 2015; Schroeder,

2007), this study also shows that same-species (i.e., chimp pairwise distances calculated in a chimp V/CV matrix) and different-species (chimp pairwise distances calculated in a human V/CV matrix) evaluations of significance change interpretation of the results.

This study shows that extant models need to be used cautiously as these "analogues" may change distance values and significance in different morphological regions depending on what species are used. In addition, this study highlights that the effect of the choice of model also varies depending on the region that is being investigated and the size of the samples being analysed. Although this method may be a conservative approach into the extrapolation of *Paranthropus* V/CV estimates (Ackermann, 1998, 2003; Schroeder, 2007), variation in this study maybe duly over or underestimated which tells us that analyses may not be as informative or appropriate as we thought and that other methods and approaches to estimate variation in *Paranthropus* should be formulated.

- Question 2b: Are extant ape models more appropriate models of *Paranthropus* variability than human models (possibly because of different magnitudes/patterns of sexual dimorphism)?

The results presented here suggest that *G. gorilla* models are the most appropriate models for studying craniodental variation in *Paranthropus*. As mentioned above, human models generally show larger significant differences and Mahalanobis'distance values where gorilla models show fewer significant differences and smaller values (for example **Cranial Analysis 1**, **Cranial Analysis 2**, **Cranial Analysis 3** in the mid-face maxilla and zygomatic (zygomatic-upper) regions). Particularly striking was **Mandibular Analysis 1,** in which SK 34 RIGHT and LEFT are treated more so like the exact individual it actually is and clustered together using the gorilla model (which is what would be expected since these two specimens represent the right and left halves of the same individual) whereas it was not in the other extant models. However, in the analysis of the mandibular corpus (**Mandibular Analysis 2**), the gorilla and human appear to show SK 34 RIGHT and LEFT as separate individuals whereas the chimpanzee model clusters them together. In this analysis, the chimpanzee model provides the largest distance values, followed by the gorilla then lastly the human. This suggests that *Paranthropus* size/sex variation may be

most comparable (though not identical) to the greater sexual dimorphism and general size variation displayed by gorillas. This is important because the choice of different, possibly inappropriate, extant models (like chimpanzees) may alter the interpretation of morphological variation and taxonomy of *Paranthropus*.

Objective 3: To understand the evolutionary processes underlying diversification in *Paranthropus*.

- Question 3a: Did the diversification of *Paranthropus* species from each other occur through random processes (i.e. drift), or did adaptation play a role?

The morphological diversification of *Paranthropus* in the vast majority of comparisons was consistent with non-adaptive (neutral) evolution; in other words, drift could not be rejected. . Neutrality tests show (detect) adaptive divergence between *P. robustus* and the two East African species – *P. aethiopicus* and *P. boisei*-, however not between *P. aethiopicus* and *P. boisei*. *P. aethiopicus* (the "Black Skull", KNM-ER 17000) dated to approximately 2.7 -2.3 Ma, is chronologically older, in relation to *P. boisei* (dated to 2.4 – 1.4 Ma) and dated more recently at 1.0 Ma, *P. robustus* (Constantino and Wood, 2004; Kimbel, 2006; Wood, 2010). This includes analyses of regions such as the upperface, zygoma, basicranium and tooth complexes. This result suggests that non-adaptive processes may have played a more important role than previously thought in the diversification of these aspects of *Paranthropus* morphology. However, drift was not the only driver of paranthropine diversity. Natural selection (adaptation) also played a significant role in *Paranthropus* morphological variation and the diversification of the lineage (see further discussion below).

- Question 3b: If natural selection acted to diversify species within the genus, then which region(s) was selection acting on? Is this consistent with our understanding of morphological/functional differences in these taxa?

In general, the results of this study may suggest that selection has played a less important role in shaping the craniodental morphology in the genus *Paranthropus* than previously thought. Instead, this study highlights the possible influence of non-adaptive evolutionary processes on

the evolution and diversity of cranial anatomy in this genus. This interpretation is based on the fact that a majority of the tests conducted in this study failed to reject the null hypothesis of drift. However, selection was detected in 7 out 18 analyses (8 out 96 comparisons/tests). Specifically, selection was detected in the following regions: midface, temporal region of the skull, the mandible (corpus, ramus and midline regions) and maxilla (including the hard palate and tooth P4 tooth complex). These areas are consistent with the current understanding researchers have of the uniquely derived characteristics of the genus *Paranthropus* and interpretations of these traits with regard to the functional capabilities and biomechanics of the genus. Specifically, the regions that the results of this study indicate have been shaped by natural selection are some of those related to the masticatory apparatus and are involved in feeding biomechanics.

These regions included those to which the muscles of mastication attach (i.e., the origin and/or insertion of the masseter, temporalis, and medial pterygoid muscles). The areas in which selection is implicated also include regions (e.g., the hard palate and mandibular corpus) that would be modified by natural selection to resist strains encountered during feeding on a diet including hard and/or tough foods. It is noteworthy, though, that the null hypothesis of drift was not rejected in analyses of other regions that also comprise the masticatory apparatus (e.g., those involving portions of the zygoma). This suggests that natural selection did not drive the evolution of all the morphological features that constitute the masticatory apparatus (Ackermann and Cheverud, 2004). Further study is required to disentangle the nuances of these results. Taken together, the results of this study are mixed with regard to whether or not the uniquely derived features of the genus *Paranthropus* are functional traits that were moulded by natural selection as dietary adaptations.

- Question 3c: Did the morphological response to selective pressures change in concert with these pressures, or is there evidence of correlated response due to selection on other variables?

Morphological responses to selection were variable across the different analyses in which selection was detected. However, there are some noteworthy trends; for example, the results of many analyses (including those of different cranial and mandibular regions and those involving

different ancestor-descendant pairs) are generally consistent in so far as they show morphological responses changed in concert with vectors. In general responses to selection vectors were in the direction of the selection. This shows in morphological features such as maxillary height, overall tooth enlargement, and the mandibular largeness and robustness. However, pressures are strongly negative for the length and depth of the palate whereas responses to selection are majority positive indicating that changes in morphological features are happening in a direction opposite to the selection There is also considerable evidence for correlated responses induced by direct selection, particularly in the external auditory meatus and temporal region (ear). The differentiation is very complex where traits may change/differ, but not because they are directly acted on by selection.

Overall, these results indicate that adaptive forces play a huge and important in shaping *Paranthropus* craniofacial morphology particularly in relation to the masticatory apparatus (not in all regions or to the full extent previously thought) and understanding which morphological areas (traits) are involved may help us answer questions about diet, biomechanism and *Paranthropus* functional capabilities. In areas where drift was rejected and selection reconstructed, selection acted on features directly and indirectly acting on more than one trait simultaneously (sometimes in opposite directions) and affecting regions in the either same or different way (Lande, 1983). It is also direct selection that acted to induce correlated selection on various traits inducing morphological changes in one or more region(s). *Paranthropus* phenotypic change in response to selection proved to be adverse and also linked some regions of the masticatory apparatus to direct or correlated selection, showing how complex paranthropine morphology diversification is. However, what these results have also shown is that .selection may

Limitations and Future Research

There are two primary limitations to the study, both of which revolve around sample size. First, *Paranthropus* fossil samples – like many hominin samples – are limited in numbers, and can be poorly preserved, distorted and/or fragmented resulting in limited samples and shared morphology. For the collection of landmarks, landmark data (including variables) and/or specimens were omitted depending on the preservation of the fossil, which made the number of

individuals small for many of the comparisons. Lack of specimens may cause misinterpretation of variation, restricts the amount and kind of studies that can be performed, and generally results in less robust conclusions. Second, because of the small sample sizes for *Paranthropus*, it is impossible to estimate variance and covariance (V/CV) with any accuracy (see Ackermann 2009). This means that extant species must be used as models to estimate fossil V/CV, which has its own problems as we know that even closely related species vary in different ways (Ackermann 2002, 2003, 2005). In this thesis, an attempt was made to minimize the problems related to this issue—i.e., multiple comparative extant samples were used as models for estimating of within-taxon variation in *Paranthropus.* Nevertheless, in the absence of large samples of *Paranthropus* fossils, there is no perfect analogue for the morphological variability in this genus, and this has undoubtedly affected the results of this study.

One particularly noteworthy finding of this thesis is the fact that both adaptive (selection) and non-adaptive processes (genetic drift) were shown to be important in shaping the morphology of the genus *Paranthropus*. Specifically, genetic drift was shown to play a role in the evolution of the facial (upper face) region (including the zygoma), and selection was implicated in the temporal region of the cranium, hard palate (maxilla) and mandible. As described above, the results here may suggest that selection was responsible for shaping some but not all of the regions that are related to the masticatory apparatus, which is consistent with the long held idea that the craniodental morphology of the genus *Paranthropus* represents a dietary adaptation. However, this idea does not explain why selection was not shown to be responsible for the morphology of other regions that are similarly related to feeding behavior. Future research will delve into these outstanding questions by including more extant comparative specimens (i.e., *Pan paniscus,* more *Homo*) and additional fossil comparative specimens, (e.g.,

more gracile and robust australopith specimens). Expanding the morphological regions and density of the landmarking would be also be beneficial as it would serve to increase the number of variables. Approaches should also be honed to more directly address questions about functional morphology and mastication (and biomechanics related to functional capabilities) linked to diet. Finally, other methods such as protein signature analyses could be used to further understand the phylogenetic relationships among the various *Paranthropus* taxa.

REFERNCES

Ackermann, R.R. (1998). A QUANTITAVE ASSESSMENT OF VARIABILITY IN THE AUSTRALOPITHECINE, HUMAN, CHIMPANZEE AND GORILLA FACE. Ph.D. Dissertation: University of Washington, St. Louis.

Ackermann, R.R. (2002). Patterns of covariation in the hominoid craniofacial skeleton: implications for paleoanthropological models. *Journal of Human Evolution*. 42(1): 167-187.

Ackermann, R.R. (2003). Using extant morphological variation to understand fossil relationships: a cautionary tale. *South African Journal of Science*. 99(1): 255-258.

Ackermann, R.R. (2005). Variation in Neanderthals: a response to Harvati (2003). *Journal of Human Evolution*. 48(6): 1-4.

Ackermann, R.R. (2009). Morphological integration and the interpretation of fossil hominin diversity. *Evolutionary Biology*. 36(1): 149-156.

Ackermann, R.R. and Cheverud, J.M. (2000). Phenotypic covariance structure in tamarins (genus *Saguinas*): a comparison of variation patterns using matrix correlation and common principal component analysis. *American Journal of Physical Anthropology*. 111(1): 489-501.

Ackermann, R.R. and Cheverud, J.M. (2002). Discerning evolutionary processes in patterns of tamarin (genus *Saguinas*) craniofacial variation. *American Journal of Physical Anthropology*. 117(3): 260-271.

Ackermann, R.R. and Cheverud, J.M. (2004). Detecting genetic drift versus selection in human evolution. *PNAS*. 101(52): 17946-17951.

Ahern, J.C., Hawks, J.D. and Lee, S.H. (2005). Neandertal taxonomy reconsidered… again: a response to Harvati et al. (2004). *Journal of human evolution*. 48(6): 647-652.

Baab, K.L., McNulty, K.P. and Rohlf, F.J. (2012). The shape of human evolution: a geometric morphometrics perspective. *Evolutionary Anthropology: Issues, News, and Reviews.* 21(4): 151-165.

Bass, W. M. (1987). *Human osteology: a laboratory and field manual* (No. 2). Missouri Archaeological Society.

Balter, V., Braga, J., Télouk, P. and Thackeray, J.F. (2012). Evidence for dietary change but not landscape use in South African early hominins. *Nature*. 489(7417): 558-560.

Benazzi, S., Kullmer, O., Schulz, D., Gruppioni, G. and Weber, G.W. (2013). Individual tooth macrowear pattern guides the reconstruction of Sts 52 (*Australopithecus africanus*) dental arches. *American journal of physical anthropology*. 150(2): 324-329.

Bookstein. F.L. (1991). *Morphometric tools for landmark data: Geometry and Biology*. Cambridge: Cambridge University Press.

Bookstein, F.L., Chernoff, B., Elder, R.L., Humphries, J.M., Smith, G.R. and Strauss, R.E. (1985). *Morphometrics in evolutionary biology: the geometry of size and shape change, with examples from fishes*. Special Publication 15. *The Academy of Natural Sciences of Philadelphia*.

Brain, C.K. (1967). The Transvaal Museum's Fossil project at Swartkrans. *South African Journal of*
Science 63(9): 378-384.

Brain, C.K. (1981). *The Hunters or the Hunted? An Introduction to African Cave Taphonomy.* Chicago: University of Chicago.

Brain, C.K. (1988). New Information from the Swartkrans cave of relevance to "robust" australopithecines. In Grine, F.E. (eds.). *Evolutionary History of the "Robust" Australopithecines*. New York: Aldine de Gruyter.

Broom, R. (1938a). More discoveries of *Australopithecus*. *Nature*. 141(1): 828-829.

Broom, R. (1938b). The pleistocene anthropoid apes of South Africa. *Nature*. 142(3591): 377-379.

Broom, R. (1947). Discovery of a new skull of the South African ape-man, *Plesianthropus. Nature.* 159(4046): 672.

Broom, R. (1949). Another new type of fossil ape-man (*Paranthropus crassidens*). *Nature.* 163(4132): 57.

Broom, R. (1950). The genera and species of the South African fossil ape-man. *American Journal of Physical Anthropology*. 8(1): 1-14.

Broom, R. (1950). *Finding the missing link*. London: Watts & Co.

Broom, R. and Robinson, J.T. (1949). A new type of fossil man. *Nature* 164(4164): 322-323.

Broom, R. and Robinson, J.T. (1950). Note on the skull of the Swartkrans ape-man *Paranthropus*
crassidens. *American Journal of Physical Anthropology* 8(3): 295-304.

Broom, R., Robinson, J.T., Schepers, G.W.H. (1950). Sterkfontein Ape-Man Plesianthropus. Transvaal Museum Memoir 4, Transvaal Museum, Pretoria.

Broom, R. and Robinson, J.T. (1952). *The Swartkrans ape-man*. Transvaal Museum Memoir 6, Transvaal
Museum, Pretoria.

Buttigieg, P.L. and Ramette, A. (2014). A guide to statistical analysis in microbial ecology: a community-focused, living review of multivariate data analyses. *FEMS Microbiology Ecology*. 90(3): 543–550. Available from: http://mb3is.megx.net/gustame/dissimilarity-based-methods/principal-coordinates-analysis. [13 November 2017].

Butzer, K. W. (1976). Lithostratigraphy of the Swartkrans formation. *South African Journal of Science*. 72(5): 136-141.

Cazenave, M., Braga, J., Oettlé, A., Thackeray, J.F., de Beer, F., Hoffman, J., Endalamaw, M., Redae, B.E., Puymerail, L. and Macchiarelli, R. 2017. Inner structural organization of the distal humerus in *Paranthropus* and *Homo*. *Comptes Rendus Palevol*. 16(5-6): 521-532.

Cerling, T.E., Mbua, E., Kirera, F. M., Manthi, F. K., Grine, F.E., Leakey, M. G., Sponheimer, M. and Uno, K.T. (2011). Diet of *Paranthropus boisei* in the early Pleistocene of East Africa. *Proceedings of the National Academy of Sciences*. 108(23): 9337-9341.

Cheverud, J.M. (1988). A comparison of genetic and phenotypic correlations. *Evolution*. 42(5): 958-968.

Clark Gros, W.E.L.E. (1970). *History of the primates*. 10th ed. London: British Museum. Available from: http://www.ibri.org/Books/Pun_Evolution/Chapter2/2.3.htm. [10/27/2017].

Clarke, R.J. (1988). A new *Australopithecus* cranium from Sterkfontein and Its bearing on the ancestry of *Paranthropus*. In Grine, F.E. (eds.). *Evolutionary History of the "Robust" Australopithecines*. New York: Aldine de Gruyter.

Clement A. and Hillson, S. (2013). 'Do larger molars and robust jaws in early hominins represent dietary adaptation?' A New Study in Tooth Wear. *Archaeology International*.16(1): 59-71.

Cofran, Z. and Thackeray, J.F., 2010. One or two species? A morphometric comparison between robust australopithecines from Kromdraai and Swartkrans. *South African Journal of Science*. 106(1-2): 40-43.

Conroy, G.C. and Pontzer, H. (2012). *Reconstructing Human Origins: a modern synthesis*. New York: V W Norton & Company.

Conroy, G.C., Falk, D., Guyer, J., Weber, G.W., Seidler, H. and Recheis, W. (2000). Endocranial capacity in Sts 71 (*Australopithecus africanus*) by three-dimensional computed tomography. *The Anatomical Record*. 258(4): 391-396.

Copes, L.E. (2012). Comparative and experimental investigations of cranial robusticity in mid-Pleistocene hominins. Ph.D Dissertation: Arizona State University, Arizona.

Copes L.E. and Kimbel, W.H. (2016). Cranial vault thickness in primates: *Homo erectus* does not have uniquely thick vault bones. *Journal of Human Evolution.* 90(1): 120-134.

Constantino, P.J. and Wood, B.A. (2004). *Paranthropus* paleobiology In: *Miscelanea en Homenae a Emiliano Aguirre*. Volumen III: Paleoantropologia. Alcala de Henares: Museo Arqueologico Regional.

Constantino, P. and Wood, B. (2007). The evolution of *Zinjanthropus boisei*. *Evolutionary Anthropology. Issues, News, and Reviews*. 16(2): 49–62.

Daegling, D.J., Judex, S., Ozcivivi, E., Ravosa, M.J., Taylor, A.B., Grine, F.E., Teaford, M.F. and Ungar, P.S. (2013). Viewpoints: feeding mechanics, diet, and dietary adaptations in early hominins. *American Journal of Physical Anthropology*. 151(3): 356–371.

Daegling, D.J., McGraw, W.S., Ungar, P.S., Pampush, J.D., Vick, A.E. and Bitty, E.A. (2011). Hard-Object feeding in sooty mangabeys (*Cercocebus atys*) and interpretation of early hominin feeding ecology. *PLoS ONE*. 6(9): 1-12.

Dean, M.C. (1988). Growth of teeth and development of the dentition in *Paranthropus*. In Grine, F.E. (eds.). *Evolutionary History of the "Robust" Australopithecines*. New York: Aldine de Gruyter.

Delson, E., Tattersall, I., Van Couvering, J., and Brooks, A. S. (eds.). (2004). *Encyclopedia of human evolution and prehistory*. New York: Routledge, Taylor and Francis Group.

Freidline, S.E., Gunz, P., Harvati, K., and Hublin, J.J. (2012). Middle Pleistocene human facial morphology in an evolutionary and developmental context. *Journal of Human Evolution*. 63(5): 723-740.

Grine, F.E. and Strait, D.S. (1994). New hominid fossils from Member 1 "Hanging Remnant", Swartkrans Formation, South Africa. *Journal of Human Evolution*. 26(1): 57-75.

Grine, F.E. (1988). New Craniodental fossils of *Paranthropus* from the Swartkrans Formation and their significance in "robust" australopithecine evolution. In Grine, F.E. (eds.). *Evolutionary History of the "Robust" Australopithecines*. New York: Aldine de Gruyter.

Grine, F.E., Sponheimer, M., Ungar, P.S., Lee-Thorp, J. and Teaford, M.F. (2012). Dental microwear and stable isotopes inform the Paleoecology of extinct Hominins. *American Journal of Physical Anthropology*. 148(2): 285–317.

Hay, R.L. (1976). *Geology of the Olduvai Gorge: A study of sedimentation in a semiarid basin*. Berkeley: University of California Press.

Hay, R.L. (1990). Olduvai Gorge: a case history in the interpretation of hominid paleoenvironments. In: L. Laporte (eds.). *East Africa. Establishment of a geologic framework for paleoanthropology*. Boulder: Geological Society of America Special Paper. 242 (2): 23-37.

Harris, J. M., Brown, F. H., Leakey, M. G., Walker, A. C., & Leakey, R. E. (1988). Pliocene and Pleistocene hominid-bearing sites from west of Lake Turkana, Kenya. *Science*. 239(4835): 27-33.

Harvati, K. (2003). The Neanderthal taxonomic position: models of intra- and inter-specific craniofacial variation. *Journal of Human Evolution*. 44(1): 107-132.

Harvati, K., Frost, S.R. and McNulty, K.P. (2005). Neandertal variation and taxonomy- a reply to Ackermann (2005) and Ahern et al. (2005). *Journal of Human Evolution*. 48(6): 653-660.

Herries, A. I., and Adams, J. W. (2013). Clarifying the context, dating and age range of the Gondolin hominins and *Paranthropus* in South Africa. *Journal of Human Evolution*. 65(5): 676-681.

Herries, A.I. and Shaw, J. (2011). Palaeomagnetic analysis of the Sterkfontein palaeocave deposits: Implications for the age of the hominin fossils and stone tool industries. *Journal of Human Evolution*. 60(5): 523-539.

Hlazo, N. (2015). *Paranthropus*: Variation in Cranial Morphology. Honours Thesis: University of Cape Town, Cape Town.

Isaac, Gl. (1978). In Leakey, M.G. and Harris, J.M. (eds.). *Koobi Fora Research Project: The Fossil hominids and an introduction to their context, 1968-1974* (Vol. 1). New York: Oxford University Press.

Howell, F.C. and Coppens, Y. (1976). An Overview of Hominidae from the Omo Succession, Ethopia. In Coppens, Y., Howell, G. LI.I. and Leakey, R.E.F. (eds.). *Earliest Man and Environments in the Lake Rudolf Basin: Stratigraphy, Paleoecology, and Evolution.* Chicago: University of Chicago Press.

Jungers, W.L. (1988). New estimates of body size in australopithecines. In Grine, F.E. (eds.). *Evolutionary History of the "Robust" Australopithecines*. New York: Aldine de Gruyter.

Kay, R.F. and Grine, F.E. (1988). Tooth morphology, wear and diet in *Australopithecus* and *Paranthropus* from southern Africa. In Grine, F.E. (eds.). *Evolutionary History of the "Robust" Australopithecines*. New York: Aldine de Gruyter.

Keyser, A. W. (2000). The Drimolen skull: the most complete australopithecine cranium and mandible to date. *South African Journal of Science*. 96(4): 189-192.

Keyser, A. W., Menter, C. G., Moggi-Cecchi, J., Pickering, T. R., & Berger, L. R. (2000). Drimolen: a new hominid-bearing site in Gauteng, South Africa. *South African Journal of Science*. 96(4): 193-197.

Kimbel, W.H. and White, T.D. (1988). Variation, sexual dimorphism and the taxonomy of *Australopithecus*. In Grine, F.E. (eds.). *Evolutionary History of the "Robust" Australopithecines*. New York: Aldine de Gruyter.

Kimbel, W.H., White, T.D. and Johanson, D.C. (1988). Implications of KNN-WT 17000 for the Evolution of "Robust" *Australopithecus*. In Grine, F.E. (eds.). *Evolutionary History of the "Robust" Australopithecines*. New York: Aldine de Gruyter.

Kimbel, W.H. (2006). The Species and Diversity of Australopiths.*Springer*. 1(1): 1-35.

Kimura, M. (1955a). Solution of a process of random genetic drift with a continuous model. *Proceedings of the National Academy of Sciences*. 41(3): 144-150.

Kimura, M. (1955b). Random Genetic Drift in Multi-Allelic Locus. *Evolution*. 9(4): 419-435.

Kimura, M. (1968). Evolutionary rate at the molecular level. *Nature*. 217(1): 624-626.

Kimura, M. (1991).The neutral theory of molecular evolution: a review of recent evidence. *The Japanese Journal of Genetics.* 66(4): 367-386.

Klingenberg, C.P., and G.S. McIntyre. (1998). Geometric morphometrics of developmental instability: analyzing patterns of fluctuating asymmetry with Procrustes methods. *Evolution*. 52(1): 1363-1375.

Kligenbgerg, C.P., Barluenga, M. and Meyer, A. (2002). Shape Analysis of symmetric structures: Quantifying variation among individuals and asymmetry. *Evolution*. 56(10): 1909-1920.

Klingenberg, C.P. (2011). MorphoJ: an integrated software package for geometric morphometrics. *Molecular Ecology Resources.* 11(1): 353-357.

Lacruz, R. S. (2008). *Primate enamel development with emphasis on South African Plio-Pleistocene fossil hominids*. Ph.D. Dissertation: University of the Witwatersrand, Johannesburg.

Lande, R. (1977). Statistical tests for natural selection on quantitative characters. *Evolution*.31 (2): 442-444.

Lande, R. (1979). Quantitative Genetic Analysis of Multivariate Evolution: Applied to Brain: Body size allometry. *Evolution*. 33(1): 402-416.

Lande, R. (1980). Genetic variation and phenotypic evolution during allopatric speciation. *The American Naturalist*. 116(4): 463-479.

Lande, R. and Arnold, S.J. (1983). The measurement of selection on correlated characters. *Evolution*. 37(6): 1210-1226.

Leakey, L.S.B. (1959). A New Fossil Skull from Olduvai. *Nature*. 184(4685): 491-493.

Leakey, R.E.F. (1976). An Overview of the Hominidae from East Rudolf, Kenya. In Coppens, Y., Howell, G. LI.I. and Leakey, R.E.F. (eds). *Earliest Man and Environments in the Lake Rudolf Basin: Stratigraphy, Paleoecology, and Evolution.* Chicago: University of Chicago Press.

Leakey, R.E.F and Walker, A. (1988). New *Australopithecus boisei* Specimens from East and West Lake Turkana, Kenya. *American Journal of Physical Anthropology*. 76(1): 1-24.

Leakey, M.D., Clarke, R.J. and Leakey, L.S.B. (1971). New hominid skull from Bed I, Olduvai Gorge,
Tanzania. *Nature.* 232(5309):308-312.

Leakey, R.E.F. (1972). Further evidence of Lower Pleistocene hominids from East Rudolf, North Kenya, 1971. *Nature.* 237(1): 264-269.

Leakey, R.E.F. and Walker, A.C., 1973. New australopithecines from East Rudolf, Kenya (III). *American journal of physical anthropology*. 39(2): 205-221.

Lee-Thorp, J.A., Sponheimer, M., Passey, B.H., de Ruiter, D.J., and Cerling, T.E. (2010). Stable isotopes in fossil hominin tooth enamel suggest a fundamental dietary shift in the Pliocene. *Philosophical Transactions of the Royal Society*. 365(1): 3389-3396.

Lee-Thorp, J. (2011). The demise of "Nutcracker man". *PNAS*. 108(23): 9319–9320.

Lockwood, C.A. (1999). Sexual Dimorphism in the Face of *Australopithecus*. *American Journal of Physical Anthropology.* 108 (1): 97–127

Lockwood, C.A., Menter, C.G., Moggi-Cecchi, J. and Keyser, A. W. (2007). Extended Male Growth in a Fossil Hominin Species. *Science*. 318 (1): 1443-1445.

Lofsvold, D. (1988). Quantitative Genetics of Morphological Differentiation in *Peromyscus* II. Analysis of Selection and Drift. *Evolution*. 42(1): 54-67.

Lucas, P.W., Omar, R., Al-Fadhalah, K., Almusallam, A.S., Henry, A.G., Michael, S., Thai, L.A., Watzke, J., Strait, D.S. and Atkins, A.G. (2013). Mechanisms and causes of wear in tooth enamel: implications for hominin diets. *Journal of the Royal Society Interface*. 10(1): 1-9.

Macho, G.A. (2014). Baboon feeding Ecology informs the dietary niche of *Paranthropus boisei*.*PLOSONE*. 9(1): 1-8.

Manly, B.F.J. (1986). Multivariate Statistical Methods: a Primer. London: Chapman and Hall.

Martinez, L.M., Estebaranz-Sάnchez, F., Galbany, J. and P̃erez-P̃erez, A. (2016). Testing Dietary Hypotheses of East African Hominins Using Buccal Dental Microwear Data. *PLos ONE*. 11(11): 1-25.

Marriog, G. and Cheverud, J.M. (2004). Did Natural Selection or Genetic Drift Produce the Cranial Diversification of Neotropical Monkeys? *The American Naturalist*. 163(3): 417-428.

McHenry, H.M. (1988). New Estimates of Body Weight in Early Hominids and Their Significance to Encephalization and Megadontia in "Robust" Australopithecines. In Grine, F.E. (eds.). *Evolutionary History of the "Robust" Australopithecines*. New York: Aldine de Gruyter.

McCollum, M. A. (1999). The Robust Australopithecine Face: A Morphogenetic Perspective. *Science*. 284(1): 301-304.

Menter, C. G., Pickering, T. R., and Keyser, A. W. (1999). International Union for Quaternary Research. In *XV International Congress Book of Abstracts*. 1(1): 124-124.

Partridge, T.C. and Watt, I.C. (2001). The stratigraphy of the Sterkfontein hominid deposit and its relationship to the underground cave system. *Palaeontologia africana*. 28(1).

Partridge, T.C., Granger, D.E., Caffee, M.W. and Clarke, R.J. (2003). Lower Pliocene hominid remains from Sterkfontein. *Science*. 300(5619): 607-612.

Pickering, T.R., Heaton, J.L., Clarke, R.J. Sutton, M.B., Brain, C.K. and Kuman, K. (2012). New hominid fossils from Member 1 of the Swartkrans Formation, South Africa. *Journal of Human Evolution.* 62(1): 618-628.

Pickering, R. and Kramers, J.D. (2010). Re-appraisal of the stratigraphy and determination of new U-Pb dates for the Sterkfontein hominin site, South Africa. *Journal of Human Evolution*. 59(1): 70-86.

Pickering, R., Kramers, J. D., Hancox, P. J., de Ruiter, D. J., and Woodhead, J. D. (2011). Contemporary flowstone development links early hominin bearing cave deposits in South Africa. *Earth and Planetary Science Letters*. 306(1-2): 23-32.

Plavcan, J.M. (2001). Sexual Dimorphism in Primate Evolution. *Yearbook of Physical Anthropology*. 44(1): 25–53.

Rabenold, D. and Pearson, O.M. (2011). Abrasive, Silica phytoliths and the Evolution of thick molar enamel in Primates, with implications for the diet of *Paranthropus boisei*. *PLoSONE*. 6(12): 1-11.

Rak, Y. (1983). *The australopithecine Face*. New York: Academic Press.

Rak, Y. (1988). On Variation in the Masticatory System of *Australopithecus boisei*. In Grine, F.E. (eds.). *Evolutionary History of the "Robust" Australopithecines*. New York: Aldine de Gruyter.

Robinson, J.T. (1954). Prehominind Dentition and Hominid Evolution. Transvaal Museum, Pretoria. 1(1): 324-334.

Robinson, J. T. (1954). The genera and species of the Australopithecinae. *American Journal of Physical Anthropology*. 12(1): 181-200.

Robinson, J.T. (1956). *The dentition of the Australopithecine.* Transvaal Museum Memoir 9, Transvaal
Museum, Pretoria.

Roseman, C.C. (2004). Detecting interregionally diversifying natural selection on modern human cranial form by using matched and morphometric data. *Proceedings of the National Academy of Sciences of the United States of America*. 101(35): 12824-12829.

Rowan, J., Faith, J.T., Gebru, Y. and Fleagle, J.G., 2015. Taxonomy and paleoecology of fossil Bovidae (Mammalia, Artiodactyla) from the Kibish Formation, southern Ethiopia: Implications for dietary change, biogeography, and the structure of the living bovid faunas of East Africa. *Palaeogeography, Palaeoclimatology, Palaeoecology*. 420(1): 210-222.

Schroeder, L. (2007). Using Mahalanobis' Generalised Distances to Investigate Morphological Relationships and Variation in Early *Homo* Dental Specimens. Honours Thesis. University of Cape Town, Cape Town.

Schroeder, L., Roseman, C.C., Cheverud, J.M. and Ackermann, R.R. (2014). Characterizing the Evolutionary Path(s) to Early Homo. *PLOS ONE*. 9(2): 1-20.

Schroeder, L. (2015). *The evolution and diversification of Pleistocene Homo*. Ph.D. Dissertation: University of Cape Town, Cape Town.

Schroeder, L., and Ackermann, R. R. (2017). Evolutionary processes shaping diversity across the *Homo* lineage. *Journal of human evolution*. 111(1): 1-17.

Schroeder, L., & von Cramon-Taubadel, N. (2017). The evolution of hominoid cranial diversity: A quantitative genetic approach. *Evolution.* 71(11): 2634-2649.

Schwartz, J.H. and Tattersall I. (2003). *The Human Fossil Record: Volume Two: Craniodental Morphology of Genus Homo (Africa and Asia)*. New York: John Wiley & Sons Publication.

Scott, G. R., & Turner, C. G. II. (1997). *The anthropology of modern human teeth: dental morphology and its variation in recent human populations*. Cambridge: Cambridge University Press.

Shipman, P. and Harris, J.M. (1988). Habitat Preference and Paleoecology of *Australopithecus boisei* in Eastern Africa. In Grine, F.E. (eds.). *Evolutionary History of the "Robust" Australopithecines*. New York: Aldine de Gruyter.

Skelton, R.R. and McHenry, H.M. (1992). Evolutionary relationships among early hominids. *Journal of Human Evolution*. 23(1): 309-349.

Skelton, R.R. and McHenry, H.M. (1998). Trait list bias and reappraisal of early hominid phylogeny. *Journal of Human Evolution*. 34(1): 109-113.

Skelton, R.R., McHenry, H.M. and Drawhorm, G.M. (1986). Phylogenetic Analysis of Early Hominids. *Current Anthropology*. 27(1): 21-43.

Slice, D. E. (2007). Geometric Morphometrics. *Annu. Rev. Anthropology*. 36(1): 261 – 281.

Smith, A.L., Benazzi, S., Ledogar, J.A., Tamvada, K., Pryor Smith, L.C., Weber, G.W., Spencer, M.A., Lucas, P.W., Michael, S., Shekeban, A. and Al-Fadhalah, K., Almusallam, A.S., Dechow, P.C., Grosse, I.R., Ross, C.F., Madden, R.H., Richmond, B.G., Wright, B.W., Wang, Q., Byron, G., Slice, D.E., Wood., S., Dzialp, C., Berthaume, M.A., Casteren, A.V., and Strait, D.S. (2015). The Feeding Biomechanics and Dietary Ecology of *Paranthropus boisei* .*The Anatomical Record*. 298(1): 145-167.

Sponheimer, M., Lee-Thorp, J., de Ruiter, D., Codron, D., Codron, J., Baugh, A.T., and Thackeray, F. (2005). Hominins, sedges, and termites: new carbon isotope data from the Sterkfontein valley and Kruger National Park. *Journal of Human Evolution*. 48(1): 301-312.

Sponheimer, M., Alemsged, Z., Cerling, T.E., Grine, F.E., Kimbel, W.H., Leakey, M.G., Lee-Thorp., J.A., Manthi, F.K., Reed, K.E., Wood, B.A., and Wynn, J.G. (2013). Isotopic evidence of early hominin diets. *PNAS*. 110(6): 10513-10518.

Stansfield, E. and Gunz, P. (2011). Skhodnya, Khvalynsk, Satanay, and Podkumok calvariae: possible Upper
Paleolithic hominins from European Russia. *Journal of Human Evolution*. 60(1): 129-144.

Strait, D.S., Grine, F.E. and Moniz, M.A. (1997). A reappraisal of early hominid phylogeny. *Journal of human evolution*. 32(1): 17-82.

Susman, R.L. (1988). New Postcranial Remains from Swartkrans and Their Bearing on the Functional Morphology and Behavior of *Paranthropus robustus*. In Grine, F.E. (eds.). *Evolutionary History of the "Robust" Australopithecines*. New York: Aldine de Gruyter.

Sutton, M. (2013). *The archaeology of Swartkrans cave, Gauteng, South Africa: new excavations of members 1 and 4.* Ph.D. Dissertation, University of the Witswatersrand, Johannesburg

Sutton, M. B., Pickering, T. R., Pickering, R., Brain, C. K., Clarke, R. J., Heaton, J. L., & Kuman, K. (2009). Newly discovered fossil-and artifact-bearing deposits, uranium-series ages, and Plio-Pleistocene hominids at Swartkrans Cave, South Africa. *Journal of Human Evolution*. 57(6): 688-696.

Suwa, G. (1988). Evolution of the "Robust" Australopithecines in the Omo Succession: Evidence from Mandibular Morphology. In Grine, F.E. (eds.). *Evolutionary History of the "Robust" Australopithecines*. New York: Aldine de Gruyter.

Thackeray, J.F. and Prat, S. 2009. Chimpanzee subspecies and'robust'australopithecine holotypes, in the context of comments by Darwin. *South African Journal of Science*. 105(11-12): 463-464.

Thackeray, F., Braga, J., Treil, J., Niksch, N., and Labuschagne, J.H. (2002a). 'Mrs. Ples' (Sts 5) from Sterkfontein: an adolescent male? *South African Journal of Science*. 98(1-2): 21–22.

Tobias, P. V. (1988). Numerous Apparently Synapomorphic Features in *Australopithecus robustus*, *Australopithecus boisei* and *Homo habilis*: Support for the Skelton-McHenry-Drawhorn Hypothesis. In Grine, F.E. (eds.). *Evolutionary History of the "Robust" Australopithecines*. New York: Aldine de Gruyter.

Ungar, P.S., Grine, F.E. and Teaford, M.F. (2008). Dental Microwear and Diet of the Plio-Pleistocene Hominin *Paranthropus boisei*. *PLoS ONE*. 3(4): 1-6.

Ungar, P.S. and Sponheimer, M. (2011). The diets of early Hominins. *Science.* 334(1): 190-193.

Von Cramon-Taubadel, N. and Smith, H.F. (2012). The relative congruence of cranial and genetic estimates of hominid taxon relationships: Implications for the reconstruction of hominin phylogeny. *Journal of Human Evolution*. 62(1): 640-653.

Vrba, E.S. (1988). Late Pliocene Climatic Events and Hominid Evolution. The Evolution of *Australopithecus boisei*. In Grine, F.E. (eds.). *Evolutionary History of the "Robust" Australopithecines*. New York: Aldine de Gruyter.

Walker, A. (1976). Remains attributable to *Australopithecus* in the East Rudolf succession. In Coppens, Y., Howell, G. LI.I. and Leakey, R.E.F. (eds.). *Earliest Man and Environments in the Lake Rudolf Basin: Stratigraphy, Paleoecology, and Evolution.* Chicago: University of Chicago Press.

Walker, A. and Leakey, R. (eds.). (1993). *The Nariokotome Homo Erectus Skeleton*. Cambridge: Harvard University Press.

Walker, A.C., Leakey, R.E., Harris, J.M., and Brown, F.H. (1986). 2.5- myr *Australopithecus boisei* from west of Lake Turkana, *Kenya. Nature*. 322(6079): 517-522.

Walker, A.C. and Leakey, R.E. (1988). The Evolution of *Australopithecus boisei*. In Grine, F.E. (eds.). *Evolutionary History of the "Robust" Australopithecines*. New York: Aldine de Gruyter.

Ward, S.C. (1991). Taxonomy, paleobiology, and adaptations of the "robust" australopithecines. *Journal of Human Evolution*. 21(1): 469-483.

Weaver, T.D., Charles, Roseman, C.C. and Stringer, C.B. (2007). Were neandertal and modern human cranial differences produced by natural selection or genetic drift? *Journal of Human Evolution*. 53(2): 135-145.

Webster, M. and Sheets, D.H. (2010). A practical introduction to landmark-based geometric morphometrics. In Alroy, J. and Hunt, G. (eds.). *Quantative Methods in Paleobiology*. *The Paleontological Society Papers*. 16(1): 163-188.

White, T.D. (1988). The Comparative Biology of "Robust" *Australopithecus*: Clues from Content. In Grine, F.E. (eds.). *Evolutionary History of the "Robust" Australopithecines*. New York: Aldine de Gruyter.

Williams, F. L. (2015). Dietary proclivities of *Paranthropus robustus* from Swartkrans, South Africa. *Anthropological Review*. 78(1): 1-19.

Wood, B. and Strait, D. (2004). Patterns of resource use in early Homo and Paranthropus. *Journal of Human Evolution*. 46(2): 119-162.

Wood, B.A. (1988). Are "Robust" Australopithecines a Monophyletic Group? In Grine, F.E. (eds.). *Evolutionary History of the "Robust" Australopithecines*. New York: Aldine de Gruyter.

Wood, B.A. (2010). Reconstructing human evolution: Achievements, challenges, and opportunities. *PNAS*. 10(2): 8902-8909.

Wood, B.A. (2013): Gritting their teeth. *Nature*. 493(1): 486-487.

Wood, B.A. (2011). *Wiley-Blackwell encyclopedia of human evolution*. New York: John Wiley & Sons.

Wood, B. A. and Harrison, T. (2011). The evolutionary context of the first hominins. *Nature*. 470(1): 347-352.

Wood, B. A. and Boyle, E.K. (2016). Hominin Taxic Diversity: Fact or Fantasy? *Yearbook of Physical Anthropology*. 159(S61): 37-78.

Wood, B. and Lieberman, D.E. (2001). Craniodental variation in *Paranthropus* boisei: a developmental and functional perspective. *American Journal of Physical Anthropology*. 116(1): 13-25.

Wood, B. and Schroer, K. (2017). *Paranthropus*: Where Do Things Stand? In Marom, A. and Hovers, E. (eds.). *Human Paleontology and Prehistory*. New York: Springer, Cham.

Available from: http://bigpictures.club/resize.php?img=http://www.ibri.org/Books/Pun_Evolution/Figures/Fig2-18.gif, [27 October, 2017].

APPENDIX A

Table A.1.1. Matrix of pairwise Mahalanobis' distances for Densified Analysis 1 generated using a *H. sapiens* variance-covariance matrix. Non-bolded, non-italicized values indicate distances that are not significant using any model. Bolded values indicate distances that are statistically significant using all models. Non-bolded, italicized values indicate distances that are significant using some, but not all models; super-scripted numbers indicate the models for which these distances are significant; values 1-9 as listed in the caption for **Table 5.3.1**.

	SK 48	**SK 79**	**OH 5**
SK 48	0		
SK 79	*70.80* ^{1,4,7}	0	
OH 5	*292.17* ^{1,4,5,6,7,9}	*389.87* ^{1,3,4,5,6,7,8,9}	0

Table A.1.2. Matrix of pairwise Mahalanobis' distances for Densified Analysis 1 generated using a *P. troglodytes* variance-covariance matrix. Non-bolded, non-italicized values indicate distances that are not significant using any model. Bolded values indicate distances that are statistically significant using all

models. Non-bolded, italicized values indicate distances that are significant using some, but not all models; super-scripted numbers indicate the models for which these distances are significant; values 1-9 as listed in the caption for **Table 5.3.1**.

	SK 48	**SK 79**	**OH 5**
SK 48	0		
SK 79	*185.49* ^{1,4,5,6,7}	0	
OH 5	36.26	*124.62* ^{1,4,7}	0

Table A.1.3. Matrix of pairwise Mahalanobis' distances for Densified Analysis 1 generated using a *G. gorilla* variance-covariance matrix. Non-bolded, non-italicized values indicate distances that are not significant using any model. Bolded values indicate distances that are statistically significant using all models. Non-bolded, italicized values indicate distances that are significant using some, but not all models; super-scripted numbers indicate the models for which these distances are significant; values 1-9 as listed in the caption for **Table 5.3.1**.

	SK 48	**SK 79**	**OH 5**
SK 48	0		
SK 79	45.66	0	
OH 5	9.56	31.38	0

Table A.1.4. Matrix of pairwise Mahalanobis' distances for Densified Analysis 2 generated using a *H. sapiens* variance-covariance matrix. Non-bolded, non-italicized values indicate distances that are not significant using any model. Bolded values indicate distances that are statistically significant using all models. Non-bolded, italicized values indicate distances that are significant using some, but not all

models; super-scripted numbers indicate the models for which these distances are significant; values 1-9 as listed in the caption for **Table 5.3.1**.

	SK 48	**SK 79**	**OH 5**
SK 48	0		
SK 79	1.72	0	
OH 5	10.31	4.86	0

Table A.1.5. Matrix of pairwise Mahalanobis' distances for Densified Analysis 2 generated using a *P. troglodytes* variance-covariance matrix. Non-bolded, non-italicized values indicate distances that are not significant using any model. Bolded values indicate distances that are statistically significant using all models. Non-bolded, italicized values indicate distances that are significant using some, but not all models; super-scripted numbers indicate the models for which these distances are significant; values 1-9 as listed in the caption for **Table 5.3.1**.

	SK 48	**SK 79**	**OH 5**
SK 48	0		
SK 79	6.41	0	
OH 5	9.03	7.16	0

Table A.1.6. Matrix of pairwise Mahalanobis' distances for Densified Analysis 2 generated using a *G. gorilla* variance-covariance matrix Non-bolded, non-italicized values indicate distances that are not significant using any model. Bolded values indicate distances that are statistically significant using all

models. Non-bolded, italicized values indicate distances that are significant using some, but not all models; super-scripted numbers indicate the models for which these distances are significant; values 1-9 as listed in the caption for **Table 5.3.1**.

	SK 48	**SK 79**	**OH 5**
SK 48	0		
SK 79	5.55	0	
OH 5	9.56	2.88	0

Table A.1.7. Matrix of pairwise Mahalanobis' distances for Densified Analysis 3 generated using a *H. sapiens* variance-covariance matrix. Non-bolded, non-italicized values indicate distances that are not significant using any model. Bolded values indicate distances that are statistically significant using all models. Non-bolded, italicized values indicate distances that are significant using some, but not all models; super-scripted numbers indicate the models for which these distances are significant; values 1-9 as listed in the caption for **Table 5.3.1**.

	SK 48	**SK 79**	**OH 5**
SK 48	0		
SK 79	6.61	0	
OH 5	13.34	3.71	0

Table A.1.8. Matrix of pairwise Mahalanobis' distances for Densified Analysis 3 generated using a *P. troglodytes* variance-covariance matrix. Non-bolded, non-italicized values indicate distances that are not

significant using any model. Bolded values indicate distances that are statistically significant using all models. Non-bolded, italicized values indicate distances that are significant using some, but not all models; super-scripted numbers indicate the models for which these distances are significant; values 1-9 as listed in the caption for **Table 5.3.1**.

	SK 48	**SK 79**	**OH 5**
SK 48	0		
SK 79	12.27	0	
OH 5	*22.50* [5,6]	9.00	0

Table A.1.9. Matrix of pairwise Mahalanobis' distances for Densified Analysis 3 generated using a *G. gorilla* variance-covariance matrix. Non-bolded, non-italicized values indicate distances that are not significant using any model. Bolded values indicate distances that are statistically significant using all models. Non-bolded, italicized values indicate distances that are significant using some, but not all models; super-scripted numbers indicate the models for which these distances are significant; values 1-9 as listed in the caption for **Table 5.3.1**.

	SK 48	**SK 79**	**OH 5**
SK 48	0		
SK 79	8.91	0	
OH 5	13.79	6.18	0

Table A.1.10. Matrix of pairwise Mahalanobis' distances for Densified Analysis 4 generated using a *H. sapiens* variance-covariance matrix. Non-bolded, non-italicized values indicate distances that are not

significant using any model. Bolded values indicate distances that are statistically significant using all models. Non-bolded, italicized values indicate distances that are significant using some, but not all models; super-scripted numbers indicate the models for which these distances are significant; values 1-9 as listed in the caption for **Table 5.3.1**.

	SK 48	**SK 79**	**OH 5**
SK 48	0		
SK 79	*11.26* [5]	0	
OH 5	1.78	5.54	0

Table A.1.11. Matrix of pairwise Mahalanobis' distances for Densified Analysis 4 generated using a *P. troglodytes* variance-covariance matrix Non-bolded, non-italicized values indicate distances that are not significant using any model. Bolded values indicate distances that are statistically significant using all models. Non-bolded, italicized values indicate distances that are significant using some, but not all models; super-scripted numbers indicate the models for which these distances are significant; values 1-9 as listed in the caption for **Table 5.3.1**.

	SK 48	**SK 79**	**OH 5**
SK 48	0		
SK 79	*40.72* [1,4,5,6,7,9]	0	
OH 5	3.87	*28.71* [4,5,6,7,9]	0

Table A.1.12. Matrix of pairwise Mahalanobis' distances for Densified Analysis 4 generated using a *G. gorilla* variance-covariance matrix. Non-bolded, non-italicized values indicate distances that are not

significant using any model. Bolded values indicate distances that are statistically significant using all models. Non-bolded, italicized values indicate distances that are significant using some, but not all models; super-scripted numbers indicate the models for which these distances are significant; values 1-9 as listed in the caption for **Table 5.3.1**.

	SK 48	**SK 79**	**OH 5**
SK 48	0		
SK 79	*14.99* [5,6]	0	
OH 5	1.26	9.77	0

Table A.1.13. Matrix of pairwise Mahalanobis' distances for Densified Analysis 5 generated using a *H. sapiens* variance-covariance matrix. Non-bolded, non-italicized values indicate distances that are not significant using any model. Bolded values indicate distances that are statistically significant using all models. Non-bolded, italicized values indicate distances that are significant using some, but not all models; super-scripted numbers indicate the models for which these distances are significant; values 1-9 as listed in the caption for **Table 5.3.1**.

	SK 48	**SK 79**	**OH 5**
SK 48	0		
SK 79	4.94	0	
OH 5	3.34	9.3	0

Table A.1.14. Matrix of pairwise Mahalanobis' distances for Densified Analysis 5 generated using a *P. troglodytes* variance-covariance matrix. Non-bolded, non-italicized values indicate distances that are not significant using any model. Bolded values indicate distances that are statistically significant using all

models. Non-bolded, italicized values indicate distances that are significant using some, but not all models; super-scripted numbers indicate the models for which these distances are significant; values 1-9 as listed in the caption for **Table 5.3.1**.

	SK 48	**SK 79**	**OH 5**
SK 48	0		
SK 79	7.82	0	
OH 5	3.75	11.27	0

Table A.1.15. Matrix of pairwise Mahalanobis' distances for Densified Analysis 5 generated using a *G. gorilla* variance-covariance matrix. Non-bolded, non-italicized values indicate distances that are not significant using any model. Bolded values indicate distances that are statistically significant using all models. Non-bolded, italicized values indicate distances that are significant using some, but not all models; super-scripted numbers indicate the models for which these distances are significant; values 1-9 as listed in the caption for **Table 5.3.1**.

	SK 48	**SK 79**	**OH 5**
SK 48	0		
SK 79	6.82	0	
OH 5	1.83	6.67	0

Table A.1.16. Matrix of pairwise Mahalanobis' distances for Densified Analysis 6 generated using a *H. sapiens* variance-covariance matrix. Non-bolded, non-italicized values indicate distances that are not significant using any model. Bolded values indicate distances that are statistically significant using all

models. Non-bolded, italicized values indicate distances that are significant using some, but not all models; super-scripted numbers indicate the models for which these distances are significant; values 1-9 as listed in the caption for **Table 5.3.1**.

	SK 48	**SK 79**	**OH 5**
SK 48	0		
SK 79	4.89	0	
OH 5	2.01	4.34	0

Table A.1.17. Matrix of pairwise Mahalanobis' distances for Densified Analysis 6 generated using a *P. troglodytes* variance-covariance matrix. Non-bolded, non-italicized values indicate distances that are not significant using any model. Bolded values indicate distances that are statistically significant using all models. Non-bolded, italicized values indicate distances that are significant using some, but not all models; super-scripted numbers indicate the models for which these distances are significant; values 1-9 as listed in the caption for **Table 5.3.1**.

	SK 48	**SK 79**	**OH 5**
SK 48	0		
SK 79	12.64	0	
OH 5	5.29	13.54	0

Table A.1.18. Matrix of pairwise Mahalanobis' distances for Densified Analysis 6 generated using a *G. gorilla* variance-covariance matrix**.** Non-bolded, non-italicized values indicate distances that are not

significant using any model. Bolded values indicate distances that are statistically significant using all models. Non-bolded, italicized values indicate distances that are significant using some, but not all models; super-scripted numbers indicate the models for which these distances are significant; values 1-9 as listed in the caption for **Table 5.3.1**.

	SK 48	**SK 79**	**OH 5**
SK 48	0		
SK 79	4.99	0	
OH 5	1.82	4.33	0

Table A.1.19. Matrix of pairwise Mahalanobis' distances for Densified Analysis 7 generated using a *H. sapiens* variance-covariance matrix. Non-bolded, non-italicized values indicate distances that are not significant using any model. Bolded values indicate distances that are statistically significant using all models. Non-bolded, italicized values indicate distances that are significant using some, but not all models; super-scripted numbers indicate the models for which these distances are significant; values 1-9 as listed in the caption for **Table 5.3.1**.

	SK 48	**SK 79**	**OH 5**
SK 48	0		
SK 79	3.80	0	
OH 5	2.48	3.29	0

Table A.1.20. Matrix of pairwise Mahalanobis' distances for Densified Analysis 7 generated using a *P. troglodytes* variance-covariance matrix. Non-bolded, non-italicized values indicate distances that are not significant using any model. Bolded values indicate distances that are statistically significant using all

models. Non-bolded, italicized values indicate distances that are significant using some, but not all models; super-scripted numbers indicate the models for which these distances are significant; values 1-9 as listed in the caption for **Table 5.3.1**.

	SK 48	**SK 79**	**OH 5**
SK 48	0		
SK 79	4.75	0	
OH 5	6.15	10.36	0

Table A.1.21. Matrix of pairwise Mahalanobis' distances for Densified Analysis 7 generated using a *G. gorilla* variance-covariance matrix. Non-bolded, non-italicized values indicate distances that are not significant using any model. Bolded values indicate distances that are statistically significant using all models. Non-bolded, italicized values indicate distances that are significant using some, but not all models; super-scripted numbers indicate the models for which these distances are significant; values 1-9 as listed in the caption for **Table 5.3.1**.

	SK 48	**SK 79**	**OH 5**
SK 48	0		
SK 79	2.20	0	
OH 5	2.26	2.64	0

Table A.1.22. Matrix of pairwise Mahalanobis' distances for Densified Analysis 8 generated using a *H. sapiens* variance-covariance matrix. Non-bolded, non-italicized values indicate distances that are not

significant using any model. Bolded values indicate distances that are statistically significant using all models. Non-bolded, italicized values indicate distances that are significant using some, but not all models; super-scripted numbers indicate the models for which these distances are significant; values 1-9 as listed in the caption for **Table 5.3.1**.

	SK 48	**SK 79**	**OH 5**
SK 48	0		
SK 79	5.18	0	
OH 5	2.56	0.6	0

Table A.1.23. Matrix of pairwise Mahalanobis' distances for Densified Analysis 8 generated using a *P. troglodytes* variance-covariance matrix. Non-bolded, non-italicized values indicate distances that are not significant using any model. Bolded values indicate distances that are statistically significant using all models. Non-bolded, italicized values indicate distances that are significant using some, but not all models; super-scripted numbers indicate the models for which these distances are significant; values 1-9 as listed in the caption for **Table 5.3.1**.

	SK 48	**SK 79**	**OH 5**
SK 48	0		
SK 79	3.78	0	
OH 5	1.62	0.51	0

Table A.1.24. Matrix of pairwise Mahalanobis' distances for Densified Analysis 8 generated using a *G. gorilla* variance-covariance matrix. Non-bolded, non-italicized values indicate distances that are not significant using any model. Bolded values indicate distances that are statistically significant using all models. Non-bolded, italicized values indicate distances that are significant using some, but not all models; super-scripted numbers indicate the models for which these distances are significant; values 1-9 as listed in the caption for **Table 5.3.1**.

	SK 48	**SK 79**	**OH 5**
SK 48	0		
SK 79	3.21	0	
OH 5	1.04	0.73	0

Table A.1.25. Matrix of pairwise Mahalanobis' distances for Densified Analysis 9 generated using a *H. sapiens* variance-covariance matrix. Non-bolded, non-italicized values indicate distances that are not significant using any model. Bolded values indicate distances that are statistically significant using all models. Non-bolded, italicized values indicate distances that are significant using some, but not all models; super-scripted numbers indicate the models for which these distances are significant; values 1-9 as listed in the caption for **Table 5.3.1**.

	SK 48	**SK 79**	**OH 5**
SK 48	0		
SK 79	17.49	0	
OH 5	6.03	8.53	0

Table A.1.26. Matrix of pairwise Mahalanobis' distances for Densified Analysis 9 generated using a *P. troglodytes* variance-covariance matrix. Non-bolded, non-italicized values indicate distances that are not significant using any model. Bolded values indicate distances that are statistically significant using all models. Non-bolded, italicized values indicate distances that are significant using some, but not all models; super-scripted numbers indicate the models for which these distances are significant; values 1-9 as listed in the caption for **Table 5.3.1**.

	SK 48	**SK 79**	**OH 5**
SK 48	0		
SK 79	*23.71* [3,7]	0	
OH 5	5.92	7.78	0

Table A.1.27. Matrix of pairwise Mahalanobis' distances for Densified Analysis 9 generated using a *G. gorilla* variance-covariance matrix. Non-bolded, non-italicized values indicate distances that are not significant using any model. Bolded values indicate distances that are statistically significant using all models. Non-bolded, italicized values indicate distances that are significant using some, but not all models; super-scripted numbers indicate the models for which these distances are significant; values 1-9 as listed in the caption for **Table 5.3.1**.

	SK 48	**SK 79**	**OH 5**
SK 48	0		
SK 79	7.21	0	
OH 5	3.99	3.23	0

Table A.2.1. Significance values: Mahalanobis' Distance values for determining significance in fossil specimens for Densified Analyses. 1- 9.

Analysis	Human Human	Human Chimp	Human Gorilla	Chimp Chimp	Chimp Human	Chimp Gorilla	Gorilla Gorilla	Gorilla Chimp	Gorilla Human
1	59.211	445.062	374.613	52.994	138.675	146.916	51.127	350.248	263.859
2	34.891	219.522	91.373	27.574	22.695	20.956	20.897	74.688	29.649
3	35.461	139.512	88.823	25.894	17.265	18.456	20.887	54.858	29.299
4	35.501	316.452	163.473	21.254	6.875	13.956	21.567	80.978	22.619
5	40.651	249.752	184.493	26.144	20.705	42.716	24.407	69.358	34.019
6	38.021	128.242	66.683	23.794	14.075	20.576	20.717	64.008	21.989
7	43.13	363.38	108.12	23.77	171.21	14.82	24.31	73.72	299.61

	1	2	3	4	5	6	7	8	9
8	40.92	201.68	53.31	28.68	89.57	68.00	24.97	75.68	74.91
	1	2	3	4	5	6	7	8	9
9	27.48	28.45	22.83	28.60	64.08	35.53	20.21	45.89	43.20
	1	2	3	4	5	6	7	8	9

APPENDIX B

Table B.1. 1. Summary of principal components analysis for all Geometric morphometric analyses 1-5 (adapted from Schroeder, 2015).

ANALYSIS	REGION	PC	% VARIANCE
1	CRANIUM	1	45.98
	DENSIFIED	2	9.96
	PALATE	3	6.46
		4	4.27
		5	3.58
		6	3.28
2	MANDIBLE	1	55.93
	CORPUS	2	11.84
		3	7.47
		4	6.86

		5	4.52
		6	3.75
3	CRANIUM MAXILLA-MIDFACE	1	44.54
		2	16.31
		3	8.58
		4	7.73
		5	6.45
		6	4.14
4	CRANIUM ZYGOMATIC-UPPERFACE-BASICRANIUM	1	60.88
		2	10.96
		3	7.67
		4	4.36
		5	4.14
		6	2.79
5	CRANIUM ZYGOMATIC-MIDFACE	1	44.72
		2	15.92
		3	9.43
		4	7.98
		5	4.80
		6	4.11

APPENDIX C

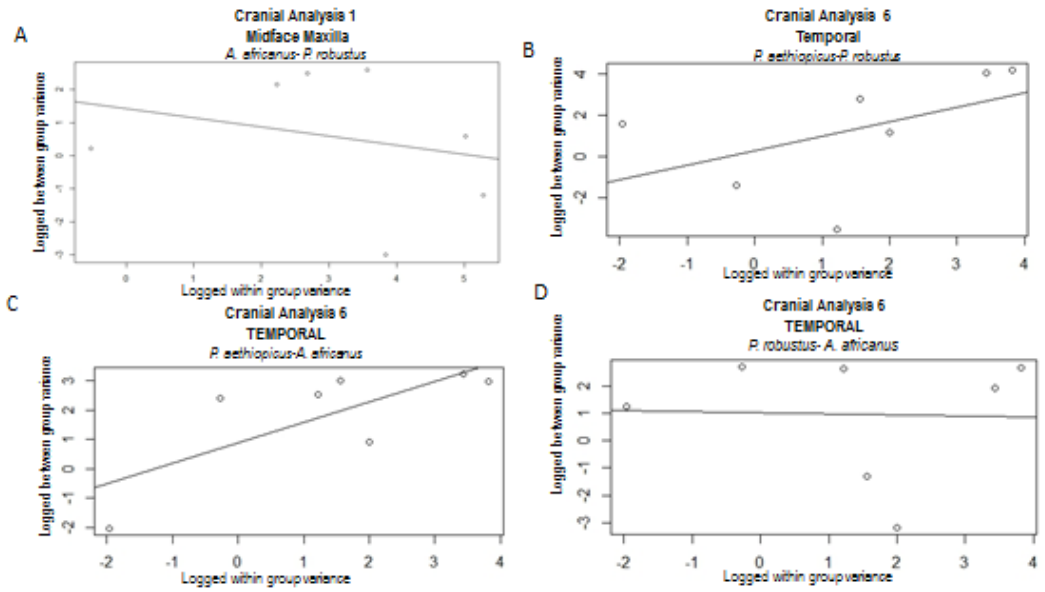

Figure C.1.1. Regression plots (logged between group against logged within group variance) for comparisons in the case drift is rejected. All analyses use a human model of within group variance. (**A**) Cranial Analysis 1 regression analysis for the comparison of *A. africanus* and *P. robustus* produces an estimated slope of -0.27 with an R^2 value of 0.07. (**B**) Cranial Analysis 6 regression analysis for the comparison of *P. aethiopicus* and *P. robustus* produces an estimated slope of 0.16 with an R^2 value of 0.04. (**C**) Cranial Analysis 6 regression analysis for the comparison of *P. aethiopicus* and *A. africanus* produces an estimated slope of 0.00 with an R^2 value of 0.00 (**D**) Cranial Analysis 6 Regression analysis for the comparison of *P. robustus* and *A. africanus* produces an estimated slope of 0.18 with an R^2 value of 0.10.

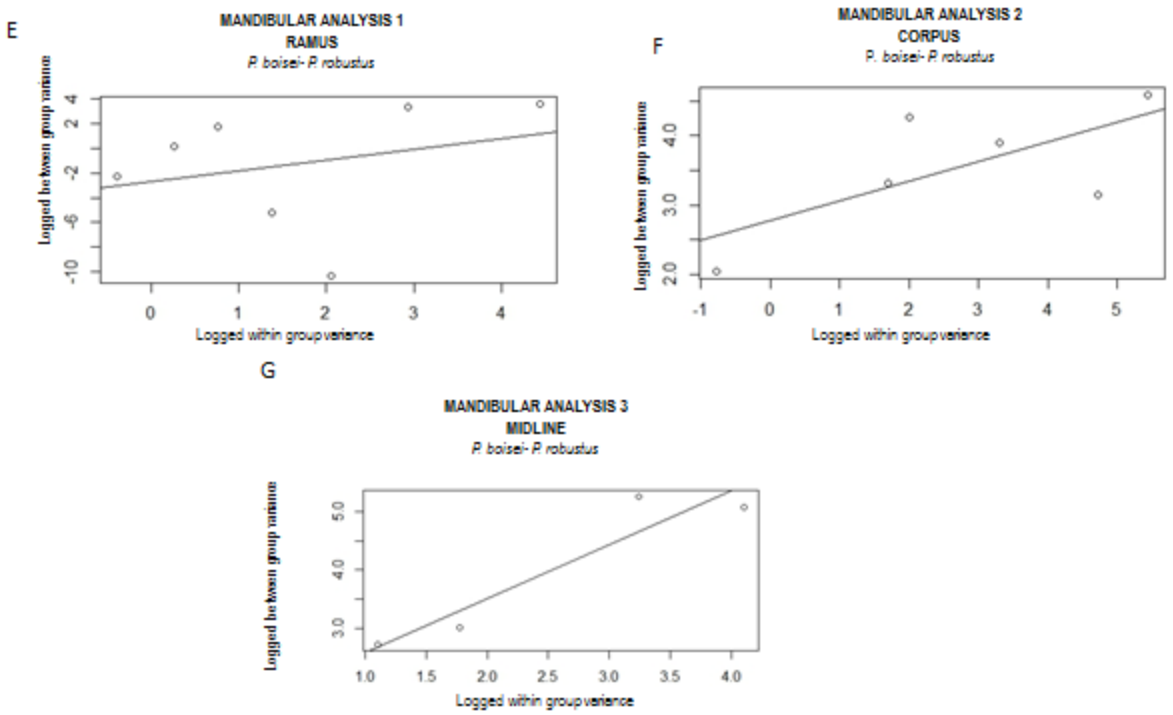

Figure C.1.2. Regression plots (logged between group against logged within group variance) for comparisons in the case drift is rejected. All analyses use a human model of within group variance. (**E**) Mandibular Analysis 1 regression analysis for the comparison of *P. boisei* and *P. robustus* produces an estimated slope of 0.28 with an R^2 value of 0.49. (**F**) Mandibular Analysis 2 regression analysis for the comparison of *P. boisei* and *P. robustus* produces an estimated slope of -0.24 with an R^2 value of 0.04. (**G**) Mandibular Analysis 3 regression analysis for the comparison of *P. boisei* and *P. robustus* produces an estimated slope of 0.14 with an R^2 value of 0.26.

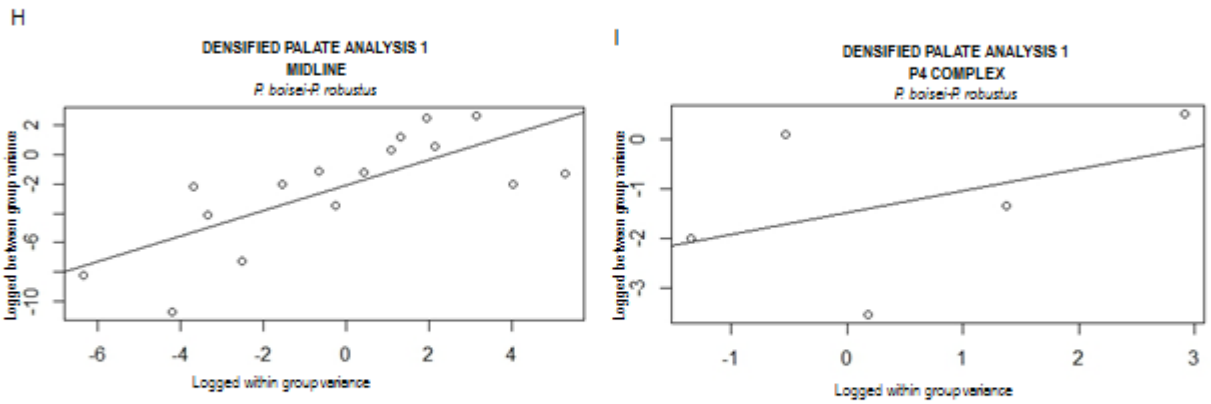

Figure C.1.3. Regression plots (logged between group against logged within group variance) for comparisons in the case drift is rejected. All analyses use a human model of within group variance. (**H**) Densified Palate Analysis 1 regression analysis for the comparison of *P. boisei* and *P. robustus* produces an estimated slope of 0.54 with an R^2 value of 0.48. (**I**) Densified Palate Analysis 5 regression analysis for the comparison of *P. boisei* and *P. robustus* produces an estimated slope of 0.89 with an R^2 value of 0.99.

Appendix D

D.1.1 Neutrality test code in R v3.24 (revised).

#adopted/written by Lauren Schroeder

#edited by Nomawethu Hlazo

dataset <- read.csv ("DatasetD9.csv", header=T, sep=";") #read data

species <- as.matrix (DatasetD9$SPECIES) #transform species names into matrix form

HUMAN <- dataset [DatasetD9$SPECIES == "HUMAN",] #call HUMAN species name

#CHIMP <- dataset [DatasetD9$SPECIES == "CHIMP",]

#GORILLA <- dataset [DatasetD9$SPECIES == "GORILLA",]

covTeethWithin <- cov (HUMAN [,2: ncol (DatasetD9)],use = "pairwise.complete") #find covariance matrix of HUMAN dataset ncol number of columns

#covTeethWithin <- cov (CHIMP [,2:ncol (DatasetD9)],use = "pairwise.complete")

#covTeethWithin <- cov (GORILLA [,2:ncol(DatasetD9)],use = "pairwise.complete")

speciesName <- unique (DatasetD9$SPECIES) #call all species names

speciesName #returns species names

View (speciesName) #views number and species name

D.1.2. Selection vector code in R v3.2.2 (revised)

#This implementation only works with two species at a time

GroupMeans1 <- apply (DatasetD9 [DatasetD9$SPECIES == speciesName [1], 2: ncol(DatasetD9)],2,mean,na.rm = TRUE) #calculates group means of species 1 in this case ARCHAIC

GroupMeans2 <- apply (DatasetD9 [DatasetD9$SPECIES == speciesName [2],2:ncol (DatasetD9)],2,mean,na.rm = TRUE) #calculates group means of species 2 in this case DMANISI

```
GroupMeans <- cbind(GroupMeans1,GroupMeans2) #column binds GroupMeans1 and
GroupMeans2

CEigenAnalysis <- eigen(covTeethWithin) #perform eigenanalysis on HUMAN covariance
matrix

CVectors <- CEigenAnalysis$vectors #names eigenvectors Cvectors

CValues <- CEigenAnalysis$values #names eigenvalues CValues

CVectors #returns CVectors

CEigenAnalysis #returns CValues


#Calculate group mean differences along eigenvectors

GroupMeans <- as.matrix(t(GroupMeans))

compMeans <- GroupMeans%*%CVectors

compMeans


#Calculate between group variance

betweenVarEigen <- diag(var(compMeans))

betweenVarEigen #returns between group eigenvalues


#regress logged between eigenvalues on logged within eigenvalues

WBEigenvalueslog <- as.data.frame(cbind(log(CValues),log(betweenVarEigen)))

names(WBEigenvalueslog) <- c("Within","Among")

print(WBEigenvalueslog)

WBESlope <- lm(Among~Within,data = WBEigenvalueslog)$coefficients[2]

WEBRSquare <- summary.lm( lm(Among~Within,data = WBEigenvalueslog))$r.squared

WBESlope
```

WEBRSquare

```
#calculate Standard error
lm(Among~Within,data = WBEigenvalueslog)
lm.r <- lm(Among~Within,data = WBEigenvalueslog)
summary(lm.r)
Resid <- lm.r$residuals
Resid2 <- Resid^2
SSR <- sum(Resid2)
SSR1 <- sqrt(SSR/((length(WBEigenvalueslog$Among))-2))
SSR2 <- sqrt(sum(((WBEigenvalueslog$Within)-mean(WBEigenvalueslog$Within))^2))
SES <-SSR1/SSR2
SES
#test to see if slope is different from 1
tstat <- (abs(WBESlope-1))/SES
pvalue <- 2*pt(tstat,df=nrow(covTeethWithin)-2, lower.tail = F)
output <- c(WBESlope,tstat,pvalue,WEBRSquare)
names(output) <- c("Slope","tstat","p.value","RSquare")
output
```

D.1.2. Code for Selection vectors in R. 3.2.4 (revised).

```
library(statmod)

library(MASS)

dataset <- read.csv("DatasetD7.csv",header=T,sep=";") #read data

species <- as.matrix(DatasetD7$SPECIES)   #transform species names into matrix form

HUMAN <- dataset[DatasetD7$SPECIES == "HUMAN",] #call HUMAN species name

covTeethWithin <- cov(HUMAN[,2:ncol(DatasetD7)],use = "pairwise.complete") #find
covariance matrix of HUMAN dataset

speciesName <- unique(DatasetD7$SPECIES) #call all species names

speciesName #returns species names

View (speciesName) # view number and species names


#This implementation only works with two species at a time

GroupMeans1 <- apply(dataset[DatasetD7$SPECIES ==
speciesName[1],2:ncol(DatasetD7)],2,mean,na.rm = TRUE) #calculates group means of species
1 in this case  P. robustus

GroupMeans2 <- apply(dataset[DatasetD7$SPECIES ==
speciesName[2],2:ncol(DatasetD7)],2,mean,na.rm = TRUE) #calculates group means of species
2 in this case P. boisei


#calculates selection vectors between two species

#assumes species 1 is the descendent and species 2 is the ancestor

VGroupMeansdescendent <- as.vector(GroupMeans1) #calls species 1 descendent

VGroupMeansancestor <- as.vector(GroupMeans2) #calls species 1 ancestor

Dmean <- VGroupMeansdescendent - VGroupMeansancestor #calculates difference vector
```

```
TDmean <- cbind(Dmean)

winv <- solve(covTeethWithin,TDmean) #multiplies inverse of covariance matrix by difference vector

selectionv <-t(winv)

Dmean #returns difference vector

selectionv #returns selection vector
```

APPENDIX E

Avizo Fire: https://vsg3d.com/
MorphoJ: http://www.flywings.org.uk/morphoj_page.htm
PAST: http://folk.uio.no/ohammer/past/
R: https://cran.r-project.org/